TECHNISCHE UNIVERSITÄT MÜNCHEN

Institut für Wasserchemie und Chemische Balneologie
Lehrstuhl für Analytische Chemie

SERS-Based Label-Free Microarray Readout for the Detection of Microorganisms

Maria Knauer

Vollständiger Abdruck der von der Fakultät für Chemie der Technischen Universität München zur Erlangung des akademischen Grades eines

Doktors der Naturwissenschaften (Dr. rer. nat.)

genehmigten Dissertation.

Vorsitzender:		Univ.-Prof. Dr. M. Schuster
Prüfer der Dissertation:	1.	Univ.-Prof. Dr. R. Nießner
	2.	Univ.-Prof. Dr. S. Scherer

Die Dissertation wurde am 02.11.2011 bei der Technischen Universität München eingereicht und durch die Fakultät für Chemie am 10.02.2012 angenommen.

"-Skal du en vei?"

"-Finnes det flere veier?"

Acknowledgements

This thesis would not have been realizable if certain people had not contributed with their support and academic knowledge.

I would like to address a special thank to Prof. Dr. R. Nießner for the friendly reception at the institute of hydrochemistry and for giving me the trust necessary to accomplish my thesis. He kindly provided financial support for the project which was not funded by an official founder.

Furthermore, I would like to warmly thank Prof. Dr. C. Haisch for the interesting topic and his academic involvement and support throughout my work. I appreciate his enthusiasm and kind, but qualitative way of leading the lasergroup, which is a very inspiring team with a most comfortable working atmosphere. I would like to thank him for his patience towards me and his great participation in discussions.

I could not thank Dr. N. P. Ivleva enough for her inspiration. Without her help and knowledge, this work would by far be of another quality. She has taught me a lot, both on an academic and on a personal level. Thank you for always, with no exception, taking time.

I thank C. Sternkopf and M. Hanzlik for developing SEM and TEM images, Dr. M. Wagner for writing the excellent mapping program.

I have had the pleasure of introducing the topic to several hardworking students for internships, bachelor- and master theses. These students are; T. Flock, M. Hübner, C. Ziegler, P. Köllner, M. Nentwig, S. Klotz and K. Schwarzmeier.

For proof-reading of this thesis, I would like to thank Dr. N. P. Ivleva, Dr. M. Knauer, K. Wutz and K. Schwarzmeier.

I would like to thank all my colleagues at IWC for their impressive participation to create an inspiring working atmosphere and for their constant helpfulness. A special thanks to my collaborates in the lasergroup. The hydrogeologists C. Mayrhofer and S. Huckele have given me strength and kept me in a good mood throughout my time at the institute and I would like to express my gratefulness towards them.

Without my friends and family, which have given me their support along my entire studies, I would not have accomplished what I have today. One large thanks to my husband Markus for everything he is.

Publications

Parts of this thesis have been published in following scientific journals:

X. Liu, M. Knauer, N. P. Ivleva, R. Niessner, C. Haisch, *Synthesis of core-shell surface-enhanced Raman tags for bioimaging,* Anal. Chem., **2010**, 82, 441-446.

M. Knauer, N. P. Ivleva, X. Liu, R. Niessner, C. Haisch, *SERS-based label-free microarray readout for the detection of microorganisms,* Anal. Chem., **2010**, 82, 2766-2772.

M. Knauer, N. P. Ivleva, R. Niessner, C. Haisch, *Optimized surface-enhanced Raman scattering (SERS) colloids for the characterization of microorganisms*, Anal. Sci., **2010**, 26, 761-766. (Awarded to hot paper)

M. Knauer, N. P. Ivleva, R. Niessner, C. Haisch, A flow-through microarray cell for the online SERS detection of antibody-captured E. coli bacteria, Anal. Bioanal. Chem., **accepted.**

Abstract

Bacteria detection in aqueous and aerosol matrix is hampered by the limited selectivity and sensitivity of existing readout methods. Whilst the problem of microbial contamination in the environmental and industrial field is rising, the need for a fast and accurate detection principle is increasing.

This thesis reports the development of a label-free SERS detection and –imaging of microorganisms on a microarray platform in aqueous media originated from both aerosol and water samples. The microarray is part of a closed flow-through system where the recognition takes place. In order to obtain reproducible and strong species specific SERS spectra from various bacteria immobilized on a chip, chemically synthesized nanoparticles were developed and applied. Hereby, different colloid sols were tested and optimized regarding their suitability as SERS media. The silver sols produced by a modified procedure of Leopold and Lendl [1] gave an enhancement factor of 10^8 for the test molecule crystal violet compared to normal Raman. The colloid preparation was carried out at room temperature and the colloids were stable for weeks. Furthermore, this SERS medium was successfully applied for label-free *in situ* detection and identification of microorganisms immobilized on an antibody by fingerprint analyses and SERS imaging (*Legionella pneumophila* (autoclaved), *Salmonella typhimurium* (heat killed) and *Escherichia coli* (living)). Furthermore, quantitative analysis of *Legionella pneumophila* (autoclaved) and *Salmonella typhimurium* (heat killed) was performed using Raman mapping. A flow-through microarray setup increased the sensitivity of the method and gave a LOD of 4485 cells/mL and LOQ of 7755 cells/mL for spiked *E. coli* (living) suspensions. This setup was successfully adapted to bioaerosol detection where heat killed aerosolized *E. coli* were detected with a LOD of 114 particles/cm^3 and LOQ of 178 particles/cm^3. Unlike conventional SERS detection of bacteria, which requires dehydration prior to detection, this system enables detection and quantification of multiple microorganisms in an aqueous environment *in situ.* Hence, it has a great potential for high-throughput detection of microbial samples. A non-destructive analysis of living bacteria cells is possible. Moreover, the "whole-organism fingerprint" SERS spectra can be adopted for further chemical characterization of microorganisms.

Table of Contents

1 Introduction 1

2 Fundamentals 4

2.1 Review of previous work 5

2.2 Microorganisms 10

2.2.1 Legionella pneumophila 11

2.2.2 Salmonella typhimurium 12

2.2.3 Escherichia coli 12

2.2.4 Potential reservoirs 12

2.3 Microarray detection of immunoassays 14

2.4 Surface-enhanced Raman spectroscopy (SERS) 18

2.4.1 Electromagnetic enhancement 20

2.4.2 Chemical enhancement 23

2.4.3 SERS media 23

2.5 SERS characterization of microorganisms 26

2.6 Microfluidics 29

2.7 Bioaerosol analysis 30

3 Materials and Methods 32

3.1 Chemicals and solvents 33

3.2 Miscellaneous devices 36

3.3 Microarray coating 38

3.3.1 Diamino-PEG-coating 38

3.3.2 Star-PEG-coating 40

3.3.3 Ag-coating 44

3.3.4 Surface control 45

3.4 Preparation of immuno-microarray reagents 46
3.4.1 Antibody immobilization 46
3.4.2 Microorganism preparation 46

3.5 Preparation of the SERS media 47
3.5.1 Silver nanoparticles 47
3.5.2 Gold nanoparticles 48

3.6 SERS measurements 50
3.6.1 SERS measurements on crystal violet 50
3.6.2 SERS measurements on microorganisms 51

3.7 Data acquisition 56

4 Results and Discussion 58

4.1 Microarray platform 59

4.2 SERS media 66
4.2.1 Silver colloid sol 67
4.2.2 Gold colloid sol 77

4.3 SERS on bacteria (stationary) 85
4.3.1 Negative control 86
4.3.2 Importance of colloid agglomeration onto the bacteria 89
4.3.3 Identification of bacteria 92
4.3.4 Quantitative analysis of bacteria 100

4.4 SERS on bacteria (flow cell) 107
4.4.1 Negative control 108
4.4.2 Identification of bacteria 109
4.4.3 Effects of environmental stress on bacteria 114
4.4.4 Quantitative analysis of bacteria 121

4.5 SERS analysis of airborne bacteria 125
4.5.1 Aerosol sampling 125
4.5.2 Identification of bacteria 126
4.5.3 Quantitative analysis of bacteria 126

5 Summary and Outlook 129

6 Abbreviations 133

7 Appendix 137

8 Literature 139

1 Introduction

"*Water is fundamental for life and health. The human right to water is indispensable for leading a healthy life in human dignity. It is a pre-requisite to the realization of all other human rights.*"

The United Nations Committee on Economic, Cultural and Social Rights,
Environment News Service, Nov. 27th 2002

The European Commission has developed an edict, the Registration, Evaluation, Authorization and Restriction of Chemicals (REACH), which regulates the drinking water monitoring requirements in the European Union. It is based on the European Commission Directive from 1980 relating to the quality of water intended for human consumption, better known as the Drinking Water Directive (80/778/EEC). This Directive was revised in 1998 (98/83/EEC). It says that in both 250 mL drinking and bottled water, no coliform cells should be present and gives suggestions for drinking water treatment [2]. Additionally, in November 2011 a new law published by the German Dinking Water Ordinance will become operative [3]. It states that all public drinking water installations must be analyzed for the presence of *Legionella* and coliforms before they are operated. According to § 14 of this ordinance, the upper concentration limit of the mentioned bacteria is 100 cfu/100 mL water. In order to detect such low concentrations quickly, a new analytical tool is needed. Microorganism analysis methods on the market are time intensive and require mostly a cultivation step prior to the detection. The drinking water community is aiming for an online and continuous analysis of bacteria in water to diminish contamination risk to the consumer.

In the past few years, Raman spectroscopy has gained increasing interest in the analysis of bacteria as the method provides component specific information by means of vibrational spectroscopy. Though, normal Raman is hampered by its low cross sections, hence limited in sensitivity. For larger and complex biomolecule structures, high signal to noise ratios require long laser exposure times which can cause burning of the analyte surface material. By introducing nano-sized metal particles to the analytes, signal enhancement (i.e. cross section improvement) results. This application, called surface-enhanced Raman spectroscopy (SERS) enables qualitative differentiation of various bacteria strains by fingerprint spectra evaluation which is difficult and time consuming by means of normal Raman. As the method is non-destructive and water compatible, online measurements are possible. Nevertheless, the sensitivity of bacteria detection based on SERS in water and

aerosol matrices is too weak to detect the small concentrations set as contaminant-free water and air by the government.

The aim of this work was to develop a new method which approaches these governmental requirements. A qualitative and quantitative detection principle for multiple bacteria strains by combining immunocomplex-microarrays with SERS was sought. The main emphasis of the work was the qualitative analysis of microorganisms relevant for drinking water analysis, by means of fingerprint spectra assignment to the respective analyte. In order to produce SERS enhancement, a reproducible and easy SERS media preparation procedure of an optimal metal colloid sol was developed. The enhancement properties of the prepared colloids were calculated from the SERS enhancement in presence of crystal violet. For quantitative evaluation purposes, a microfluidic setup was constructed and inserted as a part of the microarray platform. Hereby, a completely new way of micoarray readout was educed by a scanning process over the microarray spot. Validation of the readout method was carried out in a stationary tray. With this new development, an improvement in reproducibility, time consumption and quality of bacteria detection to conventional methods was wanted. This would ease the monitoring of drinking water and air to diminish the risk of infections.

Thesis layout

This thesis is divided into four main parts which include a thorough introduction to the fundamentals of the work, followed by an experimental part in which the procedures and their properties are described. Subsequently, the results of the research are discussed. At the end a short summary followed by an outlook can to be found. In the beginning of the fundamentals chapter, a state of the art is described with a literature review. This chapter is addressed to scientists working on surface-enhanced Raman spectroscopy (SERS) analysis of bacteria. It is written to provide the reader a quick update in the state of art of the thematic of this thesis.

Author´s words to the reader

The wide and relative new world of SERS has inspired me since I was introduced to the topic three years ago. There are so many questions and undiscovered aspects connected to this phenomenon and there, I believe, will still be decades until a complete chemical and physical understanding of SERS has been accomplished. Bacteria pollution in various media has proven to be detectable with SERS and some of the many open questions which we had in the beginning of our journey have now been answered. A sensitive and fast detection method for bacteria in aqueous and aerosol media could be established in such short time which should awake the interest to the industry to look closer at this alternative method. I believe that in the future, we will see a breakthrough of SERS in the industry to multiple applications.

2 Fundamentals

2.1 Review of previous work

In the 1970s it was found by Creighton *et al.* that the properties of surface-enhanced Raman scattering (SERS) is contributed by different metal species through electromagnetic and chemical enhancement effects and provides significant enhancement of Raman scattering [4]. Research groups worldwide have implemented a wide range of SERS substrates and media since then [5-9]. The most common are nanocolloids and coatings of Ag, Au and Cu. It was later discovered that SERS enhancement is dependent on the size, micro- and nanomorphology of the metal [10]. The optimal spherical Ag nanoparticle size for SERS was found to be between 50 nm and 60 nm by Stamplecoskie *et al.* [11]. They also highlighted the importance of control over the size and polydispersity of the particles for reproducible SERS enhancements, though only particles in the region ~20 nm to ~65 nm were examined. Willets *et al*. reported in 2009 that Ag colloids must be in the range of 20 nm to 100 nm to produce enhancement of the Raman scattered photons [12]. Other groups have tested numerous different shapes of SERS media on their enhancement properties like rods [13], bi- and trilayer particles [14] as well as metals coatings [15]. Transition metals like Pt, Pd and Rh have also been tested by Ren *et al.* [16]. This group reported an enhancement as high as four orders of magnitude using cauliflower-shaped Rh as SERS media. Enhancement was also produced in the UV spectral region (UV-SERS) on Rhodium and Ruthenium electrodes by Ren *et al.* [17]. Flower-shaped PdI_2 nanomaterials with remarkable SERS activity was reported by Wang *et al.* [18]. Tian *et al.* published a direct generation of SERS on transition metals like Pt, Ru, Rh, Pd, Fe, Co, Ni and their alloys [19]. Mainly, the literature presents SERS particles which are either produced by reduction of metal salts, by laser ablation, or electrochemically.

Silver colloids were first presented as SERS media by Creighton *et al.* in 1979 [4]. This group proved that superior enhancement can be achieved using silver surfaces in comparison to gold structures in the visible range. Ooka *et al.* showed that silver colloids interact with both amine and carboxylate groups [20]. The free electrons of the silver atom interact with the respective empty orbital of the functional groups of the analyte. Several authors (e.g., Lee and Meisel [21], Munro *et al.* [22] and Leopold and Lendl [1]) have reported different procedures to create Ag colloidal sols and characterized corresponding scattering enhancements by SERS. A silver surface in contact with water is slightly electropositive; hence it shows an affinity to electronegative regions on bacteria cell walls due to electrostatic interactions, in addition to van-der-Waal forces.

In 1989, Holt *et al*. published the first SERS analysis of bacteria. They collected SERS data from a photosynthetic bacterium cell wall and awoke the interest towards SERS analysis of microorganisms [23]. Since then, the method has gained attention of research groups worldwide. Both qualitative and quantitative information on bacteria strains, subspecies and even complex biofilms have been reported as well as *in vitro* and *in situ* SERS detection of bacteria. However, the main part of the existing *in situ* quantitative applications includes the use of labelling molecules [24-26]. Fluorescence quenching is observed in SERS, although it is known that local fields can enhance all optical fields which are in resonance with the surface plasmons. This quenching occurs especially for chromophores, probably generated by dipole-dipole coupling between the excited chromophore and the nearby metal, resulting in a shortened time of excited-state, which in return decreases the fluorescence quantum yield [27]. This is one of the reasons why fluorescence dyes are often used as labelling molecules. The detection of *E. coli* using SERS has been published numerously in the last decade. The latest publications in this area are promising for future implementation of SERS detection of real sample microorganism analysis. E.g. in 2011, Walter *et al*. published the detection of *E. coli* in a SERS flow-system [28]. They showed the qualitative evaluation of different subspecies by chemometrics. A database of multiple spectra was generated to improve the recovery rates. These results were gathered without the use of labelling molecules. Temur *et al.* carried out a quantification of *E. coli* in the range of 10^1 cfu/mL - 10^5 cfu/mL by using gold nanoparticles coated with the label 5,5'-dithiobis-2-nitrobenzoic acid (DTNB) on a sandwich immunoassay [25]. Zeiri *et al.* have shown that if silver colloids are produced in the present of bacteria, these particles enter the inner of the cell and fingerprint spectra observed are different from those collected by adding the colloid sol ex post (cell external and after) preparation [29]. This is due to the different biochemical reactions *in vitro* compared to the composition *in vivo* but also the difference in inner and outer cell matter. They additionally reported that fingerprint spectra from the same bacteria species (here *E. coli*) vary with unequal laser excitation wavelengths. Thus, when comparing SERS fingerprints of other research groups, one should simultaneously compare the experimental conditions used. Further work in this area was completed by Kahraman *et al.* in 2007 [30]. Here, two bacterium species were analyzed with SERS with the motive of revealing the dependence of laser wavelength and SERS media metal on the fingerprint spectra. They concluded that there were small changes in the fingerprints, but not as severe as Zeiri *et al*. reported. Further important work on SERS detection of microorganisms was carried out by Kahraman *et al.* [31] who exposed several bacteria to silver colloids on glass slides based on the convective

assembly. With this application, a well-ordered structure of the substrate resulted, which lead to better quality and higher reproducibility of the SERS spectra of *E. coli* and *Staphylococcus cohnii*. Laucks *et al.* [32] showed a distinction between psychro-active bacteria and *E. coli* by different SERS peak intensity ratios and absolute intensities. It was found that they were similar in reproducibility. In 2010, Wigginton *et al.* reported a membrane filter for the concentration of pathogens for SERS detection [33]. Jarvis *et al.* [34] carried out SERS detection in the interior of a microorganism to show that specific addressing of certain regions in a cell can be of advantage. For example, the cell wall components of microorganisms can be selectively enhanced [35]. Ivleva *et al*. were able to carry out qualitatively *in situ* analysis of biofilm constituents with an enhancement factor of up to two orders of magnitude [36]. They reached an amplification factor of four orders of magnitude of the Raman signal on the biofilm component specific distribution analysis [37].

Many SERS experiments on microorganisms have been reported where the authors suggest the drying of the cells prior to measurement. For instance Ravindranath *et al.* introduced the SERS-driven cross-platform based multiplex pathogen detection. On this platform, filtrated and dehydrated bacteria originated from water samples were SERS analyzed using labelling molecules [38]. Zeiri *et al.* reported in 2005 SERS fingerprint spectra of dehydrated silver coated *E. coli* cells [39]. The disadvantage of drying the analytes is a change in shape, composition and chemical reactions results. Hence these experiments cannot be compared to SERS detection of microorganisms still in water. In order to overcome these drawbacks, several research groups have developed different flow systems to preserve their analytes during measurement. Cheng *et al.* constructed a dielectrophoretic chip for the *in situ* SERS detection of bacteria in blood samples. The Raman laser was hereby focused on a concentrated bacteria slug after separation from the blood cells [40]. Yan *et al.* reported SERS spectra *E. coli* cells using nanoparticle cluster arrays [41]. Recently, Yang *et al.* published the detection of bacteria in solution using SERS labels on silver nanoparticles and optical fibers. By using a sensor based on a liquid core photonic crystal fiber a detection limit of 10^6 cells/mL was achieved of *Shewanella oneidensis* MR-1[42].

The implementation of flow cells to SERS analysis became increasingly important in the past decade as the high sensitivity of the method matches the small volumes involved in microfluidic analysis. It is known that a higher reproducibility can be achieved in flow systems than under static conditions due to the higher precision of the analyte dosage and better heat dissipation of flow systems. One of the first experiments making use of flow-injection for SERS analysis was performed by Berthod *et al.* in 1987 [43]. Para-aminobenzoic

acid was detected at different pH levels and with different concentrations by means of flow-injection analysis. Hereafter several groups implemented flow systems to the SERS analysis of organic and biochemical compounds. Wilson *et al.* constructed a flow cell for the SERS detection of geological samples [24]. They applied disperse colloidal SERS media for the determination of pigments in microorganisms. Strehle *et al.* have developed a flow cell for the online SERS measurement of crystal violet [44]. They were able to analyze separate sample volumes down to 60 nL, underlining the potential of this approach in case of limited volume. Park *et al.* described the detection of duplex dye-labelled DNA sequences in an alligator teeth-shaped PDMS micro-fluidic channel using confocal SERS microscopy [45]. A similar channel construction was used by Yea *et al.* for the ultra-sensitive analysis of cyanide water pollutant [46]. Hou *et al.* presented a micro-fluidic system based on a discharge driven vortex to a chip-detection technique [47]. Hereby, a concentration of bacteria suspensions containing *Saccharomyces cerevisiae, Escherichia coli F-amp* and *Bacillus subtilis* for SERS detection was obtained. Furthermore, a pigment in cyanobacteria has been detected in a spectroscopic-microfluidic flow cell using silver nanoparticles as SERS media [24]. Considering all these works, it becomes obvious that micro-fluidics combined with SERS detection can be useful for highly sensitive biological and environmental trace analyses. The combination of SERS and microfluidic with immunoassay techniques offers the possibility to selectively capture specific antigens on well-defined spots in the flow cell. As an example, Guven *et al.* inserted a SERS-based sandwich immunoassay using antibody coated magnetic nanoparticles for *E. coli* enumeration [48]. They reported a LOD of 8 cfu mL^{-1}, by separation of the captured bacteria with a consecutively SERS detection employing specific SERS labels.

There are several other Raman techniques with which only small sample volumes are needed and suitable for biomolecule detection. For instance surface enhanced resonance Raman scattering (SERRS) which requires that the analyte is a chromophore and that the scattering from this chromophore dominates the spectrum. The method takes use of chromophores with electronic transition which possess absorption maximum frequencies close to that of the laser excitation (i.e. in resonance). In 1991, Picorel *et al.* investigated the stability of isolated bacterial and photosystem II reaction center complexes on silver electrode surfaces using SERRS [49]. The advantage of this method is that it features higher cross sections than SERS, and so the method is more sensitive. Tip enhanced Raman scattering (TERS) involves an AFM tip coated with a thin layer of SERS metal (tip diameter ~50 nm). This method enables a nanoscaled topographic resolved analysis of all kinds of analytes. However, the tip is limited in durability as the metal atoms detach with time and is hard to

reproduce. Neugebauer *et al.* examined Staphylococcus epidermis cells by means of TERS for better understanding of the fingerprint spectra of whole cells [50]. Further Raman applications which should be mentioned are coherent anti-Stokes Raman spectroscopy (CARS), surface-enhanced hyper Raman spectroscopy (SERHS), ultra-violet SERS and surface-enhanced infrared spectroscopy [51, 52].

SERS is a new application on the field of bioaerosol detection. It is still a challenge to collect real samples non-destructively for the implementation to a SERS readout device, though one group has reported important proceedings; Sengupta *et al.* characterized in 2005 aerosolized microorganisms by collecting a nebulized bacteria suspension in a cuvette by an impactor [53]. A laser beam was focused in the cuvette and generated photons which were detected as fingerprint spectra of the bacteria. In 2007, the same group published an extended development of their readout system experimenting on *E. coli* cells and pollen [54]. In chapter 4.5 of this thesis, an alternative analytical system for airborne microorganisms is presented, which possesses a comparable low LOD to the existing methods.

2.2 Microorganisms

Analytics of microorganisms has attracted increasing attention worldwide due to the immense threat of bioweapons as well as the rising risk of foodborne and airborne pathogen contaminations. These microorganisms can represent a severe threat to human health if they are in the right environments and, depending on the species, direct contact occurs between humans and contaminated food, aerosols or liquids.

Microorganisms can be divided into two main groups, the gram positive and gram negative bacteria which differ in their cell wall components and can be identified by a staining procedure. Additionally, these main groups are divided in two subassembly groups, the aerobic and the anaerobic bacteria. In general, all bacteria consist of proteins, RNA, DNA, phospholipids, lipopolysaccharides, peptidoglycans, glycogens and a small amount of inorganic ions and small molecules. Gram positive cells possess a cell wall which holds a dry matter consisting of 30 – 70 % murein lattice which is mainly made of peptidoglycanes [55]. The protein content is relatively low compared to the cell wall of gram negative cells, which holds a dry matter consisting of less than 10 % murein lattice. Characteristic is the presence of teichoic acids, chains of 8 - 50 glycerine- and ribitmolecules, in gram positive species. Gram negative cells have porins which cross the cellular membrane for molecule transports but do not possess teichoic acids. In this work, only gram negative species were examined. Their cell wall is composed of a plasma membrane, peptidoglycane and an outer membrane of lipopolysaccharides (LPS). In *Salmonella typhimurium* (*S. typhimurium*) and *Escherichia coli* (*E. coli*), these LPS consist of highly branched sugars linked to a glycosamine containing lipid and often determine the somatic antigen specificities [56]. These polysaccharides can contain as many as six primer sugars. A major component of this core is known as O-phosphorylethanolamine. On these sugar-core structures, side chains are present which bear species-specific epitopes. The main function of these sugar chains is to protect the bacteria from destruction as the antigenic proteins on the cell wall can otherwise rouse immune response. The surface membrane of bacteria cells are negatively charged due to surface phosphate and carboxylate groups composing the core region of LPS molecules [57].

Bacteria can secrete various substances, such as polysaccharides, by metabolic activity. These polysaccharide chains produce a sticky gel surrounding the bacteria which have a protecting function. In addition, they are useful due to their adhesion properties and preventing the cells from dehydration. The production varies with respect to the surrounding

temperature and matrices. Not all species tend to produce these sugar chains, though it is well known for some of the bacteria used in this thesis, such as *E. coli*, and *S. typhimurium*.

Some microorganisms, like fecal coliforms, (e.g. *E. coli*) and hydrogen sulfide producing bacteria, are used as indicator bacteria for water contamination [58, 59]. These are not dangerous to human health if ingested, but if they are detected the probability of finding pathogenic bacteria which may be present in feces (e.g. *Salmonella* and *Legionella*) is large. The reason for the analysis of such indicator bacteria is that there exists no online method for the simultaneous detection of multiple pathogenic bacteria in water. According to EU regulations, the absence of indicator bacteria in 250 mL water sample is the requirement for drinking water quality [2]. This fact highlights the importance of a rapid, reliable and sensitive detection method, as additionally no applicable tool exists for the complete analysis of fecal pollution in water. Most of the commercial analytic tools for bacteria detection are time consuming and many require an enrichment of the bacteria present, such as platen-based counting, immunoassays [60] and gel electrophoresis [61]. Though, pathogens can be in a so-called viable but not culturable (VBNC) state and cannot be cultivated due to thermal damage, longer detention in drinking water or exposure to chlorine [62]. For some bacteria in drinking water e.g. *E. coli*, *Salmonella* and *Legionella*, this state is reversible. For instance, *Legionella* can be revitalized by the growth in amoebas. Enrichment independent techniques are also available, for instance cytometric methods. Nevertheless, no qualitative information can be gained, as this technique is based on the scattering events of fluorescence markers, caused by laser excitation [63]. For the qualitative and quantitative analysis of pathogens without the need of cultivation, methods like fluorescence *in situ* hybridization (FISH) [64] and polymerase chain reaction (PCR) [61] are available. Although microbial risk assessment is an evolving discipline, methods have not been effectively developed to address the severity of the risk at the watershed level [58]. Large improvements in nanotechnology and surface chemistry have allowed developing several new methods for microarray readout [65-68]. Though, a challenge is to develop appropriate readout methods with miniaturized analytical platforms already on the marked, to detect pathogenic germs of low concentration.

2.2.1 Legionella pneumophila

Legionella pneumophila (L. pneumophila) are rod-shaped gram negative bacteria with 20 µm length and a thickness of 0.5 µm [69]. They are to be found in water reservoirs and pipes, but also in the soil. A criterion for the survival of *Legionellas* in free nature is the presence of other bacteria species as they cannot decompose carbohydrates for nutrition and

energy uptake. If *Legionellas* are transferred to aerosol state, they can cause diseases like Legionella-pneumonie or Pontiac-fever through respiration. The infection dosage is 10^4 - 10^5 cfu/L. A common detection method is the use of ELISA on urine samples. This can take up to several days as an enrichment of the cells is required.

2.2.2 Salmonella typhimurium

Salmonella typhimurium (S. typhimurium) are rod-shaped gram negative bacteria of 2 – 5 µm length and have a diameter of 0.7 – 1.5 µm [69]. They belong to the *Salmonella enterobacteriaceae* family which can be found in soil, on plants or in human and animal fecal. Foodstuff and dairy products can be contaminated with *Salmonella* and by consumption of these products, intestine infections can cause Salmonellosis or Typhus abdominalis diseases. The infectious dose varies among *Salmonella* strains. A common detection method is the platen-based cultivation of stool samples.

2.2.3 Escherichia coli

Escherichia coli (*E. coli*) belong to the family of *enterobacteriaceae* and are rod-shaped gram negative bacteria with a length of 2 – 6 µm and diameter of 1.1 – 1.5 µm [69]. It is an acid producing (lactose positive), polycariotic bacterium without cell core and contains DNA, cytoplasma, ribosomes and mesosomes. They are oxidase negative (i.e. no cytochrom c oxydase enzyme) and possess flagellae equally distributed over the cell surface. The flagellaes are rotating due to concentration differences of proteins between the two sides of the cell membrane. Energy is gained by mixed acid fermentation. *E. colis* produce vitamin K and nourish on sugars and amino acids. A cell division occur every 20 min if they are not exposed to high concentration of salt or low pH values. They are normally found in animal and human intestines. Cheese, meat and milk can be contaminated by *E. coli* through the host animal and even harvested foodstuff which has been treated with fertilizer can be contaminated. Although most strains are non-pathogenic to humans, some subspecies are able to produce toxins and can cause perilous diseases. The infection dosage is less than 100 germs. Fastest detection methods of *E. coli* contamination are ELISA and PCR tests.

2.2.4 Potential reservoirs

Bacteria tend to build biofilms on interfaces. These biofilms are aggregates of microorganisms on a surface which tend to produce a matrix of extracellular polymeric substance and grow under laminar and turbulent flow as well as when the water is stagnant [70]. Some of the microorganisms can divide within about 20 min which results in a rapid

growth of the biofilm. Such cluster consists of nutrition elements, extruded media and cells. After a certain time period, the number of cells increases so much that the bacteria cluster burst and single cells are flushed away which might end up in the drinking or in the shower water. Fecal coliform bacteria can reach rivers and lakes through discharge from animals, especially birds, or through usage of fertilizers, but also from human originated sewage or waste-effluent from paper fabrics. Meat can be contaminated during the slaughtering process or when stored. Surface bacteria can end up inside the meat when handled before cooking. These inside bacteria are hard to kill as the temperature does mostly not get high enough and can cause severe illness if consumed.

2.3 Microarray detection of immunoassays

The growing concerns of germs in drinking water have occupied researchers for years, trying to develop a fast, nevertheless selective high-throughput detection principle. A great variety of methods has been applied for water monitoring, most of them time consuming and based on a previous enrichment of the analytes [71]. In the past decade, high-throughput screening methods using immunoassays on microarray technologies have been applied as miniaturized analytical tools in modern biology and biochemistry [67]. An unprecedented capability for the simultaneous analysis of thousands of biochemical interactions is thereby realizable. Biomolecules like DNA/RNA and oligonucleotides, proteins, peptides, carbohydrates, toxins and microorganisms have been characterized in water, tissue and blood samples using microarrays [72-74]. The first functional microarray was made in 1991 by Fodor *et al.* as a light-directed, spatially addressable parallel chemical synthesis [75]. Microarray systems have been developed that make use of fluorescence and chemiluminescence as detection principle, for microorganisms and other biomolecules, by introducing a labelling molecule for specific detection [60, 76]. However, the application of labelling reagents requires larger reactants volume, additional preparation steps and is time consuming.

Microarrays can provide fully automatic high-throughput analysis with parallel detection of numerous analytes, and only require minor probe volumes. The use of laser techniques opens the possibility to quickly scan distinct areas of the microarray for spectroscopic analysis. Raman spectroscopy is a composition specific method (see section 2.4) which can be combined with microarray technology [66]. Through surface plasmon resonance effects, the low cross section of Raman can be increased by bringing the target molecules in the proximity of nano-roughened metal particles. This highly sensitive effect is called surface-enhanced Raman scattering (SERS) and is a convenient technique for bacteria detection as the analysis can be carried out in water, which is a weak Raman scatterer [36]. The main implementation of SERS nowadays is in the detection of proteins [77]. Here, quantitative calibration has been carried out using the relative intensities of SERS signals. Several groups have reported the combination of microarray platform with SERS detection [44, 78, 79]. However, a label-free *in situ* microarray detection based on SERS has not yet been developed.

A microarray system allows higher reproducibility of SERS detection in flow cells, compared to stationary analyte detection, due to the fact that the analytes are stagnant. When

the Raman signal is collected from a flowing stream (mobile analyte detection), the samples pass through a laser beam. At the laser focus, SERS signals from different aggregates are accumulated and averaged [80]. Hence, a quantitative analysis is associated with large standard deviations. Another advantage of immunoassays is that any desirable number of spots of different antibodies of multiple targets can be added and analyzed.

Bacterial cells and viruses can produce an immuno-complex with certain antibodies [81]. Antibodies (immunoglobulines) are designed by nature to defend against viruses, bacteria and parasites and possess a specific affinity to the antigen which triggered its synthesis. They selectively bind small molecules such as biopolymers, pesticides, toxins and pharmaceuticals. An immunoassay takes advantage of the specific binding of an antibody to its antigen [82]. Monoclonal antibodies are in contrast to polyclonal antibodies homogeneous due to the fact that they are produced from a single population of identical cells [83]. Such monoclonal antibodies were first reported by Milstein and Köhler in 1975 and are used as a unique analytical reagent armed with extraordinary specificity and binding affinity [84]. The functional group recognized by the antibody is called epitope or antigen determinate [85]. Electron microscope experiments have proved a Y-shaped geometry of the antibody and immuno-complexes develop at the end-site of the antibody's Fab-fragment [86]. Monoclonal antibodies are convenient as they only bind to one site of a particular molecule, and therefore provide a more selective and accurate test. Possible interactions between antibody and antigen can be caused by four different interacting forces: dispersion, electrostatic and hydrophobic interactions as well as hydrogen bonding between the immune reactants. They play an important role in stabilizing the immune complex. In order to obtain a strong and specific binding, a complementary geometry must exist between the interacting species so that several physical forces develop [87]. Based on these facts, a great influence of the pH value, the ionic strength of the solvent and buffer involved on the binding procedures, is to be expected. These binding processes have to be taken into account when interpreting the results. In fact, stable antigen-antibody bonds are found at a pH range of 6 to 8. Beyond that range, the immune complexes undergo dissociation. Equation 1 describes the kinetic of the association/dissociation reactions [88]. This equilibrium is expected to hold, if the affinity constants are independent of analyte concentration, i.e. if the binding of an antibody at one antigen does not affect the binding at an adjacent antigen.

$$Ag + Ab \underset{k_d}{\overset{k_a}{\rightleftharpoons}} [Ag\text{-}Ab] \qquad \text{(eq. 1)}$$

Ag − Antigen

Ab − Antibody

k_a − Association constant

k_d − Dissociation constant

Immunoassays can be divided into two classes, the homogeneous and the heterogenous system. In comparison to homogeneous systems, the heterogeneous (e.g. enzyme immunoassays) possess a greater sensitivity towards hapten detection. Systems which contain a solid phase surface, mostly of synthetic material or modified glass carriers, on which unlabelled immune reactants (antigens or antibodies) are immobilized, are called enzyme-linked immunosorbent assays [89]. A microarray immunosensor is a multiplex flow-through microarray which utilises a heterogeneous platform on which the recognition takes place. This platform possesses immobilized antigens applied by microprinting or microstructuring processes.

There are several applications of microdosing, which are all generally based on two different methods of spot generation at the glass slide surface. One of the techniques operates with “free flying” droplets. A pumping system allows a single droplet to leave a capillary through piezoelectricity, which acts between the edge of the capillary and the liquid (e.g. Ink-jet spotter with piezo-pump). The second method deposes the droplets directly onto the chip surface. This only takes place if the attracting forces between the droplet liquid and the chip surface are stronger than those between liquid and pin. Microarraying in this work is carried out with a contact spotter (BioOdyssey calligrapher mini-arrayer, *BioOdyssey,* Munich, Germany) illustrated in figure 1.

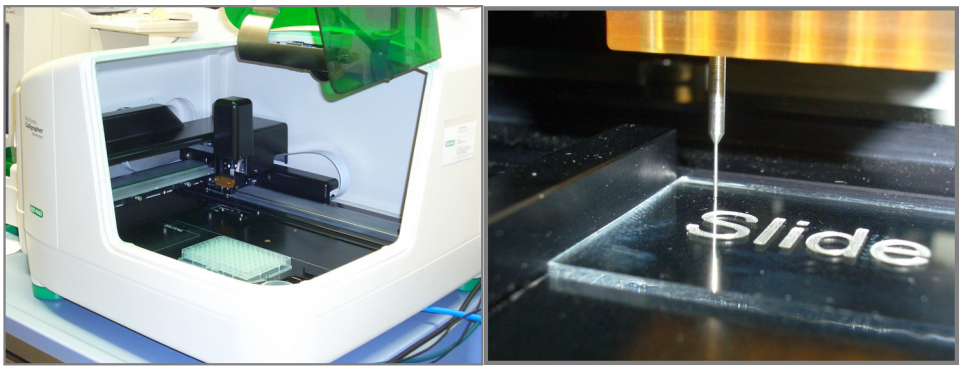

Figure 1: Contact spotter

2.4 Surface-enhanced Raman spectroscopy (SERS)

Raman spectroscopy (RS) is a vibrational spectroscopic method that provides highly specific information about material properties. RS can be applied for label-free analyte detection, revealing molecular fingerprints. However, conventional Raman microscopy (RM) is hampered for the characterization of microorganisms by its limited sensitivity (for recent review see ref. [90]). SERS enables enhancement of low Raman scattering and allows obtaining fingerprint spectra of different analytes even to the single molecule level [91]. The vibrational bands obtained by SERS are much narrower than those revealed by fluorescence spectroscopy and can be collected from bacteria without labelling [35]. Additionally, SERS is sensitive and has a fluorescence quenching effect [36]. There has been a huge progress in characterizing and identifying microorganisms with colloidal SERS media in the past [12, 34, 35, 92].

SERS was discovered in 1974 as Fleischman *et al.* observed a large signal enhancement by measuring pyridine adsorbed on electrochemically roughened silver [93]. They contributed this signal enlargement to an increased surface area. This enhancement effect was later described as electromagnetic enhancement (EME) based on surface plasmon resonance and chemical enhancement (CE) which is based on charge transfer effects between the metal and analyte. Though, the theory of the phenomenon is not yet fully understood. Raman scattering is induced by an induced dipole μ either caused by a change in polarity α or a change in the electromagnetic field E. SERS is caused by an increase in either α (chemically) or E (electromagnetic). Enhancement factors up to 10^{14} can be reached through these effects compared to normal Raman intensities. Such amplification of the scattered photons can be reached at “hot spots”, where the analyte is positioned at a site of high field enhancement.[91, 94-96]. The cross section of SERS can reach 10^{-16} cm^2/molecule. Typical cross sections of normal Raman are 10^{-30} - 10^{-25} cm^2/molecule. Younger literature describes the physical characteristics of the enhanced scattering of photons caused by EME and CE in dependence of the wavelength of the electromagnetic waves [97]. Equation 2 and 3 describe the dependencies of SERS enhancements. The SERS signal I^{SERS} is proportional to the excitation intensity I_L and the effective SERS cross section σ_{eff}^{SERS} .

$$\sigma_{eff}^{SERS} = \sigma_{ads}^{R} A(\nu_L)^2 A(\nu_S)^2 \qquad \text{(eq. 2)}$$

$$I^{SERS}(\nu_S) \propto N \cdot I_L \cdot \left|A(\nu_L)\right|^2 \cdot \left|A(\nu_S)\right|^2 \cdot \sigma_{ads}^{R} \qquad \text{(eq. 3)}$$

A − Field enhancement
I^{SERS} − Intensity of SERS signal
N − Number of particles involved in SERS process
σ − SERS cross-section
ν_L − Frequency of incident light
ν_S − Frequency of scattered light
I_L − Excitation intensity

In figure 2, the concept of SERS enhancement on a bacterium surrounded by several metal particles, which are much smaller in size than the analyte, is illustrated. The metals are partly chemisorbed on the bacteria cell wall which allows charge transfer effects. Enhancement occurs in close proximity of metallic nanostructures (for details see section 2.4.1 and 2.4.2). A large variety of molecules and larger molecular structures can be analyzed with high precision. A particular advantage of SERS for the characterization of biomolecules is the fact that it can be carried out in aqueous medium since water is a weak Raman scatterer. Furthermore, due to the enhancement of the Raman scattering only short laser exposure times and laser energies are needed. One of the drawbacks of SERS is the limited reproducibility of quantitative analysis as signal intensity is dependent on SERS media size and distance to the analyte. In NR, the intensity of the collected signal is proportional to the concentration of the analyte.

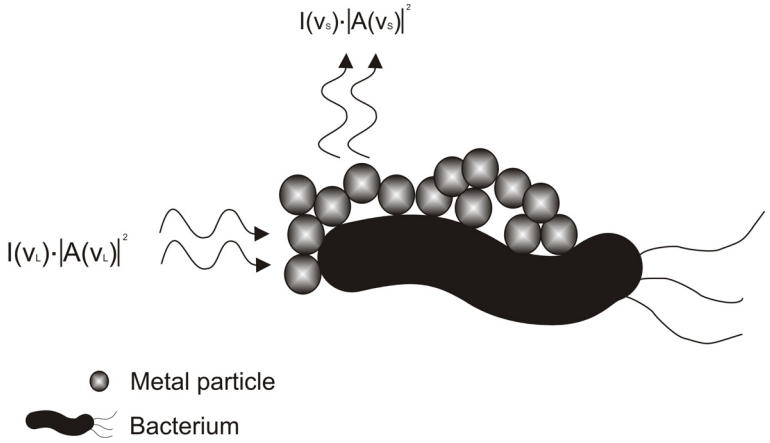

Figure 2: Schematic of a SERS enhancement incident on a bacterium covered by metal nanoparticles. SERS occurs only at sites with close proximity of metal and analyte.

As the SERS media's size and shape are hardly reproducible, the assortment of quantitative information is a challenge. This thesis will discuss an alternative way to overcome this aspect of reproducibility.

A variety of metal structures (Ag, Au and Cu) is used to induce the SERS effect. These metals are utilized in different formats e.g. as metal plates, colloids, rods, coatings etc. [5-9]. When SERS media are added to the analyte which is exposed to a laser beam, a field enhancement occurs. With larger analyte molecules, it must be considered that the enhancement decreases with increasing distance to the SERS metal (see eq. 6). Furthermore, a direct contact of the analyte with the SERS media can cause distortion in the molecular structure and therefore a change in fingerprint spectrum. Thus, SERS spectra are only to certain extend comparable to normal Raman spectra due to changes in polarity and molecule symmetries. In fact, some IR active bands can appear in SERS spectra.

Closely spaced interacting particles create so-called "hot spots" which exhibit extra field amplification. However, such high amplification can only be obtained at very restricted areas (within 1 nm distance between metal and analyte, see figure 3) and is hardly reproducible. A hot spot is most probable if the analyte is sited between several metal particles. In this thesis, the importance of directed particle agglomeration to obtain "hot spots" and how it can be employed to detect cells in water is discussed.

2.4.1 Electromagnetic enhancement

Electromagnetic enhancement (EME) of the scattered photons is based on the surface plasmon resonance effect occurring when light hits a metal particle. Hence, strong optical fields which are generated on the metal surface can become resonant to the incident laser light or the scattered electrical field (i.e. an excitation of the plasmon resonance). EME occur if the metallic sphere is small compared to the incident optical wavelength. This effect contributes to the largest part of the overall signal amplification. It has been proven that electromagnetic incidents create an enhancement of factor 10^4 or more (up to 10^7) [98]. The EME $A(\nu)$ of a perfectly spherical metal particle is mathematically described in equation 4 and highlights the dependence of size of the particle r, its distance to the analyte d and the dielectric constant ε of the surrounding media. However, one has to bear in mind that an enhancement is only possible for metals with rough surfaces. This is due to the mobility of the plasmons in the metal hence, the electromagnetic field can be scattered in multiple directions, both parallel and perpendicular to the surface. Surface plasmons are oscillations of the electrons in the conduction band at the surface of the metal particle excited by an energy source.

$$A(\nu) \propto \left(\frac{r}{r+d}\right)^3 \cdot \frac{\varepsilon_{metal} - \varepsilon_{surrounding}}{\varepsilon_{metal} + 2\varepsilon_{surrounding}} \qquad \text{(eq. 4)}$$

r - Radius of metal particle

d - Distance between analyte and metal particle

ε - Dielectric constant

Brown *et al.* calculated by means of modelling using finite element methods (FEM) the electric field enhancement between two silver nanoparticles (figure 3), derived from the first approximation of Raman enhancement $G_{(r,w)}$ from previously reported SERS papers (see equation 5) [99].

$$G_{(r,w)} = I\left|\frac{E_{(r,w)}}{E_{inc(r,w)}}\right|^4 \qquad \text{(eq. 5)}$$

where $E_{(r,w)}$ is the predicted total electric field at position r, and $E_{inc(r,w)}$ is the electric field associated with the incoming electromagnetic radiation. The requirement was that the incident light had to be perpendicular to the line joining the centres of the particles.

In order to calculate the enhancement exactly for each experiment, the size of the metal particle and its surface plasmon resonance has to be known. Furthermore, the number of particles per analyte molecule is needed. Additionally, the distance between the metal and the analyte, the orientation of the molecule in respect to the normal of the surface, the incident radiation energy and electric properties of the metal are depending factors. In the case of water/metal interfaces, at which the surface plasmon resonance occurs, the two dielectric constants have opposite signs and the electromagnetic enhancement factor $G_{em}(\nu_S)$ can be expressed with proportionality of d^{12} (see equation 6) [91].

$$G_{em}(\nu_S) = \left|A(\nu_L)\right|^2 \left|A(\nu_S)\right|^2 \propto \left|\frac{\varepsilon(\nu_L) - \varepsilon_0}{\varepsilon(\nu_L) + 2\varepsilon_0}\right| \left|\frac{\varepsilon(\nu_S) - \varepsilon_0}{\varepsilon(\nu_S) + 2\varepsilon_0}\right| \left(\frac{r}{r+d}\right)^{12} \qquad \text{(eq. 6)}$$

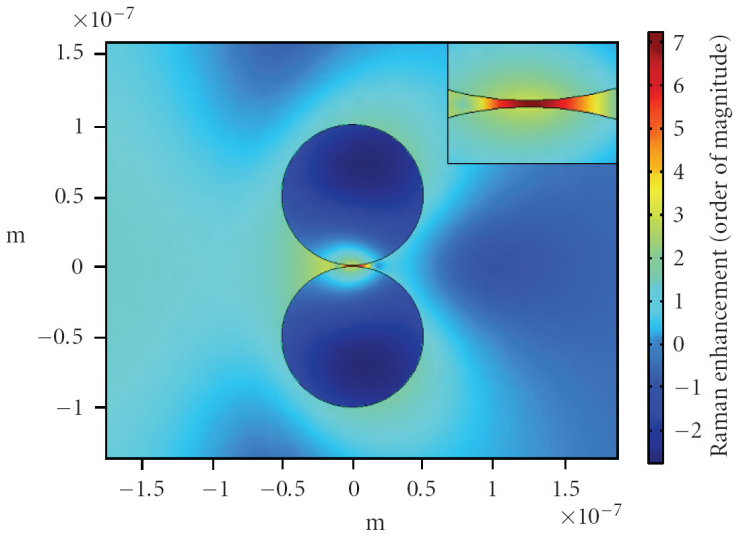

Figure 3: A model of the electromagnetic enhancement between two silver nanoparticles with radius 50 nm which are separated by 1 nm. Laser wavelength is 514 nm. The red colour indicates the maximum Raman enhancement and the blue colour the minimum enhancement [99].

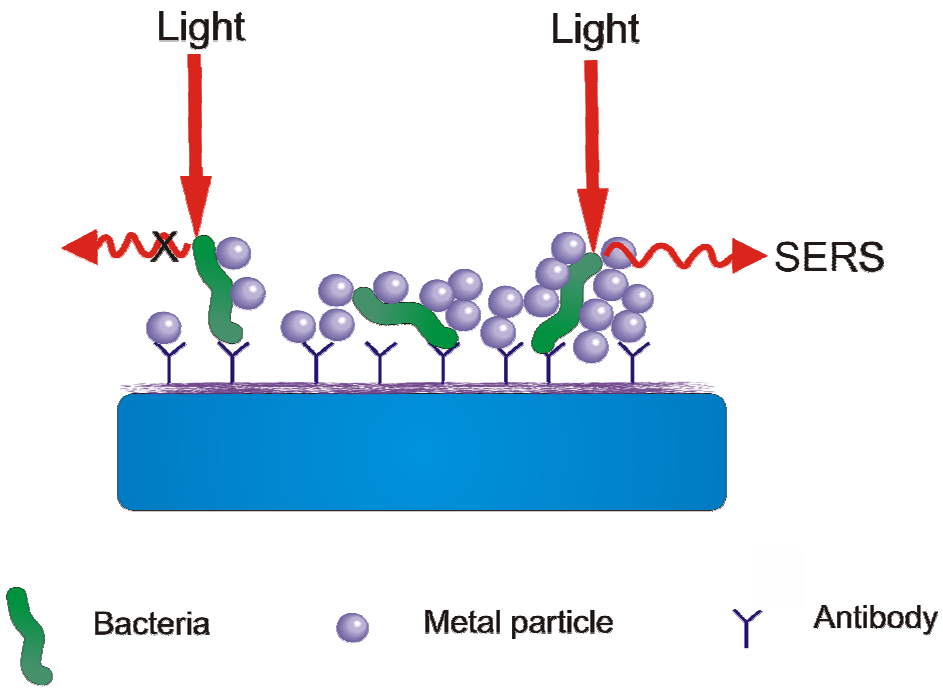

Figure 4: Illustration of an artificial microarray spot at which a SERS experiment on bacteria is reflected. On the left hand side of the microarray spot, a laser beam is focused on a bacterium surrounded by few nanoparticles. Here, no SERS enhancement occurs. On the right, a second bacterium is presented on which the laser light is focused. It is surrounded by enough metal particles in close range to the laser focus and obeys the requirements for SERS enhancement.

In figure 4, the scheme of an artificial SERS experiment on bacteria is illustrated. Here, it is visible that SERS occurs if the above requirements are obeyed. Moreover, the probability that field enhancement is produced is higher in proximity to noble metal particles. A common way of calculating the enhancement factor is to determine the analyte's SNR in a normal Raman experiment then derive the enhancement factor of the analyte's SERS spectrum by comparison.

2.4.2 Chemical enhancement

If the analyte molecule and the SERS metal form an adsorbate/metal complex, charge transfer effects, also called chemical enhancement effects, occur. The metal electrons move freely within the particle's conduction band and can overlay the HOMO of the chemisorbed molecule. A free transfer of electrons is possible if the metal's Fermi level and the analyte's HOMO/LUMO are close in energy. It is suggested that transitions from the Fermi level to the excited state or from the ground state to the Fermi level are involved and it is presumed that the contribution of chemical enhancement to the total SERS enhancement is small [100]. A theory which has been discussed by SERS researchers over the years is the contribution of ballistic electrons and present defects in the metallic structure [101]. The generated holes in the metallic structure couple to the molecular orbitals of the analyte, resulting in an inelastic tunnelling of the ballistic electrons to the LUMO of the chemisorbed molecule. A strong emission of Raman shifted photons occurs with the return of these electrons [97]. A third theorem is discussed by Lombardi *et al.,* where they explain the contribution of Herzberg-Teller coupling mechanism [100].

2.4.3 SERS media

Since the first observation of the SERS effect, a variety of metals (Ag, Au, Cu and other noble metals) have been applied for its generation. These metals can be adopted in various shapes to produce the wanted electric field enhancement [5-9, 102]. Ag, Au and Cu are convenient as they fulfill the plasmon resonance condition in the Near Infrared and visible range. The optimal diameter of such nanoparticle substrates and media was found to be between 20 nm and 100 nm [12]. Highly SERS active inter-particle spaces can be produced by controlled agglomeration of the colloids [94]. Adding salt (e.g. NaCl, KCl or KNO_3) to the colloid sol causes the metal particles to coagulate in the dependence of the salt concentration. This effect is called the chloride effect described by Li *et al*. [103]. Chloride is a better choice for colloid aggregation if the molecule of interest is unable to aggregate the colloid by itself, since in case of silver for instance, it only gives rise to a single ν(Ag-Cl) peak at

240 cm^{-1} [104]. In order to obtain reproducible enhancement factors and spectral features by SERS measurements, reproducible production of SERS substrates and media featuring uniformly shapes and sizes of nanostructures is crucial. This is an essential prerequisite to achieve stable surface plasmon resonance frequencies, which again result in reproducible SERS band positions and band intensities. Another important contribution to reproducible SERS measurements is the controlled aggregation of the metal nanoparticles. To produce high Raman enhancements, the nanoparticles must be in close range to the analyte. If the colloid sol is polydisperse, this can limit the reproducibility of enhancement strengths. For the synthesis of colloid sol as media for sensitive and reproducible SERS measurements, different parameters have to be taken into consideration e.g. reaction temperature, stirring time and power, reactants volume, as well as the way and order of reactant's addition in order to overcome these limiting factors [105].

In this thesis, silver and gold nanoparticles have been investigated regarding their enhancement properties by detecting bacteria in aqueous solution. These transition metals possess a high mobility of their electrons. Silver is known as the metal with the highest electrical and thermal conductivity of all elements and reflect light efficiently. Silver stays solid up to 961 °C and gold up to 1064 °C which is convenient by laser exposure. Due to the high melting points and durabilities one can suppose that the bondings are strong and not directional. Crystalline silver consists of cubic closed packed atoms and its density equals 10.49 g/cm^3. The reflection spectrum shows a plasma edge at 320 nm, this is where the plasma resonance of pure silver occurs not depending on the morphology. Gold crystallizes in a lattice faced centred cube and possess a density of 19.30 g/cm^3. Its plasma edge is to be found at different wavelengths depending on its morphology.

Characterization of the silver colloids

According to Petit *et al.* [106], the size distribution of colloidal nanoparticles can be derived from extinction spectra obtained by an UV-Vis spectrometer. A narrow absorption peak with steep flanks indicates monodisperse particles. In such case, the diameter D of the silver nanoparticle can be calculated using equation 7. A redshift of the absorbance maximum can be caused by two phenomena: a wide distribution of particle sizes and/or larger particles, or by agglomeration of the primary particles. Shoulders in the absorption spectra appear when the particles are polydisperse. The particle sizes correlate to the absorption signal intensity, i.e. stronger absorption indicates smaller particles.

$$FWHM = 50 + \frac{230}{D} \qquad \text{(eq. 7)}$$

To measure the diameter of the particles more exactly, TEM images can be developed and a mean value calculated of the particles diameter. As equation 7 only holds for silver particles, size distribution analysis by means of transmission electron microscopy is convenient for gold nanoparticles.

2.5 SERS characterization of microorganisms

Compared to common fluorescence- or chemiluminescence-based readout techniques, the signals obtained by SERS contain a wealth of information which gives additional selectivity beyond the selectivity of antibodies. An overview of the cell wall components expected to be detected on bacteria cell walls, including their SERS vibrational modes is presented in figure 5 – 7 and table 1. The cell wall LPS consists of highly branched, complex polysaccharides linked to a glycosamine-containing lipid [56]. This polysaccharide chain moiety can contain as many as six neutral sugars, for example L-glycero-D-mannose, glucose, galactose, mannose, rhamnose and abequose which are illustrated in figure 5 and 6. The lipid layer in the outer cell wall contains endotoxines connected to the outer core region. The outer membrane also contains porines which are composed of chains of amino acids. Characteristic peaks in normal Raman of amino acids are 1355 - 1360 cm^{-1}, 1287 - 1292 cm^{-1}, 1240 – 1242 cm^{-1}, 1175 cm^{-1} and 1540 cm^{-1} [107]. One other major component of the cell membrane is the phosphatidyl-choline, also called yellow fat (see figure 7). Here, aldehydes, phosphate and amine functional groups are present.

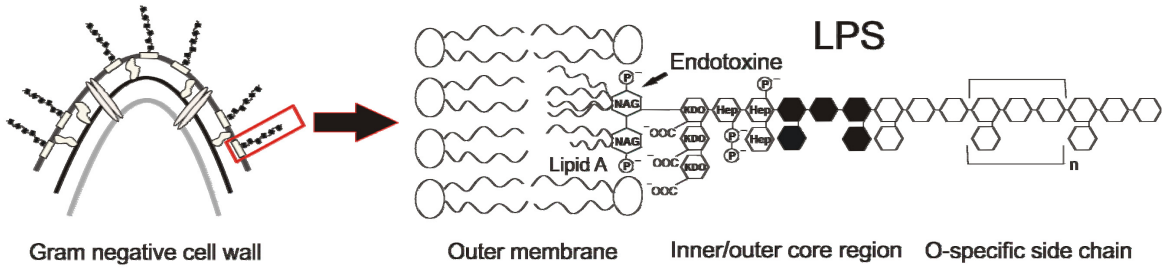

Figure 5: Composition of the LPS in the gram negative bacterium outer cell wall.

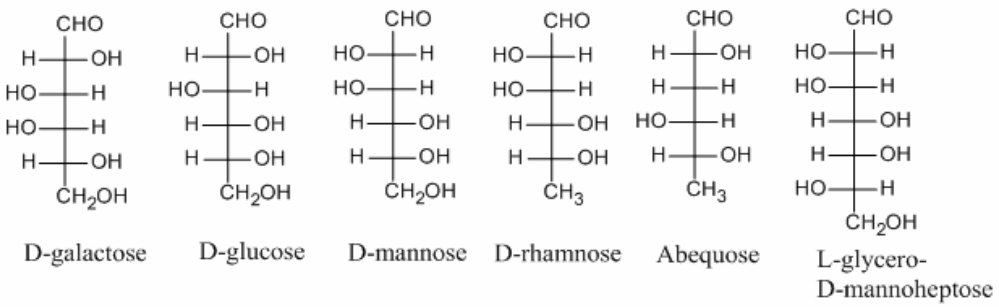

Figure 6: Sugars which build a chain structure in LPS.

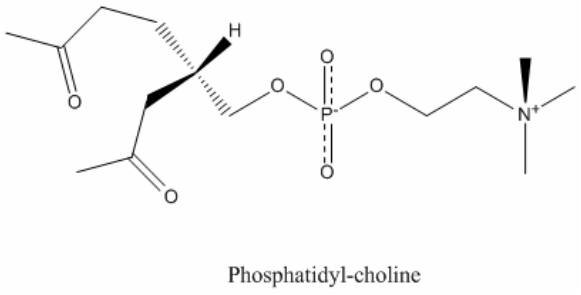

Figure 7: Phosphatidyl-choline found in the bacterium cell membrane.

Table 1: SERS vibrational modes of bacteria cell wall components.

Component	Vibrational mode	Wavenumber [cm^{-1}]	Reference
Polysaccharides	v OH	3200	
	In plane δ OH	1420 -1330	
	δ COH	~1270	[108]
	δ HCO	~1270	[108]
	δ HCC	~1270	[108]
	Ass ring breath C-C	1145 – 1160	[108, 109]
	Ass ring breath C-O	1145 – 1160	[108, 109]
	Glycosidic ring	735, 560	[108]
Tertiary amines	NH	1630	[110]
Sugars	POC	1030	[110]
	δ Ring I	747	[54]
	δ COO^- (w and b)	578	[54]
Amino acids	δ C-H (b) (proteins)	1367	[54]
	v COO^- (s) sym.	1367	[54]
	Aromatic AA in proteins	1173	[54]
	v CN (s) (tyrosin, porine, valin)	806 – 894	[54]
Lipids	N-H	1527, 1583	[54]
	δ C-H (b)	1527, 1583	[54]
	v C=C (s)	1527, 1583	[54]
	δ CH_2	1440 – 1460	[109]

Proteins	Amide I	1640 – 1680	[109]
	Amide II	1540 – 1645	[111]
	Amide III	1250 – 1310	[32, 34, 108, 109, 112]
	δ NH_2 (t)	1145	[108]
	ν CC aromatic ring	1000	[34, 108]
	ρ CH_2	720 – 730	[34]
	Aromatic ring skeletal	625	[34]
Other	Carbohydrates	560	

ν-valence / δ-deformation / w-wagging / b-bending./ t-twisting / s-stretch / ρ-rocking

2.6 Microfluidics

In this work a flow cell was constructed and combined with a microarray for SERS detection of bacteria. The implementation of flow cells to SERS analysis became increasingly important in the past decade as the sensitivity of the method is convenient for small volumes. It is known that more reproducible results can be achieved with flow conditions than with static conditions because of the higher precision of analyte addition. The use of flow-through cells in microarray analysis carries many advantages compared to conventional stationary systems. For instance, it is possible to reduce the assay time and the quantity of unspecific bound analytes, as well as to improve the sensitivity [67]. Furthermore, an automation of the application is possible [76, 113]. Additionally, the volume of reactants can be reduced as the flow rates are easily optimized. Hence, less waste is generated. In comparison to stationary systems, a flow-through system is a closed compartment in which pathogenic bacteria can be detected without the risk of contamination of the sample and operator.

For immobilization of analytes, a laminar flow is important to decrease the critical layer at the flow cell walls, where the flow rate equals zero but also to prevent high pressures in the flow cell [114]. In continuous-flow microfluidics, external pressure sources, external mechanical pumps or integrated mechanical micropumps are most convenient for producing a constant flow rate. To calculate the flow conditions in the flow cell, the equation of Reynold can be used (see equation 8). The Reynold's number is dimensionless and dependent on the flow rate ν, travelled length of the fluid l, the density of the fluid ρ and its dynamic viscosity μ. If Re > 2000, a turbulent flow is defined and for Re < 2000 a laminar flow [115]. A disadvantage of using laminar flow conditions is that the mixing of the fluid is less effective than in a turbulent flow. The choice of flow cell and capillary material is important in microfluidics as it can influence the properties of the reactants and, in the case of SERS analysis, the physical properties of solution. Fluidic resistance increases drastically (factor 4) as the channel dimensions are reduced. High pressure drops are necessary to move liquid through smaller conduits. This has to be taken into consideration during flow cell construction for microfluidic purposes.

$$\mathrm{Re} = \frac{\nu \cdot l \cdot \rho}{\mu} \qquad \text{(eq. 8)}$$

2.7 Bioaerosol analysis

Bioaerosols are defined as particles in air of biological origin, like microorganisms, herbal particles and biogenic matter from metabolism of animals and plants. They exist in a size range of 10^{-2} µm to 100 µm [116]. Bacteria are typically in the range of 0.25 – 25 µm. Bioaerosols can be associated with particulate matter or surrounded by a thin layer of water, which increases their aerodynamic diameter. In the research of indoor environment and bioaerosol contamination, the focus has long been held on infectious diseases precursors and allergens due to legal requirements of public air quality [117]. An overview to the risks of bioaerosol exposure to human health has been published by Brooks *et al.* [118]. According to Hasegawa *et al.,* bioaerosols are cultivable, hence express a severe threat to human health if they are pathogenic and present in indoor air [119].

Common samplers used are Andersen sampler, surface air sampler (SAS), sterilizable microbiological atrium (SMA), Reuter centrifugal sampler (RCS), Coriolis® wet sampler and other impactors and impingers which all capture bioaerosols efficiently [120]. The choice of sampler is important as a gentle collection in fluids can prevent the bacteria from bursting. Other sampling methods used are aerosol filters, sedimentation, electrostatic precipitation and thermal precipitation [121, 122]. The most common detection principle applied in combination with the above listed samplers is agar plate cultivation. Though, a characterization of the bioaerosol samples by cultivation requires a complex after-treatment including eventual filter suspension followed by a dilution, streak of the sample, nutrition preparation, multiple controls of the colony number, final analysis and calculation of the cfu/m^3. This can take up to 95 days [122]. Culture-based techniques can also underestimate the microbial population as less than 10 % may be culturable [117]. Other detection methods are PCR, ELISA, microscopy and gel electrophoresis. There are several physical forces which influences the properties of a bioaerosol. A gravitational force limits the detention time in air and electrostatic forces can attract single particles to another or to a solid surface. Additionally, the Brownian motion can force the particles to collide and produce clusters of bacteria which sediment. An aggregation with abiotic particles is possible. The survival of microorganisms in air is dependent on relative humidity, temperature, gas composition (O_2, O_3, N_2, NO_2, SO_2) and UV-radiation.

The qualitative and quantitative analysis of air-transported bacteria is a challenge and requires a fast detection principle without the need of cultivation to prevent severe outbreak diseases. For particle counting in aerosols an aerodynamic particle sizer (APS) or a

condensation nucleus counter (CNC) can be implemented as reference analysis. They are able to count particles of 0.8 µm – 30 µm and 3 nm – 4 µm aerodynamic diameters respectively.

3 Materials and Methods

3.1 Chemicals and solvents

The following chemicals and solvents were used without further purification if not otherwise stated.

Table 2: Chemicals and solvents.

Product	Company	
Acetone	Carl Roth GmbH	Karlsruhe, Germany
$AgNO_3$	Sigma-Aldrich	Taufkirchen, Germany
Anti-*E. coli* polyclonal O157:H7 1 mg/mL Goat	KPL Inc.	Gaithersburg, MD-USA
Anti-*Legionella* polyclonal, Cat # B65051G, 2.62 mg/mL Rabbit	BioDesign International	Saco, USA
Anti-*Salmonella* polyclonal, Cat # G5V61-500, 2 – 2.5 mg/mL Goat	BioDesign International	Saco, USA
Ascorbic acid	Sigma-Aldrich	Taufkirchen, Germany
Biotin-NHS	Sigma-Aldrich	Taufkirchen, Germany
Casein	Sigma-Aldrich	Taufkirchen, Germany
CTAB	Sigma-Aldrich	Taufkirchen, Germany
Cyclohexane	Carl Roth GmbH	Karlsruhe, Germany
DMAP	Sigma-Aldrich	Taufkirchen, Germany
DMF	Sigma-Aldrich	Taufkirchen, Germany
DMSO	Sigma-Aldrich	Taufkirchen, Germany
DSC	Sigma-Aldrich	Taufkirchen, Germany
E. coli DSM 1116 shock frozen	DSM nutritional products GmbH	Grenzach, Germany
EtOH	Sigma-Aldrich	Taufkirchen, Germany
GOPTS	Sigma-Aldrich	Taufkirchen, Germany
$HAuCl_4$	Sigma-Aldrich	Taufkirchen, Germany
Hellmanex II	Hellma GmbH	Mühlheim, Germany
HCl 37 % fuming	VWR International	Darmstadt, Germany

HNO_3	Merck KGaA	Darmstadt, Germany
H_2O_2 (Westar Supernova Kit)	Cyanagen	Bologna, Italy
HRP-streptavidin	Vector Laboratories	Burlingame, CA-USA
H_2SO_4	VWR International	Darmstadt, Germany
Isopropanol	Carl Roth GmbH	Karlsruhe, Germany
KH_2PO_4	Sigma-Aldrich	Taufkirchen, Germany
K_2HPO_4	Sigma-Aldrich	Taufkirchen, Germany
Legionella pneumophila autoclaved	Max-Pettenkofer-Institut	Munich, Germany
LB-Medium Lennox	Carl Roth GmbH	Karlsruhe, Germany
LB Medium NZCYM	Carl Roth GmbH	Karlsruhe, Germany
Luminol (Westar Supernova Kit)	Cyanagen	Bologna, Italy
MeOH	Sigma-Aldrich	Taufkirchen, Germany
$NaBH_4$	Sigma-Aldrich	Taufkirchen, Germany
Na-citrate	Sigma-Aldrich	Taufkirchen, Germany
NaCl	Sigma-Aldrich	Taufkirchen, Germany
Na_2CO_3	Sigma-Aldrich	Taufkirchen, Germany
$Na_2(CO_3)_2$	Sigma-Aldrich	Taufkirchen, Germany
NaN_3	Sigma-Aldrich	Taufkirchen, Germany
NaOH	Sigma-Aldrich	Taufkirchen, Germany
$NH_3O{\cdot}HCl$	Sigma-Aldrich	Taufkirchen, Germany
PEG-diamine 2000 Da	Huntsman	Rotterdam,The Netherlands
Pluronic F127	Sigma-Aldrich	Taufkirchen, Germany
Salmonella typhimurium ATCC 14028 heat inactivated	Istituto Zooprofilattico Sperimentale Dell`Abruzzo e del Molise “G. Caporale”	Teramo, Italy
Star-PEG	SusTech	Darmstadt, Germany

Carbonate buffer (pH 9.6)

0.20 g (31 mmol) NaN_3, 1.59 g (15 mmol) Na_2CO_3 and 2.93 g (35 mmol) $NaHCO_3$ was dissolved in 1 L MilliQ water.

PBS-buffer (pH 7.6)

1.36 g (10 mmol) KH_2PO_4, 12.20 g (70 mmol) K_2HPO_4 and 8.50 g NaCl (145 mmol) was dissolved in 1 L MilliQ water.

3.2 Miscellaneous devices

Tabelle 3: Miscellaneous devices

Product		Company	
APS	APS 3310	TSI GmbH	Aachen, Germany
Cabinet desiccator	UM 400, Max. 120°C	Memmert GmbH	Büchenbach, Germany
Cuvette (Cytometer)	Plasticbrand© PMMA	Brand GmbH	Wertheim, Germany
Cuvette (UV-VIS)	Rotilabo®, PMMA, 10 mm, 280 - 800 nm	Carl Roth GmbH	Karlsruhe, Germany
Immunomat	-	Atto-tec GmbH	Siegen, Germany
Flow cytometer	Cell Lab Quanta SC	Beckman Coulter GmbH	Aachen, Germany
Membrane pump	N 035:1.2 AN18	KNF Neuberger	Freiburg, Germany
Microtiter plate	BD – Falcon™ 384 well, PP, low binding, flat bottom	VWR International	Darmstadt, Germany
Microtiter-plate shaker	Titramax 100	Heidolph	Schwalbach, Germany
Microscope slides 76x26 mm	Calcium carbonate/Sodium glass	Carl Roth GmbH	Karlsruhe, Germany
Nebulizer	Glass	Carl Roth GmbH	Karlsruhe, Germany
Neutralizer	Kr 85, Nr. 2/93	TSI GmbH	Aachen, Germany
Raman Microscope	Leica DMLM microscope, Renishaw 2000 spectrometer	Renishaw GmbH	Gloucestershire, UK
Rotameter	Rota L 16/630-8609	Rota GmbH	Wehr, Germany
Scale	AT 261 P-1200	Mettler-Toledo GmbH	Giessen, Germany
Spotter	BioOdyssey Calligrapher Mini Arrayer	BioOdyssey	Munich, Germany
Stealth solid pin	SNS 9 ArrayIt	BioRad Laboratories GmbH	Munich, Germany

Syringes	10 mL steril PP/PE	Carl Roth GmbH	Karlsruhe, Germany
TEM	JEM 2010 (LaB6 cathode)	JEOL GmbH	Munich, Germany
Ultrapure water purification system	Milli-Q plus 185	Millipore	Schwalbach, Germany
Ultrasonic bath	RK 102/6379IA	Bandelin electronic KG	Berlin, Germany
UV-Vis spectrometer	Beckmann UV-DU 650	Beckman Clouter Inc.	Fullerton, CA-USA
Vortexer	TopMix FB 15024	Fisher Scientific	Schwerte, Germany
Wet sampler	Coriolis® FR	Bertin technologies	Aix-en-Provence, France

3.3 Microarray coating

3.3.1 Diamino-PEG-coating

A coating procedure from Wolter *et al*. [65] was applied on glass slides. Glass slides are chemically and physically stable and exhibit negligible background signals for Raman measurements. This surface material is homogeneous, efficient and passive [123]. A modification of a glass-slide surface and a monolayer-coating is possible [124, 125]. Figure 8 illustrates the activation through three steps. Step one implies the substitution reaction of alcohol end groups by silane. This silanization is carried out on a glass slide activated with hydrochloric and sulphuric acid by the organosilane GOPTS (3 -glycidyloxypropyltrimethoxysilane). Second step implies the nucleophilic ring opening reaction of oxacyclo propane (figure 9). Hereby, an anionic substance attacks an oxacyclo propane and cause the ring to open. The reaction is regio-selective and occurs in the presence of assymmetric cyclic ether at the site of the less substituted carbon atom (e.g. primary carbon atom). The configuration at a steric center maintains as it does not take part in the reaction [126]. The third step includes the introduction of activated carbo-ester at the free amino-groups by nucleophilic substitution. The reaction is catalysed by the nucleophilic 4-dimethyl-aminopyridine (DMAP). By an addition of triethylamine, DMAP is deprotonized producing a free electron pair which attacks the primary carbon of di-N-succinimidyl carbonate (DSC). An intermediate which is stabilized by charge delocalization results (see figure 10). The N-hydroxysuccinimid (NHS) activated carboxylate ester is subsequently attached to the amino-group at the highly electrophilic carbon atom of a carbodiimid. It is important to carry out these two final steps as a silanized suface often possesses hydrophobic properties [127, 128]. In this work, PEGs were implied as modification reagents. After an immobilization of haptens on the diamino-PEG modified surface, remaining active amine functional groups were deactivated by casein to prevent unspecific binding.

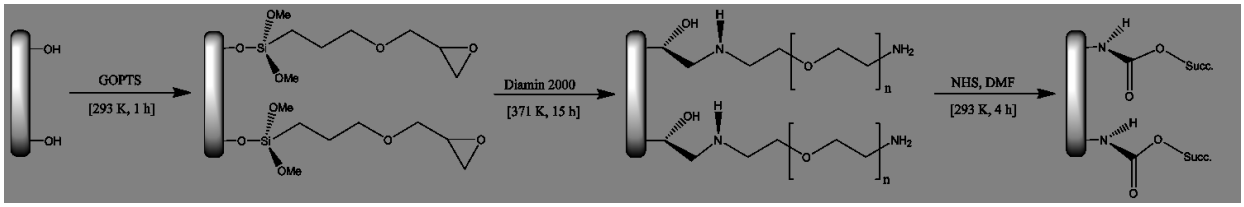

Figure 8: Diepoxy-PEG modification steps 1-3 of a glass-slide.

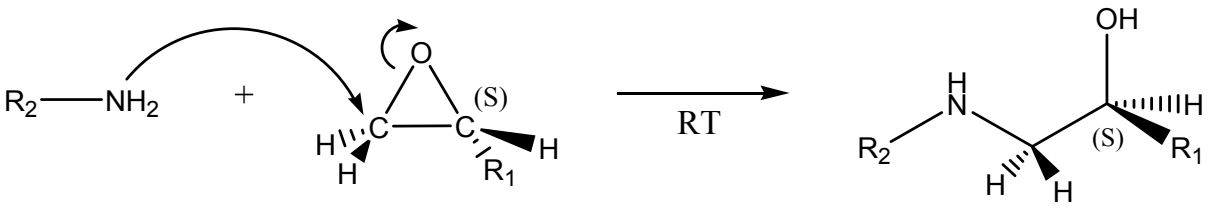

Figure 9: Step 2: Nucleophilic ring opening of an oxacyclo propane.

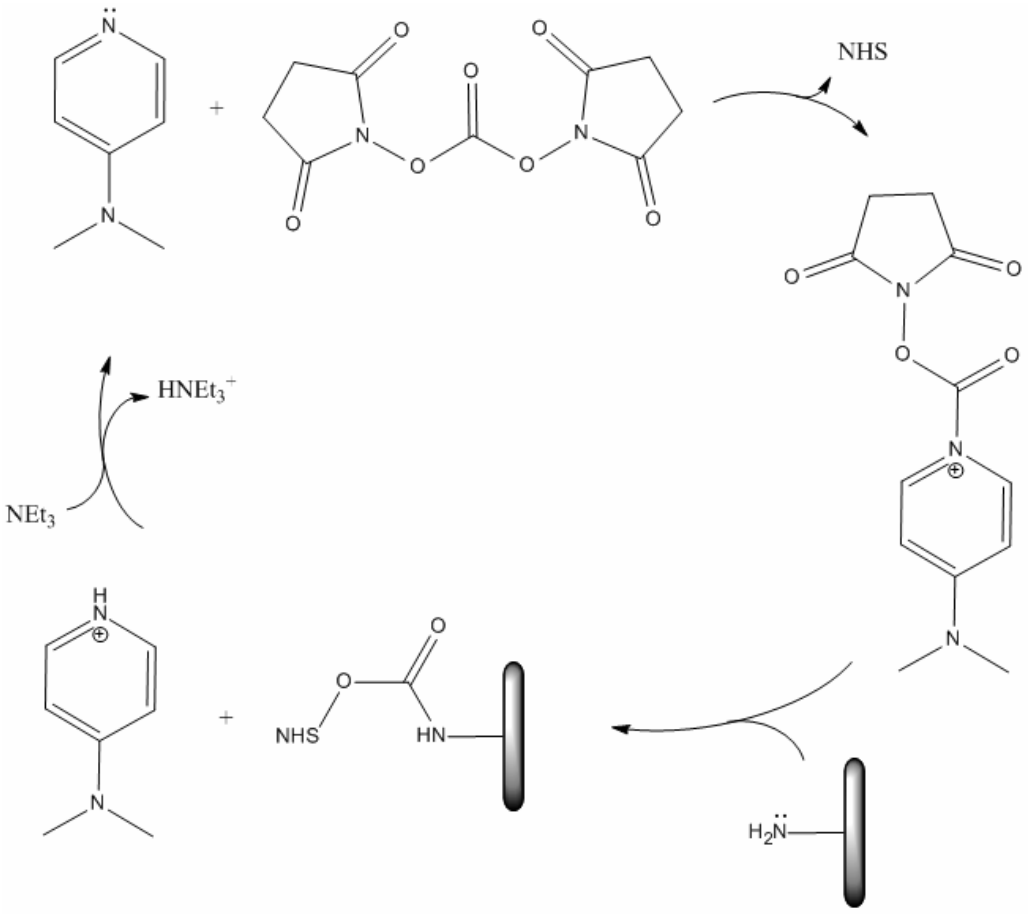

Figure 10: Step 3: NHS-activation of free amino-groups catalysed by DMAP.

Preparation of diamino-PEG-coating

Conventional glass slides were first carved on one edge with a diamond carver (*Proxxon NG 2/S*) in order to recognize on which side a coating had been carried out. Then the glass slides were put in a chip reservoir containing 2 % Hellmanex solution and left 1 h in ultrasonic bath to rinse. Subsequently, the chips were put on a shaker over night (15 h) at room temperature followed by an additional hour in ultrasonic bath. The treated slides were thoroughly washed five times in 200 mL MilliQ water and dried under nitrogen flow.

Cleaning

The prepared glass slides were dipped in 200 mL of methanol/hydrochloric acid solution (1:1) and left shaking for 1 h at room temperature. A washing step in water followed where the chips were rinsed five times in 200 mL demineralized water. Subsequently, they were dipped in concentrated sulfuric acid and left shaking for 1 h at room temperature. An additional washing step in water followed and the slides were again dried under nitrogen flow. Hereafter, the carved side of the chips were lied facing down in a petri-dish.

Silanization

At room temperature, 600 µL GOPTS were added to each slide and covered with a second slide with the carved side facing upwards forming a sandwich. After one hour the chips were separated carefully by hand and covered in 200 mL ethanol in which the slides were left for 1 h to rinse in an ultrasonic bath. The ethanol was exchanged with 200 mL methanol and the set of slides were left a following hour in ultrasonic bath. Finally, the rinsing step in ethanol was repeated followed by a drying under nitrogen flow.

Diamino-PEG-ylation

10 g diamino-PEG were molten in a beaker at 98 °C. 600 µL was pipetted over the silanized side of the glass chips which again were covered with other silanized glass chips as sandwiches. The PEG-ylation was carried out 15 h at 98 °C in closed petri-dishes. Still hot slides were dipped in 200 mL MilliQ water and left in an ultrasonic bath for 15 min and additionally rinsed with fresh MilliQ water. A final drying step in nitrogen flow was carried out. The chips were stored at room temperature in a desiccator under inert atmosphere.

3.3.2 Star-PEG-coating

A specific binding of biomolecules on synthetic surfaces is crucial for chip applications. Both the elimination of nonspecific protein adsorption and the specific binding of proteins in their initial and functional structures are normal problems faced [129]. The star-shaped PEG multilayer surface has the advantage of being able to reach higher polymer

segment density on the glass surface than the monolayered and linear diamino-PEG chains. In that way, a more even distribution of binding sites can be created. These star-PEG coatings eliminate eventual nonspecific interactions between analyte and the surface sterically and simultaneously allow specific binding of haptens. Further advantages of this surface material are a fast and straight forward application, ultra-thin coating (30 nm), high functionality and versatility, one step coating procedure for functional coatings, total elimination of nonspecific protein adsorption and haptens are allowed to bind in their initial conformation [130]. Star-PEG end-groups can be diversely functionalized, hence hapten binding sites possessing various functionalities can be synthesized. A general scheme of the star-PEG structure is shown in figure 11. The stars are characterized by a number of polymer chains which emerge in different directions out of a central core.

The CH-chains ("arms") with terminal NOCs enable the haptens to bind more strongly and precisely. One method to achieve high grafting density is to use block copolymers of ethylene glycol with other polymers that serve as surface anchoring block (e.g. diamino-PEG). This approach has the advantage of allowing even small attractive forces between the anchoring segments of the block polymer and the surface to create a higher degree of polymerization, which results in a strong attachment. In addition, such coatings can be prepared through simple spin- or dip-coating from aqueous solution. When a diamino-PEG-activated biochip is to be coated, conventional sandwich coating procedure in non-aqueous solution is applied. Hence, complicated chemical preparation is not necessary. The end groups can be used for further functionalization. Backbone consists of 80 % polyethylene oxide (PEO) and 20 % polypropylene oxide (PPO). PPO is statistically implemented to the star arms in order to separate sequences of ethene oxide units from each other. This causes the protein repellent characteristic of the polymer coating and breaks the crystallinity of PPO which again causes a higher chemical stability of the polymer chain. Isocyanate end groups are reactive towards -OH and $-NH_2$ functional groups. The molecular weight lies between 3000 g/mol and 18000 g/mol. To ensure long term durability of the prepared chips, it is preferable that the polymer chains attach covalently to the substrate [131]. The reactive endgroup of the applied star-PEG is schematically drawn in figure 12.

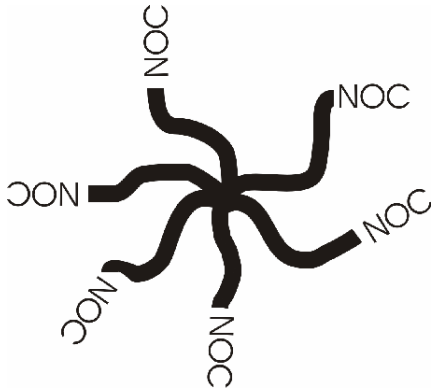

Figure 11: Scheme of a six-armed star-PEG [130].

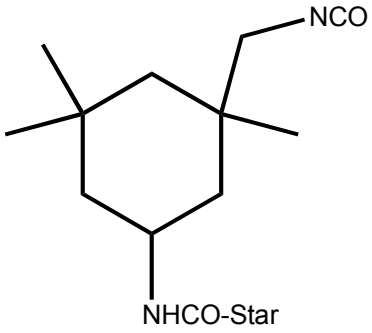

Figure 12: Reactive end group of a star-PEG arm [132].

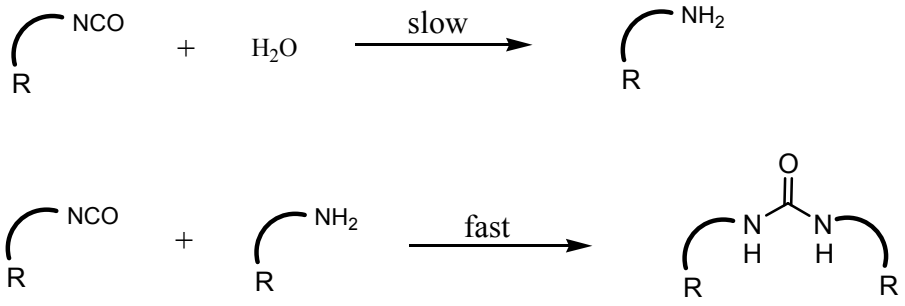

Figure 13: Formation of six-arm star diisocyanate prepolymers and chain extension due to diurethane linkages represented at one star polymer arm [130].

By solving the prepolymeric compounds in water, hydrolysis of present isocyanate groups, i.e. NOC-terminated reactive stars, to primary amines takes place (figure 13). These amines react easily with excess isocyanates to produce urea arrangements which connect two star compounds to one another. As the hydrolysis step is rate limiting, whereas the cross-linking reaction, i.e. dimerization and trimerization of the non-hydrolyzed arms with produced amine derivatives is fast, a mechanical stability of the star-PEG surface can be reached after

five minutes. After fifteen hours total cross-linking of the surface is accomplished. Hence, after dissolving the prepolymers in water for five minutes, the coating on a glass chip is carried out. It is not desirable to allow further cross-linking, as the number of NOC-terminated reactive arms available for surface and hapten binding decreases with time. The cross-linked polymers possess hydrophilic characteristics and by contact with water their hydrophilic features increase. Small water molecules can diffuse between the cross-linked arms of the dimer- and trimer star-PEGs to create hydrogen bonding. THF is used as a solvent for the prepolymers prior to the addition of water. Theoretically, the prepolymers could also be added without solving in THF, but this would be more time consuming as the polymers would have to be solved in the water added, and as mentioned, such reaction is slow [133]. In case of amino-activation and given that NH_2-PEG and star-PEG are interacting attractively, the arms of the star-polymers are directed towards the diamino polymers, hypothetically less functional groups would be available to the added haptens (see figure 14). Gray end-groups indicate NCO functional groups available to haptens, black end-groups indicate the ones which interact with the linear polymers. If the glass carrier is activated with diamino-PEG, addition of water to the prepolymers should be avoided, as a competitional reaction would occur between NH_2-PEG and the primary amine produced by the hydrolysis (see figure 15). In this case, a sandwich coating is preferable followed by a washing step in water to stop further cross-linking.

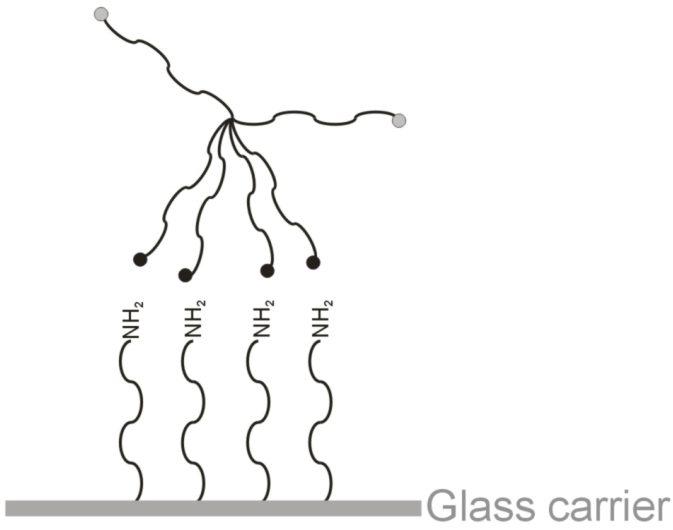

Figure 14: Interaction between a six-armed star-PEG and NH_2-PEGs.

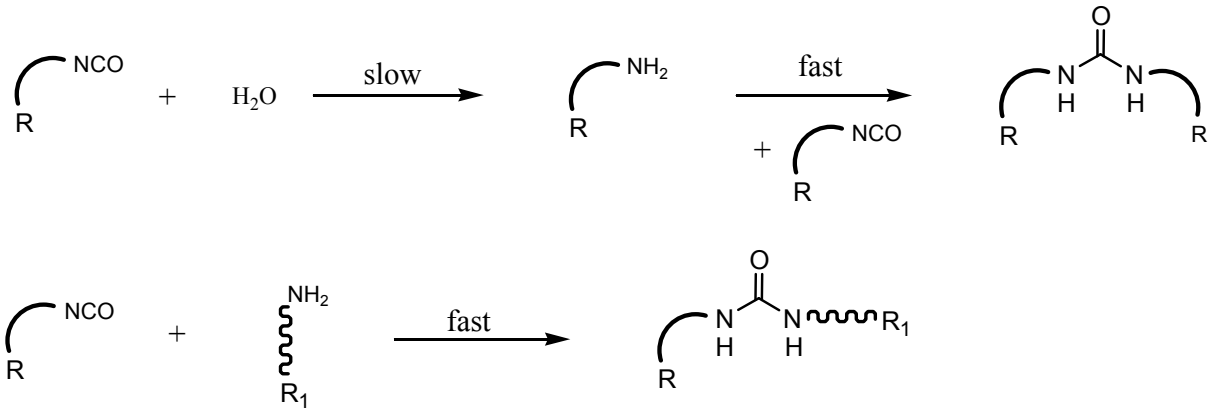

Figure 15: Competitional reactions between water and diamino-polymers (see figure 13).

Preparation of star-PEG-coating

50 mg star-PEG (SusTech, Darmstadt, Germany) were solved in 2 mL THF and left stirring for 10 min. The star-PEG solution was directly added without solving in water to an activated diamino-PEG-ylated slide which was covered with a second slide with the carved side facing upwards forming a sandwich. After 3 min the chips were carefully separated by hand and vortexed for 5 min in demineralized water to cancel further cross-linking on the glass surface. Both chips were dried in nitrogen flow and after 20 min they were ready for antigen immobilization.

3.3.3 Ag-coating

Microarrays coated with silver ions reach high capacities for covalent antibody binding due to the high density and homogeneous morphology of the ions. If a glass slide is activated by means of etching, free hydroxide groups can react with present silver ions to produce a layer of silver particles on top of the glass platform (see figure 16). Thiol and amino functionalized epitopes of antibodies bind covalently to the silver coated layer.

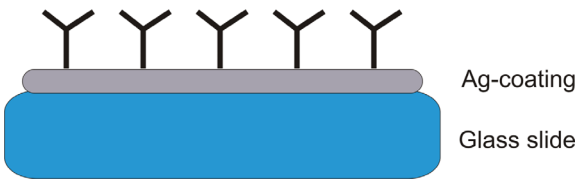

Figure 16: Antibody immobilization on a glass slide coated with silver ions.

Preparation of Ag-coating

Conventional glass slides were first carved on one edge then put in a chip reservoir containing 2 % Hellmanex solution and left 1 h in ultrasonic bath to rinse. Subsequently, the slides were left on a shaker over night (15 h) at room temperature. The cleaned slides were thoroughly washed five times in 200 mL demineralized water and dried under nitrogen gas flow. The prepared glass slides were dipped in 200 mL of methanol/hydrochloric acid solution (1:1) and left shaking for 1 h at room temperature. A washing step in water followed, where the chips were rinsed five times in 200 mL demineralized water. Subsequently, they were dipped in concentrated sulphuric acid and left shaking for 1 h at room temperature. An additional washing step in water followed and the slides were again dried under nitrogen flow. Hereafter, the etched slides were put in colloid sol C. After 72 h, the chips were taken out of the sol and dried in air. A thin layer of Ag was visible to eye as a grey film on top of the glass slide.

3.3.4 Surface control

To control the surface coverage of diamino-PEG-ylated chips, a flow cell was made of one coated chip and a polycarbonate chip. For the preparation of this control flow cell, an adhesive foil was glued between the coated chip and the chip made of polycarbonate to create a flow-through application. The “immunomat” (made at the Chair for Analytical Chemistry (TUM), Munich, Germany) was used as readout device with a surface-control program. Hereby, 1 µL/mL anti-streptavidin in PBS was added as primary antibody and 1 µL/mL anti-mouse IgG in PBS as secondary antibody. For chemiluminescence reaction, Luminol and horseradish peroxidase was added. For data analysis, LabVIEW (National Instruments, Texas, USA) was used.

3.4 Preparation of immuno-microarray reagents

3.4.1 Antibody immobilization

Prior to the antibody immobilisation an N-hydroxysuccinimide (NHS) activation was carried out on the amino PEG-ylated glass chips (4 h). For the antibody immobilization on the star-PEG- and Ag-coated chips, no activation step was needed. Briefly, 600 µL of a solution of 80 mg (0.31 mmol) DSC, 4 mg (0.03 mmol) DMAP, 1.6 mL absolute DMF and 125 µL triethylamine were added to a PEG-ylated chip and reacted as sandwich. The activated chips were cleaned in MeOH two times 10 min in an ultrasonic bath. Subsequently, the chips were dried under nitrogen flow. In order to prevent denaturation of the spotted antibodies, a solution of 0.005 % Pluronic F127 and 10 % trehalose in PBS was prepared as antibody stabilizer. This solution preserved the spots hydrated throughout the entire incubation time of 15 h. Also, an uneven spreading of the spots was prevented with the aid of Pluronic F 127 which acts as strong protein structure stabilizer. The individual spotting solutions, containing 2.62 g/L anti-*Legionella* antibodies, 2 - 2.5 g/L anti-*Salmonella* antibodies or 1.0 g/L anti-*E. coli* antibodies, were pipetted into cavities of a 384-well microtiter plate. Antibody solution was then spotted with a contact spotter (BioOdyssey Calligrapher miniarrayer from Bio-Rad, Munich, Germany). A solid pin (SNS 9) was used to create spots of 1 nL sample volume with a final spot diameter of 500 µm. The spotting procedure was carried out at 50 % humidity and 15 °C plate temperature. After an incubation at 20 °C for 15 h in petri-dishes containing 200 µL H_2O, the chip surface surrounding the spots was inactivated in 2 % casein in PBS by vortexing for 1:45 min and left shaking at RT in 2 % casein in PBS for 5 h. The chips were finally cleaned in water and PBS. Storage of the chips was possible for several weeks in PBS containing 0.1 % NaN_3 at 4 °C without degradation.

3.4.2 Microorganism preparation

S. typhimurium and *L. pneumophila* cell suspensions were diluted in PBS and stored in freezer at -18 °C. Shock-frozen *E. coli DSM 1116* cells were cultivated in LB Media (Lennox) over night at 37 °C and washed twice in PBS by centrifugation. The cells were then either autoclaved, heat killed or used as living colonies and stored in refrigerator at 4 °C. Prior to detection all cell suspensions were diluted in PBS or carbonate buffer to reach the desired concentrations. The cell concentrations of *E. coli* were determined by flow-cytometry using SYTO9.

3.5 Preparation of the SERS media

The particle size distribution of each colloid solution was tested using a UV-Vis spectrometer (Beckmann UV-DU 650, Beckmann Coulter, CA-USA) (procedure is described later). TEM pictures were developed with JEM 2010 (LaB_6 cathode) (JEOL (Munich, Germany) with an accelerating voltage of 200 kV.

3.5.1 Silver nanoparticles

For all described silver colloid preparation procedures, a glassware washing procedure including a KOH-bath followed by an HCl-bath was carried out. In that way residual particles on glass walls can act as catalysts, initiating premature agglomeration, were removed.

Colloid sol A – Ag-nanospheres

Silver colloid sol A was prepared using the procedure of Creighton *et al.* [4]. Briefly, 14.98 mg $NaBH_4$ (0.4 mmol) were dissolved in 60 mL MilliQ water in excess in an ice bath and split in 6-mL batches. 0.85 mg $AgNO_3$ (0.005 mmol) in 2 mL MilliQ water were added drop wise under vigorous stirring (1200 rpm) to generate particles with a narrow size distribution. The resulting lightly greyish sols were stored in the dark at 4 °C.

Colloid sol B – Ag-nanospheres

Silver colloid sol B was prepared using a procedure according to Lee and Meisel [21]. Briefly, 18 mg (0.1 mmol) $AgNO_3$ were dissolved in 100 mL MilliQ water in a 250 mL round bottom flask and divided in batches of 25 mL. These batches were heated to the solution's boiling point, and 0.2 mL (0.07 mmol) of 1 % tri-sodium citrate were quickly added. The mixture was left stirring (600 rpm) for 1 h under reflux. Finally, the heat source was removed and the solution was stirred (600 rpm) for another 30 min. After reaching room temperature the greyish colloid sols were stored in the dark at 4 °C.

Colloid sol C – Ag-nanospheres

Silver colloid sol C was prepared using a modified [105] procedure of Leopold and Lendl [1]. Briefly, 17 mg (0.1 mmol) $AgNO_3$ were dissolved in MilliQ water (10 mL). 100 mL of 11.6 mg (0.17 mmol) $NH_2OH{\cdot}HCl$ solution containing 3.3 mL NaOH (0.1 M) was prepared [1] and divided in 9 mL batches in centrifuge tubes. To the reducing agent, 1 mL of $AgNO_3$ was added in a flow rate of 0.67 mL s^{-1} without stirring. Finally, the centrifuge tube was inverted once to complete the mixing. The yellow/greenish colloid sols were stored in the dark at 4 °C [105].

3.5.2 Gold nanoparticles

For all described gold colloid preparation procedures, a glassware washing procedure including aqua regia followed by a KOH-bath and an HCl-bath was carried out.

Colloid sol D - Au-nanospheres

Gold colloid solution D was prepared using the procedure of Jana *et al*. [134]. Briefly, 9.07 mg (23.0 µmol) $HAuCl_4 \cdot 3H_2O$ and 7.76 mg (26.4 µmol) trisodium citrate dihydrate were dissolved in 100 mL MilliQ water. To weigh in the chloroauric acid, a plastic applicator had to be used in order to prevent oxidation of Au(III) on an metallic applicator. An ice cold 0.01 M $NaBH_4$ solution was freshly made from 1.15 mg (30.4 µmol) sodium borohydride and 3 mL MilliQ water. Then, 4 x 20 mL of the gold solution were pipetted into 4 sterile centrifugation tubes. To each batch, 600 µL borohydride solution were pipetted and the tubes were inverted 3 times. This reaction mixture was left for 4 hours at room temperature to allow the borohydride to react completely and stored at 4 °C.

Colloid sol E - Au-nanospheres

Gold nanospheres sol E was prepared after the procedure described by Frens *et al.* [135]. For this purpose, a 0.25 mM solution of $HAuCl_4 \cdot 3H_2O$ was prepared by dissolving 10.0 mg (25.4 µmol) in 100 mL MilliQ water. Addtionally, 0.04 M trisodium citrate solution was made by dissolving 0.05 g (0.2 mmol) in 5 mL MilliQ water. The gold solution was put into a round bottom flask. It was stirred under reflux and 3 mL (0.1 mM) of the citrate solution was added. Its color changed from a pale yellow to a pale green, then blue and finally to wine-red. When the reaction mixture turned wine-red, it was stirred under reflux for another 30 min. After cooling down to room temperature, the red colloid sol was stored at 4 °C.

Colloid sol F - Au-nanorods

A seed mediated method for producing gold nanorods developed by Gao *et al.* was followed [136]. For the preparation of the seed sol, the borohydride was applied as reducing agent. 1.8 mg (4.6 µmol) $HAuCl_4 \cdot 3H_2O$ and 1.5 mg (5.1 µmol) trisodium citrate dihydrate were dissolved in 20 mL MilliQ water. Then, an ice cold 0.01 M $NaBH_4$ solution was freshly made from 0.23 mg (6.1 µmol) sodium borohydride and 600 µL MilliQ water. This solution was pipetted into the gold citrate solution, stirred for 30 s and then left alone for 4 hours to allow the borohydride to react completely. In the meantime, the growth sol was prepared; A mixture of 5.24 mg (13.3 µmol) $HAuCl_4 \cdot 3H_2O$, 1.50 g (4.1 mmol) CTAB, 1.00 mL acetone and 0.75 mL cyclohexane in 50 mL MilliQ water was heated up to 60 °C under stirring. In the

beginning, the mixture was an orange suspension that turned into a yellow suspension while heating. Then it was cooled down to room temperature. 10 mL of growth sol were filled into a centrifuge tube. After adding 125 µL seed suspension, 5.0 µL of a freshly prepared 0.01 M $AgNO_3$ solution and 500 µL of a freshly prepared 0.01 M ascorbic acid solution (AA) were also added. After adding AA, the preparation turned colorless and after 10 min it turned to a pale violet which became darker during the next 2 h. After 2 h, the dark violet nanorod sol was given into 4 different dialysis tubes by using sterile syringes. The tubes were prepared by cutting off 15 cm long pieces from a hose of dialysis membranes, which were closed at the ends by plastic clips. The ends of the hose had to be folded to become leak-proof. Then, the 4 tubes were put into 600 mL MilliQ water which was stirred at 30 °C. The water was changed after an hour 3 times and then left alone over the night. The suspensions were then injected into clean 50 mL narrow-necked volumetric flasks. The sols (approx. 11 mL) were diluted with MilliQ water to give 50 mL sol. The flasks were stored at room temperature.

Colloid sol G - Au-nanorods

Preparation of nanorods without the use of seeds was carried out as published by Jana *et al.* by using CTAB polymers as stabilizing agents [137]. Briefly, in a beaker glass, 3.61 g (9.91 mmol) CTAB were diluted in 50 mL MilliQ water under stirring and heating (80 °C). This 0.2 M CTAB solution was cooled down to room temperature. Then, 18.22 mg (46.3 µmol) $HAuCl_4 \cdot 3H_2O$ were added under stirring. Furthermore, 1.81 mg (11.1 µmol) $AgNO_3$ were added to the gold-brown solution. After 17.6 mg (0.100 mmol) ascorbic acid were added, the solution turned colorless and was stirred for 30 min. Hereafter, 1.95 mg sodium borohydride were diluted in 0.5 mL ice-cold MilliQ water. 10 mL CTAB-Au solution were given into 4 sterile centrifugation tubes by using sterile syringes. To each batch, 1 µL of the 0.05 M ice-cold borohydride solution was added. Each tube was inverted 5 times and then left for 2 hours. The suspensions turned dark-brown within 10 minutes. To prevent a precipitation of CTAB, the batches were heated to 45 °C. The 4 dark-brown sols were given into 4 dialysis hoses as described above and dialyzed at 45 °C for 3 hours in 800 mL MilliQ water. The water was changed every 30 min. The nanorod colloid sol was stored at room temperature.

3.6 SERS measurements

All SERS spectra were obtained with a Renishaw 2000 Raman microscope system (Renishaw, UK) (see figure 17) using either a He-Ne laser (λ_0 = 633 nm, laser power at spot: 7 mW) or an Argon laser (λ_0 = 514 nm, laser power at spot: 7 mW). Wavelength calibrations were performed by measuring silicon wafers through a ×50 objective, evaluating the first-order phonon band of Si at 520 cm^{-1}.

3.6.1 SERS measurements on crystal violet

The SERS measurements on crystal violet (CV) were carried out in a microtiter plate using a ×50 objective with a numerical aperture (NA) of 0.75. In a cavity of the plate, CV was added to a diluted silver colloid sol (1:6) containing the desired NaCl concentration (0.01 – 0.04 M). The colloid sol was diluted, so that no excessive agglomeration of colloids would hinder SERS enhancement. If not stated differently, the exposure time was set to 1 s for all CV spectra presented in this study. Signal to noise ratios (SNR) were compared between spectra collected from colloid sol A-G. Mean values and standard deviations of three measurements were calculated. The limit of detection was defined to SNR ≥ 3 of the vibrational band at 1171 cm^{-1} in these experiments.

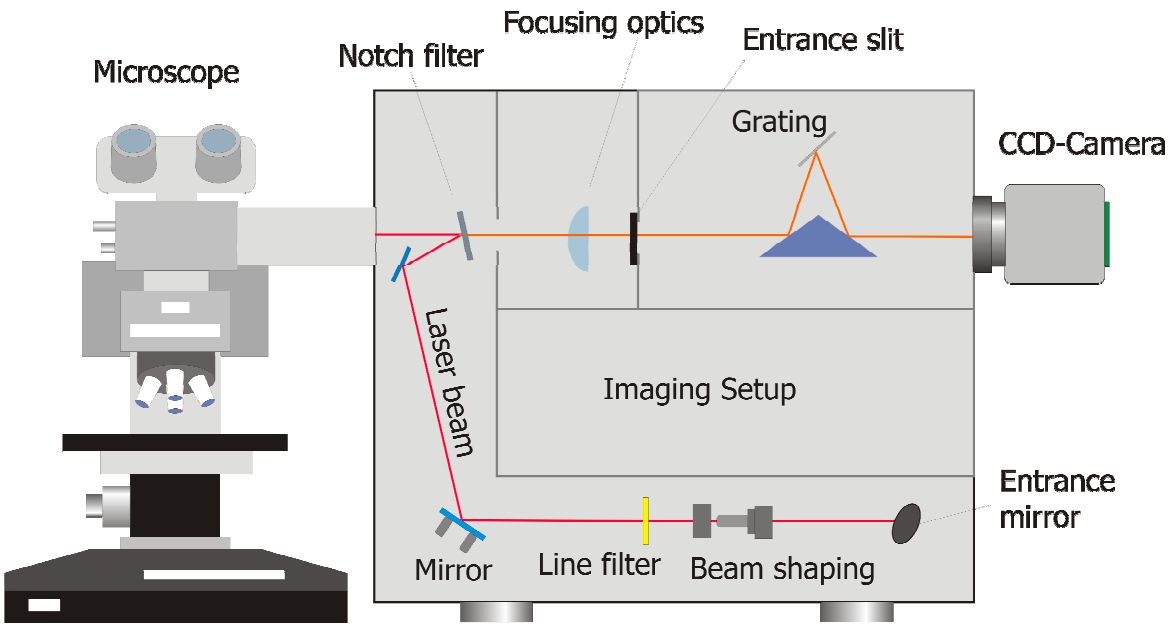

Figure 17: Raman spectrometer connected to a microscope.

3.6.2 SERS measurements on microorganisms

SERS spectra of bacteria were measured using a water immersion objective (×63, NA 0.9, lateral resolution ~ 1 µm). The laser exposure time varied for different experiments and is explicitly mentioned for each experiment.

Stationary SERS measurements

The microorganism supensions were pipetted and incubated for 1 h on a spotted glass chip containing the respective coatings and antibodies. In order to eliminate unspecific bound microorganisms, the chip was thoroughly washed in PBS. The chip was then placed in a polycarbonate tray which was filled with colloid sol (see figure 18). By marking the spots with a pen, their coordinates could be retrieved with a microscope. As the polycarbonate tray is transparent, there was possible to visualize the antigens with both top and bottom illumination which eased their localisation. The polycarbonate tray was cleaned by MilliQ water and 1:5 (H_2O:HNO_3) if silver colloids were used and, aqua regia if gold was used as SERS media.

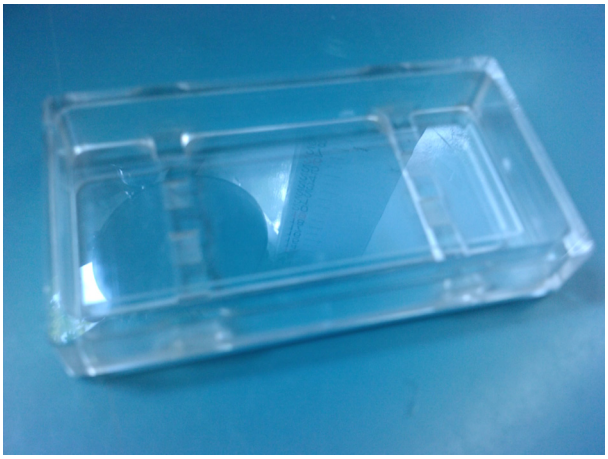

Figure 18: Polycarbonate tray for stationary measurements.

SERS measurements in a flow cell

To improve sensitivity and reproducibility of the detection method, a flow cell was developed to replace the polycarbonate tray used in stationary measurements (see figure 19). The flow channel was constructed for a laminar flow of the reactants. Additionally, the flow channel was thin enough to allow efficient interaction between bacteria and antibodies, thus minimizing the loss of antigens which did not come in contact with the antibodies. Furthermore, it was important to enable back pressure stability and eliminate leakage. This was accomplished by eight screws which stabilized the lid with an even distribution of pressure, as well as with an o-ring placed about the flow cell. The flow cell was made of stainless steel and was of 60 mm length, 0.25 mm height and 0.5 mm width. Total volume of the flow-channel was 7.5 µL. The flow cell was designed in a way to fit perfectly to the DM LM microscope platform of Leica Microsystems GmbH (Wetzlar, Germany) (see figure 20).

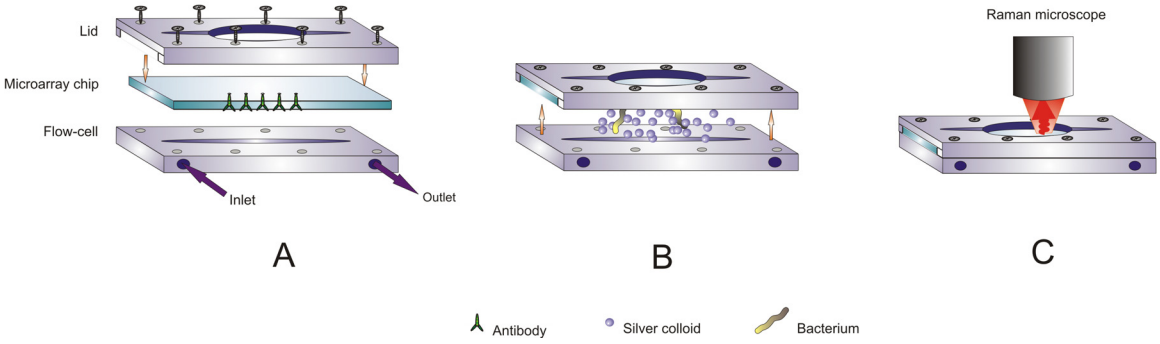

Figure 19: Illustration of the stainless steel flow cell. A) The microarray chip, holding antibodies facing down into the flow cell, was placed in between the lid and the flow cell which were held together by eight screws. B) The antigens and metal colloids were added. C) SERS measurements were carried out through the microarray chip. For better visualization, the scale in this picture is not real.

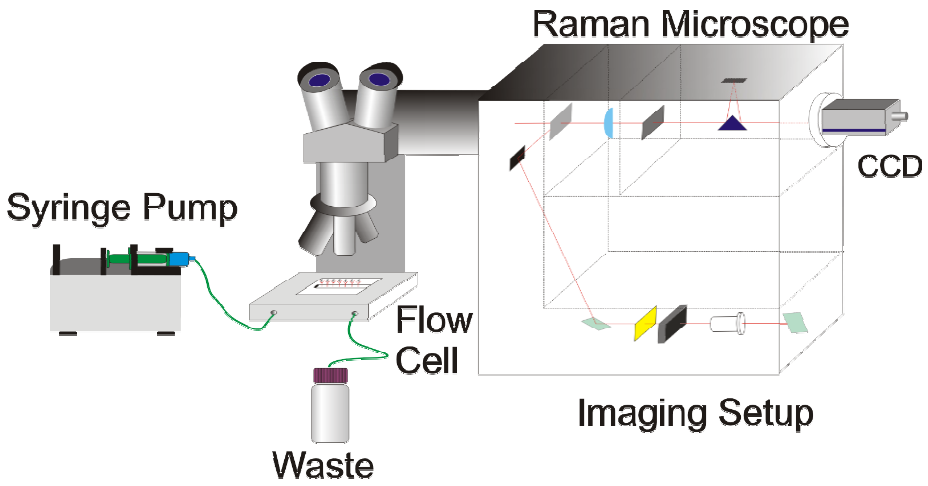

Figure 20: Setup of the flow system connected to the Raman microscope.

The antibody spots were placed in a row by means of a contact spotter and had a diameter equal to the width of the inner flow cell (500 µm). The distance between neighbour spots centre was 1300 µm. Reactants were flushed through the cell using a syringe pump (Harvard Pump 11 from Harvard Apparatus, March-Hugstetten, Germany) with a flow rate of 60 µL/min, resulting in a Reynold´s number of Re = 4 (laminar flow). Firstly, 0.5 mL antigen suspension was added, left stagnant for 30 min, and then further 0.5 mL antigen solution was added. Excess cells were flushed out with 0.5 mL PBS. Finally, the flow channel was filled with silver colloid sol (containing 0.03 M NaCl). By focusing the laser-beam through the microarray platform consisting of glass-based plates, the microorganism detection was carried out. The flow cell was cleaned by MilliQ water and 5:1 (H_2O:HNO_3) solution after each experiment.

SERS measurements on bacteria aerosols

For qualitative and quantitative measurements of aerosolized bacteria suspensions by means of SERS, a production and collection procedure was developed. The collection of bioaerosol was carried out in an air tight grounded glovebox compartment of 1 m^3 to which an external particle free gas flow was connected (see figure 21). The chamber had a constant humidity of 20 %. By means of a ventilator, the air was kept in continuous movement. Background measurements were carried out with an APS after cleaning the compartment with EtOH followed by flushing with particle free air over night.

The bacteria cells were cleaned by centrifugation in water prior to aerosolization to remove eventual residues of buffer ions, to prevent the formation of a crystal film around the bacteria cells. The generation of the bioaerosol was carried out from a three-necked bottle was filled with 10 mL bacteria cell suspension of known concentration in MilliQ water. This suspension was nebulized by means of a cross-flow glass nebulizer for a distinct time period to obtain the required aerosol concentration in the compartment. Particles with aerodynamic diameter between 0.8 µm and 14.5 µm were used. The concentrations were chosen so that in one droplet ≤ 5 µm Ø a single bacterium cell was present in order to avoid the generation of agglomerates. This was calculated with the assumption that no aggregates were present after heat inactivation of the bacteria cells. Particle free air with a flow of 4 L/min (controlled by a rotameter) was used for the nebulization process and removed by free flow through an absolute filter (HEPA) as pressure balance. The aerosolized suspension was flushed through a drying chamber containing blue gel to eliminate water droplets surrounding the particles. Subsequently, the dried particles were neutralized by a Krypton-85 source to prevent an electrostatic attraction to the walls of the compartment which was made of steel. For aerosol concentration measurements three readings by means of APS were carried out. Hereby, it was made sure that the particle concentration in the aerosol chamber was constant prior to collection. The bioaerosol was finally collected by means of a Coreolis® wet sampler holding 5 mL PBS at 150 L/min flow for 10 min. 0.5 mL of the bacteria suspension was withdrawn for concentration measurements by means of flow cytometry. The remaining suspension was added to the microarray flow cell for SERS analysis. Hereby, the flow cell was flushed with 0.5 mL PBS at 0.06 µL/min using a syringe pump. Subsequently, 2.5 mL analyte suspension was added at 0.06 µL/min followed by a flushing of the microarray with 0.5 mL PBS at 0.06 µL/min. Finally, 0.8 mL silver colloid sol C containing 0.03 M NaCl was added at 0.06 µL/min.

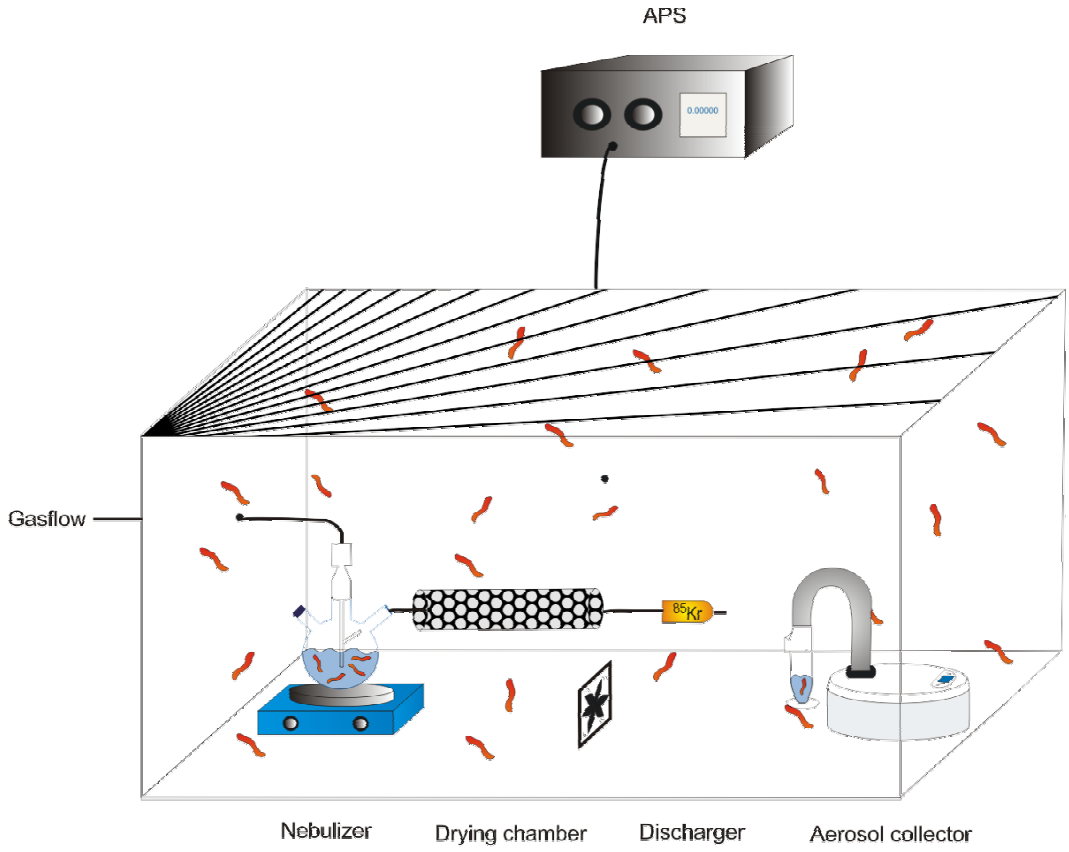

Figure 21: Setup of aerosol collection for SERS measurements.

3.7 Data acquisition

The raw data was analyzed with either LabSpec_4.02 (HORIBA Jobin Ivon Inc., Edison New Jersey, USA), Matlab (MatWorks, MA, USA) or WiRE™ (Renishaw, Gloucestershire, UK). Maps were created based on one vibrational mode at distinct wavenumber (baseline corrected). The limit of detection for each spectrum was defined as signal to noise ratio of ≥3. For the quantification, both LOD and LOQ were determined according to IUPAC. LOD was calculated with 3 s method and LOQ was calculated with 10 s. Single spectrum measurements were evaluated by Origin® 7G (OriginLab corporation, North Hampton, MA-USA). For data acquisition of larger number of collected spectra, MatLab was applied. A program was written by Dr. Michael Wagner for map evaluation. Hereby, one spectrum was chosen for baseline correction, to represent all spectra in one map. In this particular spectrum, ten points were equally distributed within the noise on each side of the peak which was chosen for mapping evaluation. By means of these twenty points surrounding the peak, an average baseline was calculated. To ensure that the peak maximum and baseline correction held for all spectra collected, the parameters chosen were added and tested to several other spectra in the map. It was important to take into consideration the appearance of asymmetric peaks, shifted maxima, SNR differences, baseline correction which is necessary due to spectral changes from luminescence reactions, optics, external light etc. The number of hits within the map was mathematically derived by the program.

The parameters for the quantitative evaluation of bacteria in solution, based on SERS mapping of microarray spots, were optimized for different experiments. When analyzing discrete numbers like the number of hits per SERS map, there are several aspects which have to be taken into consideration by choosing the map area and scanning steps. The empirical probability, of collecting information of total output of components, increases with increasing map area (maximum the size of analyte spot) and decreasing mapping steps (minimum the length of bacterium). The scanning steps should not be smaller than the length of one bacterium as a double counting would falsify the result. With increasing map area and decreasing mapping steps, the time of measurement increases which is undesired. The time of laser exposure (t_{ex}) influences the signal to noise ratio (SNR) of a SERS spectrum. The longer the t_{ex}, the stronger the metal nanoparticles agglomeration is, due to increasing temperature of solution, and the higher the SNR of the SERS signal. Because a hit is defined as observing a peak at a certain wavenumber with SNR ≥ 3, it is important for the statistic that t_{ex} is constant for every experiment. Furthermore, the incident of bacterium immobilization to an antibody

plays a role in the statistic of SERS mapping. Therefore, in a quantitative experiment, n measurements are carried out for every concentration of bacteria solution and the mean value μ with its standard deviation s is recorded for calibration.

4 Results and Discussion

4.1 Microarray platform

The microarray platform which was chosen for this thesis, developed by Wolter *et al.* [65], was made of a glass-chip coated with functionalized polymers for antibody immobilization. However, the coverage of *L. pneumophila*, *S. typhimurium* and *E. coli* on these antibody spots using the stationary platform was inefficient. The reason for this was investigated as a part of the optimization step for the combination of microarrays with SERS detection. This was a crucial point on the way to a more sensitive readout method, for quantitative analyses in particular. In figure 22, the coverage of autoclaved *L. pneumophila* cells immobilized on polyclonal antibodies extracted from rabbit blood is shown. The high concentration of the added bacteria suspension (1 mL of 10^{10} cells/mL) was chosen to insure a saturation of antigen-antibody coverage. This was calculated in relation to antibody concentration on the surface (1.3 mg/mL). Theoretically, full surface coverage of the bacteria cells on the microarray spot was expected. The areas where no whole bacteria binding are highlighted with blue circles in figure 22. The same scenario of poor coverage was observed using heat inactivated *S. typhimurium* and autoclaved *E. coli DSM 1116* as antigens. This could either be caused by something not visible in the microscope magnification (i.e. smaller than 0.05 µm) blocking the binding sites for the whole cells, or the antibody coverage on the PEG-ylated chip was insufficient due to inhomogeneous coating.

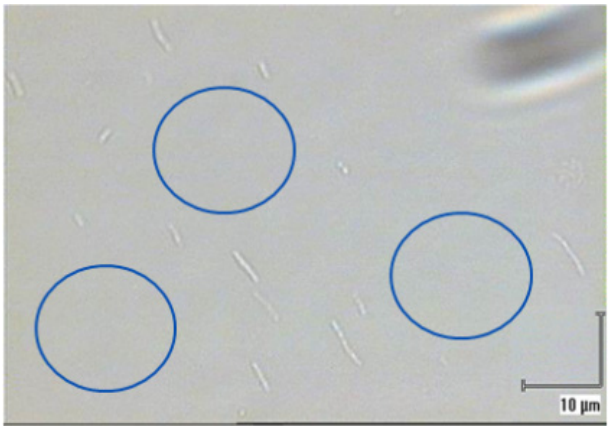

Figure 22: Optical image of an anti-*Legionella* spot loaded with a concentration of 10^{10} cells/mL of *L. pneumophila*. The blue circles indicate sites on the antibody spot where no whole cells were present.

To exclude the latter, alternative coatings of the glass chip were tested on behalf of their immunocomplex coverage efficiency. The chips were evaluated visually by microscopic imaging. As amine end-groups of antibodies bind covalently to Ag coatings, this platform was chosen as an alternative. The coating was homogeneous according to a surface test. Numerous SERS experiments using Au- and Ag-coatings to bind antibodies against bacteria and bacteria directly are described in literature and show good coverage of antibodies [68, 138]. In figure 23 the coverage of *L. pneumophila* cells (1 mL of 10^{10} cells/mL) on an anti-*legionella* spot, on a Ag-coated chip is shown. The immobilization was inefficient.

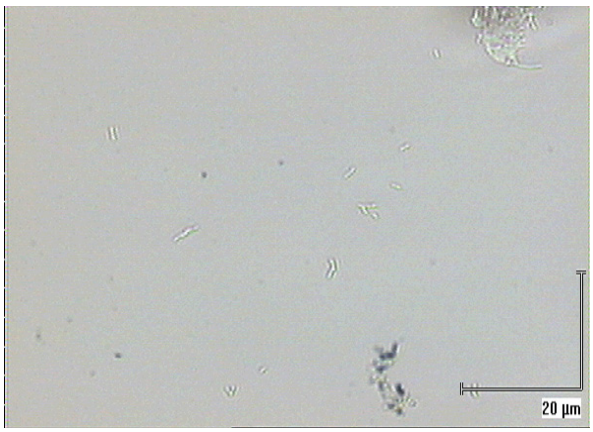

Figure 23: An optical image of a Ag-coated glass chip holding anti-*Legionella* antibodies covered by autoclaved *L. pneumophila* cells (10^{10} cells/mL). The coverage was poor.

A further surface coating with star-shaped polymers was tested regarding the coverage of *L. pneumophila* cells immobilized on anti-*legionella* spots. Star-PEGs are self-assembled on the glass chip and controlled by the addition of water. The procedure is straight forward and known for excellent antibody binding capacities [130]. Thus, chosen as a second alternative to diamino-PEG-coating. The immobilization of *L. pneumophila* cells (1 mL of 10^{10} cells/mL) on star-PEG coated glass holding antibodies against *Legionella* is shown in figure 24. No advancement compared to the coverage on diamino-PEG surface was detected.

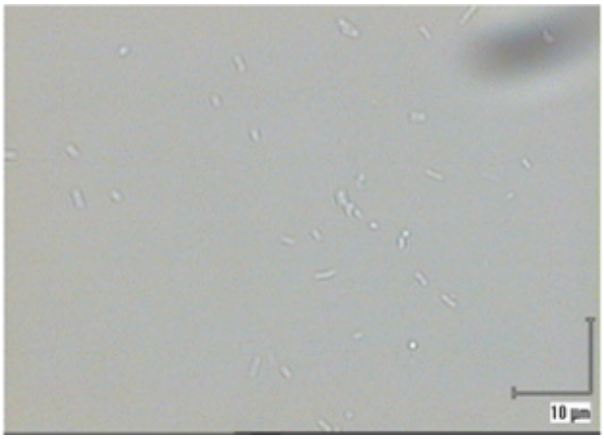

Figure 24: An optical image of a star-PEG-coated glass chip holding anti-*Legionella* antibodies covered by autoclaved *L. pneumophila* cells (10^{10} cells/mL). The coverage was poor.

It was shown that an insufficient coating was not the reason for the poor coverage of intact bacteria cells, as both alternatives show the similar phenomenon of areas where no whole cells bound. The presence of cell fragments, probably originated from the high pressure and temperature during autoclaving and boiling, was presumed. SERS experiments on the diamino-PEG-ylated surface additionally revealed that fragments, not visible to eye, were most likely present as different fingerprint spectra were maintained on the sites with no whole cells. These fingerprint spectra, collected at the sites around the whole cells, were dedicated to fragments. In figure 25, some examples to the fingerprints found by examining a spot covered by autoclaved *L. pneumophila* cells are shown. Here, the vibrational band of COO^- stretch sym. in the range 1340 – 1440 cm^{-1} is frequently visible, which supposes that sugar strains and amino acid residues were released during autoclaving. Amide II at 1500 cm^{-1} and Amide III at 1250 – 1310 cm^{-1} are additionally suggesting that large fragments of the cell wall were unleashed and bound covalently via their amide groups to the antibodies on the diamino-PEG surface. The fragments were thereby blocking the antibody binding sites. This again resulted in poor coverage of whole cells. A similar phenomenon could be seen for *S. typhimurium* and *E. coli* cells (see figures 26 and 27). It can be presumed that sugar strains produced by the cells themselves were still present in the suspension and were one of the reasons why the vibrational band of COO^- stretch sym. was appearing such currently for all three species analyzed.

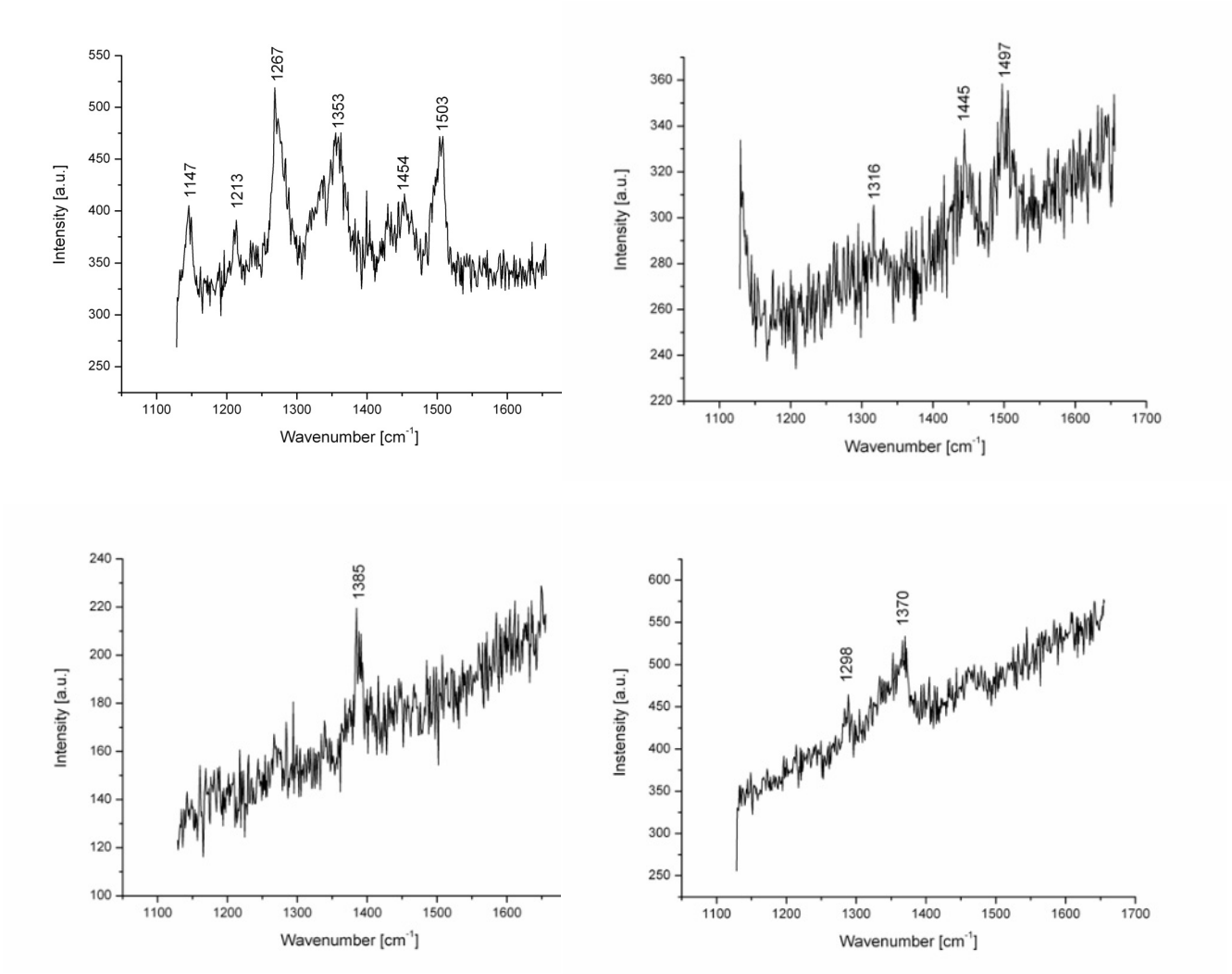

Figure 25: Fingerprint spectra of *L. pneumophila* fragments immobilized on a diamino-PEG-ylated chip holding corresponding antibodies. The fragments were probably released by autoclaving and blocked the binding sites of intact cells.

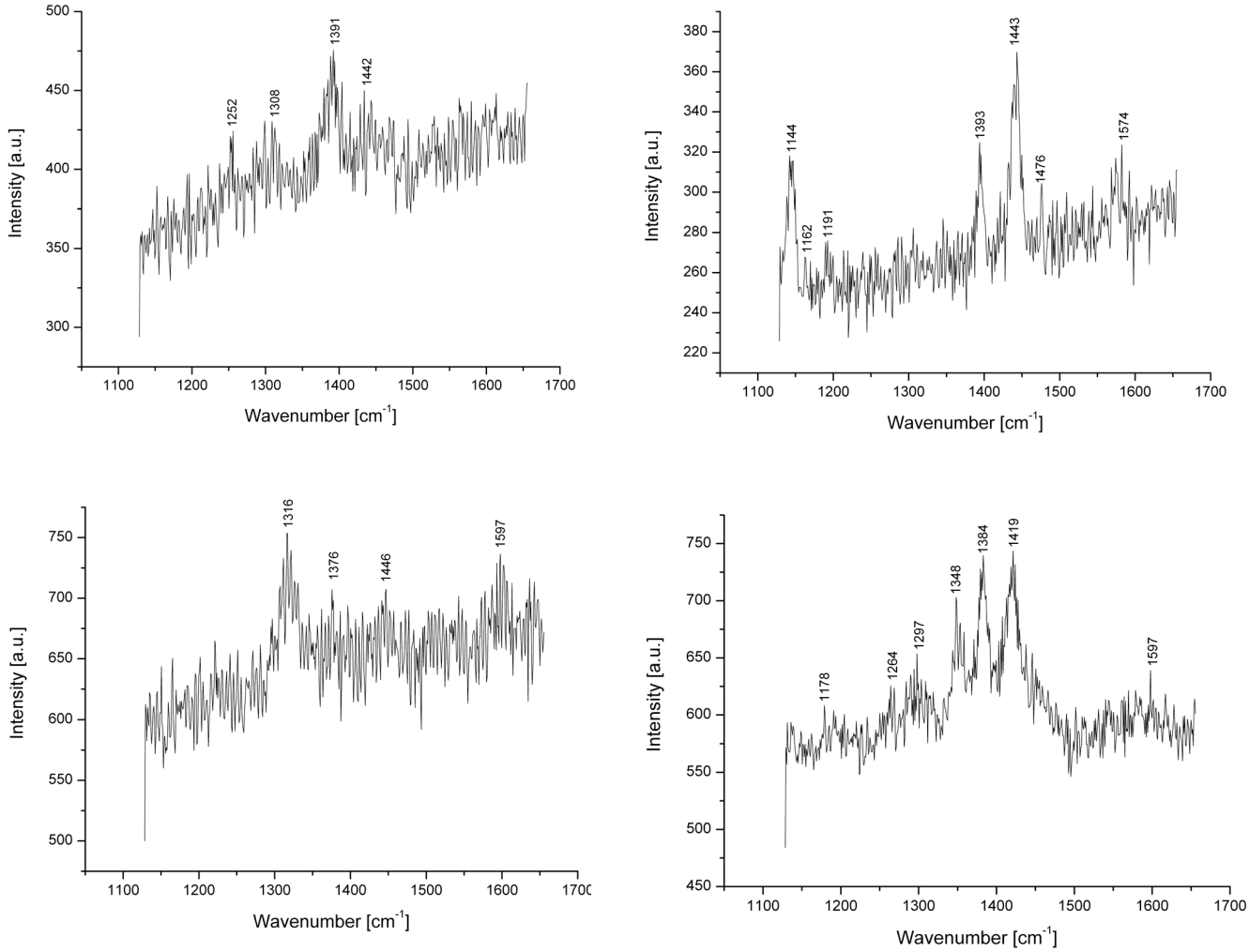

Figure 26: Fingerprint spectra of heat-inactivated *S. typhimurium* fragments immobilized on a diamino-PEG-ylated chip holding corresponding antibodies. The fragments were probably released by boiling and blocked the binding sites of intact cells.

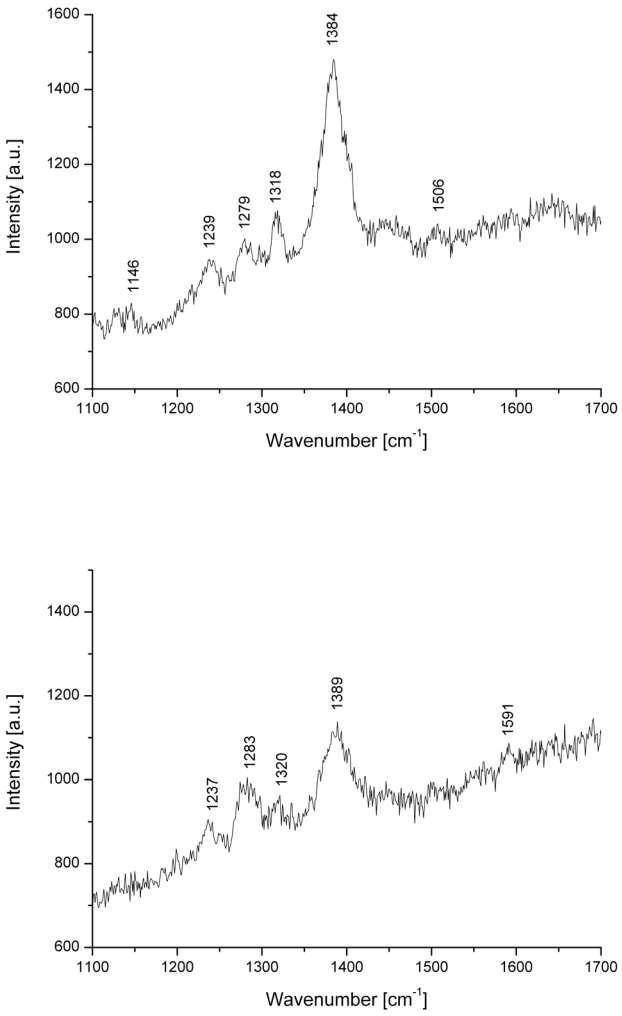

Figure 27: Fingerprint spectra of *E. coli* fragments immobilized on a diamino-PEG-ylated chip holding corresponding antibodies. The fragments were probably released by autoclaving and blocked the binding sites of intact cells.

In the case of *E. coli*, there were mainly two types of fragment spectra which appeared (see figure 27). Here, vibrational bands at ~1390, ~1320, ~1280 and ~1240 cm^{-1} were detected which again supposed that sugar strains and amino acid residues were released during autoclaving. Both spectra showed similar peak positions, though the signal intensity ratios were different. The vibrational bands at ~1390 cm^{-1} and ~1320 cm^{-1} have an intensity ratio of (4:1.2) and (4:1) in the spectra of figure 27 (top and bottom respectively). The vibrational bands at ~1320 cm^{-1} and ~1280 cm^{-1} have an intensity ratio of (1.9:1) and (1:2) respectively. Furthermore, slight shifts in wavenumber were observed.

A suspension of living *E. coli* cells, which had not been exposed to large heat or pressure changes, and most probably did not contain any fragments, were added to a amino-PEG-ylated microarray holding corresponding antibodies. This was to prove the hypothesis of antibody binding sites blocking caused by fragments. According to figure 28, the coverage efficiency of living *E. coli* cells is higher due to the lack of fragments. In the left images, heat killed cells have been immobilized onto the antibody platform. Here, the coverage was poor. A higher sensitivity of quantitative analysis it is therefore to be obtained when the analytes are living cells than for analysis of cells inactivated by heat or autoclaving. Moreover, higher reproducibility of the detection can be reached.

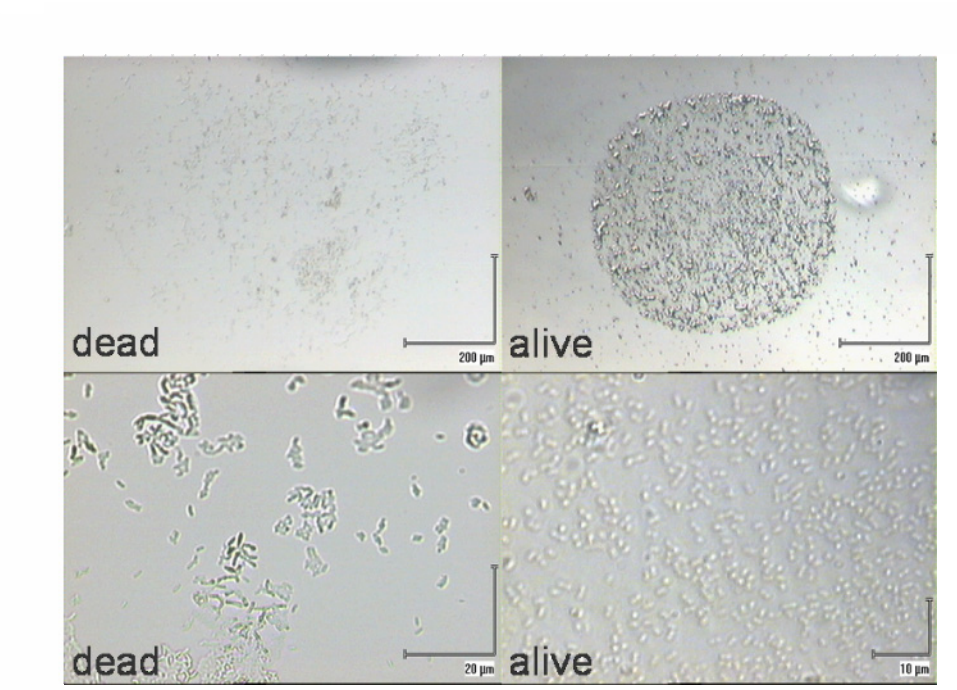

Figure 28: Optical images of dead and living *E. coli* cells added to anti-*E. coli* antibody-microarray. (left) The coverage was poor if the cells had been killed, probably due to cell fragments blocking the binding sites on the antibodies. (right) Living *E. coli* cells covered the antibody spot homogenously.

4.2 SERS media

Reproducible production of SERS media with well-defined shapes and sizes is a challenge, but at the same time crucial to achieve stable surface plasmon resonance frequencies and hence, reproducible enhancement factors and spectral features by SERS measurements. However, little investigation on reproducibility or stability of the SERS active particles has been published. Firstly, in order to achieve reproducible results, the employed colloidal sols, and therefore their synthesis have to be reproducible. Different parameters must be taken into consideration (e.g. reaction temperature, stirring power and time, reactants volume as well as the way and order of reactant's addition). Secondly, a monodisperse initial sol is crucial as highly SERS active interparticle spaces can be produced by controlled agglomeration of the colloids [94]. Addition of salts to the colloid sol in different concentrations causes the particles to coagulate.

Several colloid sols of silver and gold particles were tested as SERS media for the analysis of bacteria. Hereby, a thorough examination of the nanoparticles was completed where the effect of changing reaction parameters on the nanoparticles and on the resulting Raman cross sections were investigated. By means of the test molecule CV, the SERS enhancement factor was calculated for each prepared sol. CV is a widely used Raman reporter molecule which is also implemented as a labelling molecule for microorganism SERS detection [26]. Kneipp *et al.* showed that CV provides an extremely large effective cross section, and carried out single molecule analysis in the presence of Ag colloid sol [91].

4.2.1 Silver colloid sol

Colloid sol A (reducing agent: $NaBH_4$)

By dividing the original reactant volumes described by Creighton et al. [4] into ten batches (where the tenth batch was not used due to high level of uncertainty) a more uniform development of silver colloids was achieved. The plasmon absorption maximum lied at 376 nm for three separate preparations, which indicated a good reproducibility (figure 29a). Furthermore, the UV-Vis analysis revealed a polydisperse sol as a weak shoulder was present at 420 nm. In consequence, equation 1 is not valid for these colloids. Significant changes of the absorption spectra, such as absorption band broadening within 25 min and shift of the shoulder to 430 nm, indicated very limited stability of the colloids. This stability factor made them unsuitable for routine SERS measurements (figure 29b).

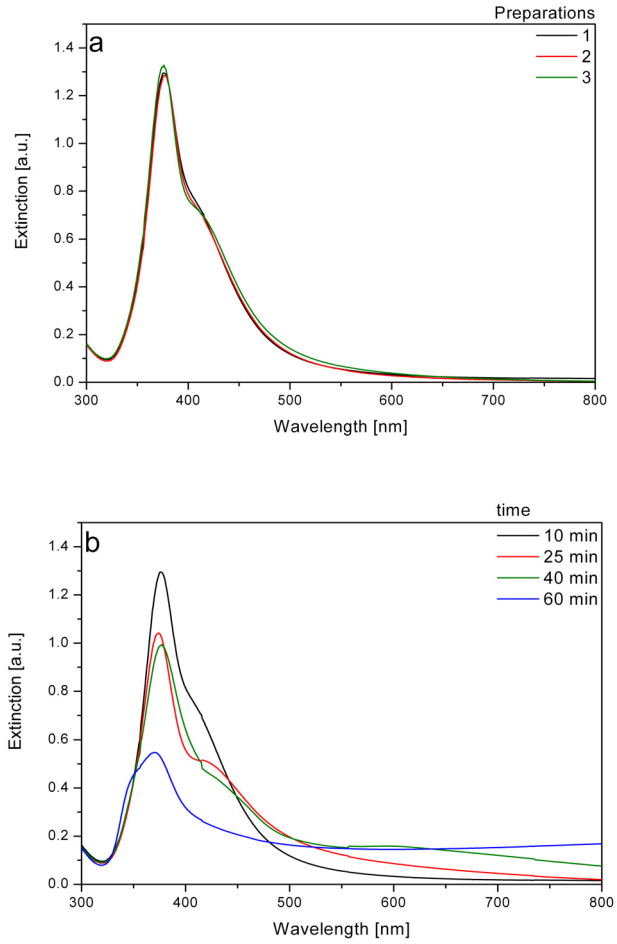

Figure 29: UV-Vis spectra of silver colloid sol A. (a) The synthesis was reproducible over three preparations. A weak shoulder was present at 420 nm. (b) Sol A showed limited stability. After 25 min the shoulder had shifted to 430 nm and developed significantly.

Colloid sol B (reducing agent: Na-citrate)

The original reactant volumes were divided in ten batches to increase the reproducibility, where the tenth batch was not used due to high level of uncertainty. However, the plasmon absorption maximum lied between 417 nm and 441 nm for five repeated preparations, indicating a limited reproducibility in the production (figure 30a). Additionally, a widening of the extinction signature in the UV at 350 nm within the five different preparations, suggests that the sol was polydisperse. Thus, equation 1 could not be applied to calculate the particle diameter. These colloids had a shelf life of over three weeks (figure 30b), but the limited reproducibility of the production procedure restrains the applicability as SERS media.

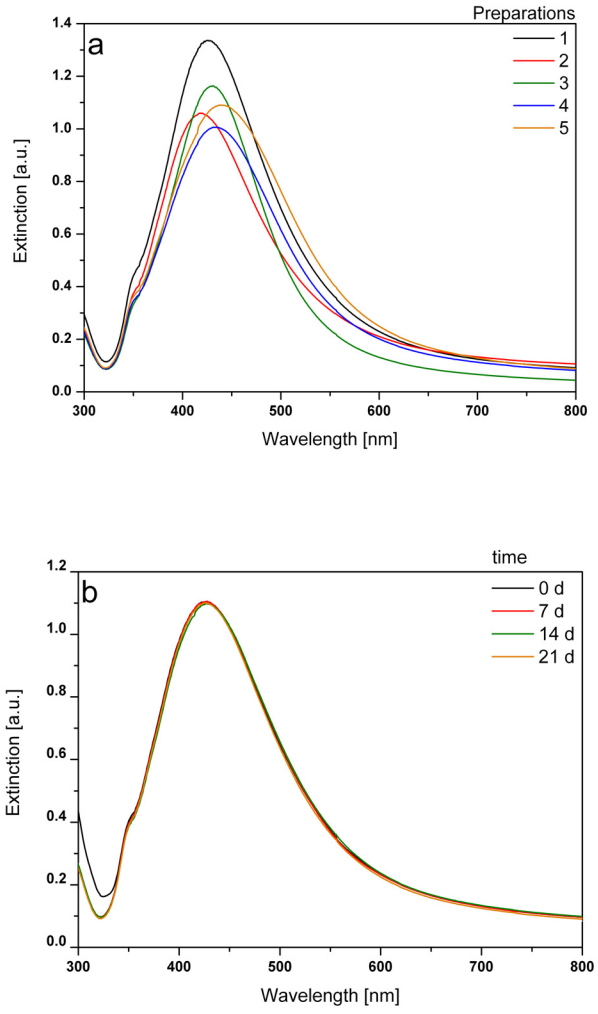

Figure 30: UV-Vis spectra of silver colloid sol B. (a) Limited reproducibility was observed throughout five preparations. (b) Sol B was stable for more than three weeks.

Colloid sol C (reducing agent: $NH_2OH•HCl$)

Again, the stock solutions were divided in ten batches to increase the reproducibility. An important aspect of the silver sol preparation was the rate of silver nitrate addition. It was found that a rapid addition using an Eppendorf pipette was the optimal procedure. Silver nitrate was added while swirling the pipette once over the reducing agent which maintained stagnant. After the rapid addition, the mixture was carefully swirled by rotating the centrifuge tube once. The final monodisperse colloidal solution had a yellowish color and contained particles of ~26 nm (figure 31a). The absorption maximum was found at 403 nm for all analyzed batches and showed good reproducibility throughout five separate preparations (figure 31b). These colloids had a shelf life of over three weeks, an important feature regarding their routine applications as SERS media (figure 31c). Advantages of the proposed procedure are the straight forward, fast and inexpensive production and the high reproducibility as well as the long shelf life of the resulting particles.

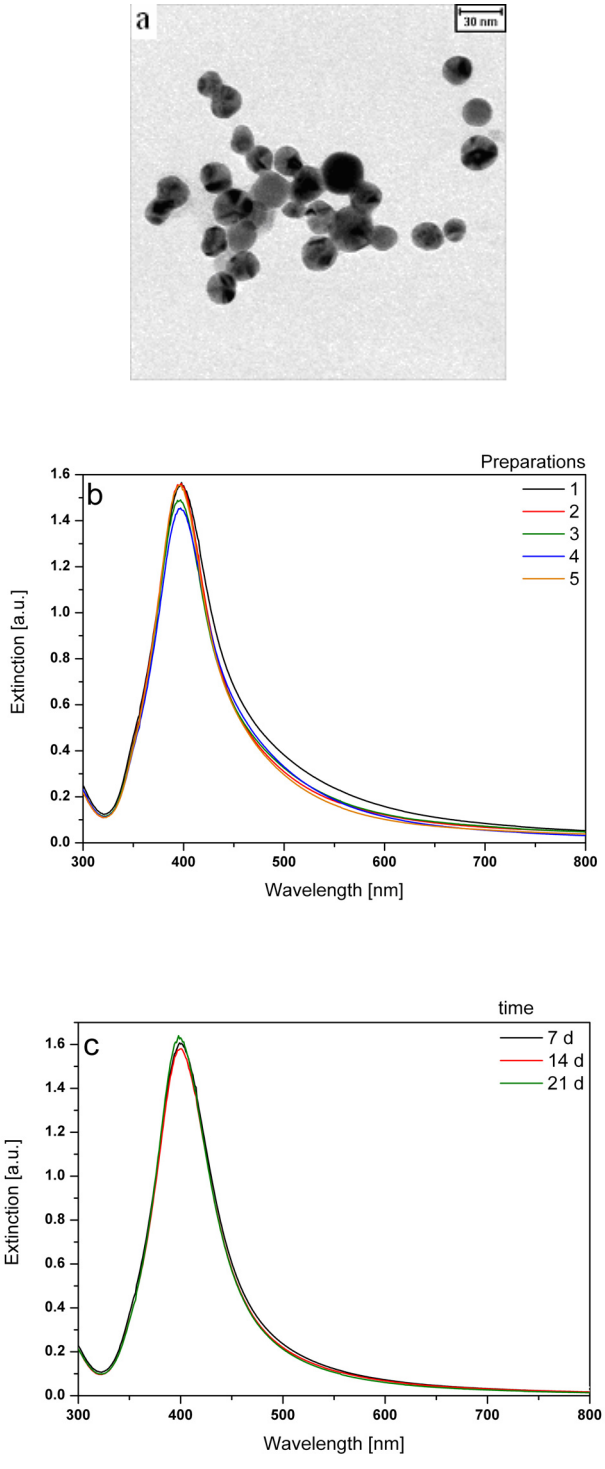

Figure 31: Characterization of silver colloid sol C. (a) The TEM image shows the narrow size distribution of the colloid sol with particle sizes of ~26 nm. (b) UV-Vis spectra illustrate a reproducible production over five preparations. (c) UV-Vis spectra of colloid sol C show substance stability over three weeks.

The stability of colloidal dispersions can be related to their Zeta potential due to its dependence on degree of repulsion between adjacent, similarly charged particles. Therefore, colloid sol C was examined towards its electric properties using a Zetaphotometer. The potentials ζ were calculated according to the Smoluchowski theory (equation 9) and was dependant on the electrophoretic mobility μ_e of the particles and the dielectric constant of dispersion medium ε_r and the permittivity of free space ε_0. The dynamic viscosity of the dispersion medium η is indirect proportional to μ_e.

$$\mu_e = \frac{\varepsilon_r \varepsilon_0 \zeta}{\eta} \qquad \text{(eq. 9)}$$

According to the American Society for Testing and Materials (ASTM) Standard D, high potentials, both positive and negative can be related to electrically stabilized colloids (see table 4) [139]. These potentials are describing the interfacial Helmholtz double layer of the particles, which again controls the character and manner of particle behaviour towards specific functional groups of the antigens.

Table 4: Zeta potential versus stability of colloid.

Zeta potential [mV]	Stability of colloid
0 - ± 5	Rapid coagulation of flocculation
± 10 - ± 30	Incipient stability
± 30 - ± 40	Moderate stability
± 40 - ± 60	Good stability
± 61→	Excellent stability

The Zeta potentials were examined for colloids prepared in different vessels in order to predict the optimal compartment for production. These results could additionally be used to examine the stability of the colloid sol. The more charged particles of opposite prefix, the higher the probability of interparticle attraction and the higher the instability. Figure 32 and 33 show the differences of using sterile and non-sterile tubes respectively. The nanoparticles which were prepared in such centrifuge tubes made of polypropylene had different properties. It was proven that the particles prepared in sterile tubes were mainly incipient stable (55 %

particles between ± 10 mV and ± 30 mV). 12.5 % particles had a Zeta potential between 0 mV and ± 5 mV and were according to table 4 rapidly coagulating. The Zeta potentials measured were of positive and negative integers, though most particles were of negative potential (71.3 % particles). Particles prepared in non-sterile tubes were to 75.4 % of negative potential and 11.5 % of positive potential. Overall, a more stable colloid sol was prepared in sterile tubes than in non-sterile, as the potentials were of higher values both positive and negative. 60.7 % particles possessed a Zeta potential between ± 10 mV and ± 30 mV and 9.8 % between 0 mV and ± 5 mV. Figure 34 describes the Zeta potential of the particles which were produced in glass ware. Here, a sol of higher stability was found. 62.6 % particles possessed a Zeta potential between ± 10 mV and ± 30 mV and 14.9 % between 0 mV and ± 5 mV. Here, 78.7 % of total particles possessed a negative Zeta potential. The disadvantage of the production in glass ware was the tedious cleaning procedure. Furthermore, the production was less reproducible in glass ware than in centrifuge tubes. Although a more stable sol was produced in glass, the production in sterile tubes was chosen as the best approach due to the reproducible and straight forward preparation. Additionally, adsorption spectra proved a shelf life of over three weeks which was long enough for the application.

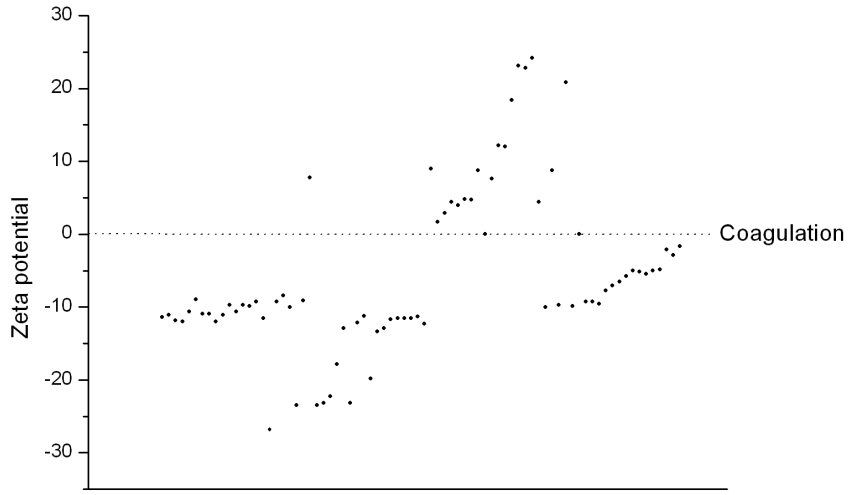

Figure 32: Zeta potentiogram of particles prepared in sterile centrifuge tubes.

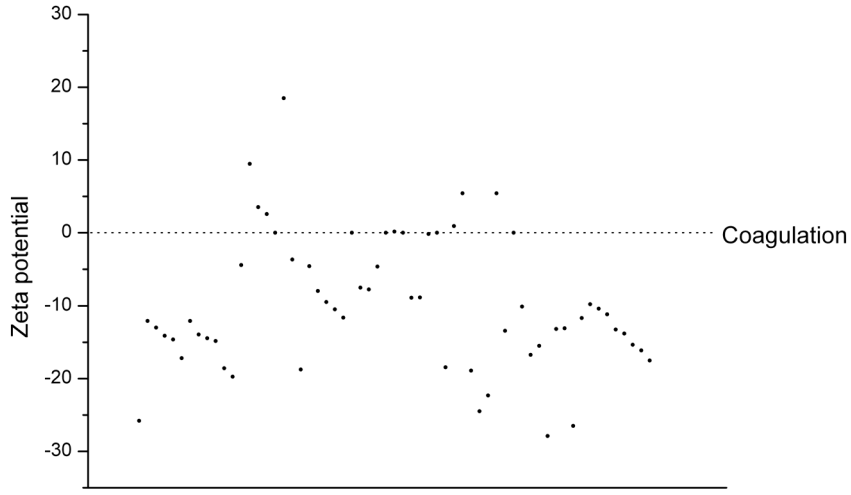

Figure 33: Zeta potentiogram of particles prepared in non-sterile centrifuge tubes.

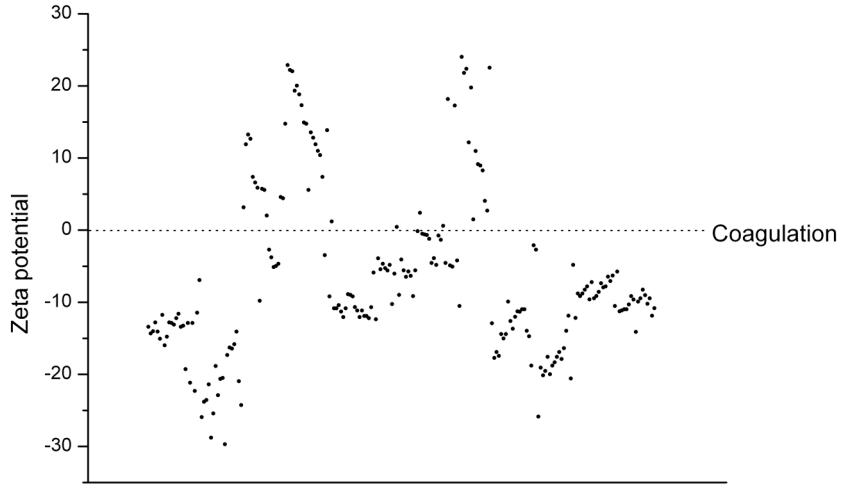

Figure 34: Zeta potentiogram of particles prepared in glass ware.

The Zeta potentials revealed that the silver nanoparticles were present in both negatively and positively charges after production in all three reaction compartments. As the bacteria cell wall consists of different functional groups, it is most probable that different charged particles are attracted to variable functional groups on the bacteria. Not all particles showed a

movement when the electrodes were activated. In glass ware, sterile and non-sterile centrifuge tubes, 2.5 %, 13.1 % and 0.4 % of the particles had a Zeta potential of 0 mV respectively.

There were certain parameters which were important to keep constant to produce reproducible silver sol C. Reducing agent hydroxylamine hydrochloride has a tendency of withdrawing water from the surroundings and should therefore be stored in an dessiccator. It was observed that the production of silver colloids was influenced in this case due to the change in molecular weight of the reducing agent. The synthesis with agglutinated reducing agent showed more polydisperse and larger particles compared to the synthesis using dry reducing agent (could be observed by a redshift of the UV-Vis spectrum). Additionally, a change in reaction temperature influenced the outcome of the sol's size distribution. A reaction temperature of 19 °C was found to be optimal. An examination of the colloid sol, e.g. by UV-Vis, prior to the SERS experiments was therefore crucial. A similar agglomeration phenomenon as with the agglutinated reducing agent could be observed when adding chlorides to the colloid sol. With increasing concentration of salt, the particle sizes within the colloid sol increased (see figure 35). This effect was used in this thesis to force agglomeration in a controlled manner to reach optimal particle sizes for SERS enhancement.

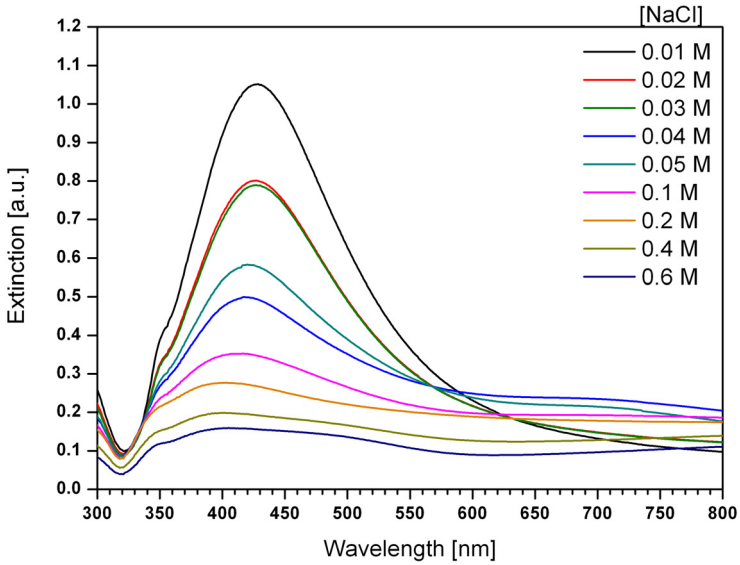

Figure 35: UV-Vis spectra of silver colloid sol C where different concentrations of NaCl were added. The higher the concentration of salt in the sol, the larger the particles grow due to agglomeration.

Enhancement factor

The silver colloids A, B and C were tested as SERS media on the test molecule CV regarding their enhancement and stability of the Raman signal (see table 5). With NR, 10^{-4} M CV (0 M NaCl) was detected with a SNR of 4.6. Here, neither colloids nor salt were added. Sodium chloride in concentrations between 0.01 M and 0.04 M was used as agglomerating agent and added to the different colloid solutions before the Raman measurements, containing various CV concentrations (10^{-5} M – 10^{-12} M). After adding chloride to the metal colloids, their stability declined with time because of agglomeration. Due to this fact, the salt was added to the colloids shortly (ca. 10 s) before the colloids were used to obtain accurate and comparable results. In the case of the colloid sol produced by sodium borohydride (colloid sol A), enhancement factors of 10^4 were obtained by using NaCl concentration of 0 M, 0.02 M and 0.04 M and factors of 10^3 with 0.01 M and 0.03 M NaCl. Colloids produced with tri-sodium citrate (colloid sol B) reached an enhancement factor of 10^8. This increase was obtained by adding 0.01 M to 0.04 M NaCl in 0.01 M steps. When no salt was added, a signal enhancement of factor 10^3 was obtained. The addition of 0.03 M NaCl was found to give the largest signal enhancement of CV using colloid sol C. In this case, we obtained a signal amplification of all CV concentrations tested, at the highest a factor of 10^8. 0.02 M and 0.04 M NaCl generated a signal enhancement of factor 10^8, but showed SNR ratios ≤ 3 for CV concentrations of 10^{-8} M (for 0.02 M NaCl) and 10^{-9} M (for 0.02 M and 0.04 M NaCl). An enhancement factor of 10^4 was obtained by adding 0.01 M NaCl, and a factor of 10^3 with 0 M NaCl. In all further experiments involving microorganisms, the silver colloid sol C prepared according to the modified procedure of Leopold and Lendl was used and 0.03 M NaCl were added before mixing to the analytes, due to the high enhancement factors reached in these experiments. Colloid sol B was not employed due to its limited reproducibility. For a summary of the results see table 7. Here, their adsorption maxima, stability, obtained enhancement factors, reproducibility of production and preparation temperatures are listed

Table 5: Signal to noise ratios of SERS signals of CV mixed with different colloid sols and salt concentrations using He-Ne laser (633 nm) (±: 1s).

Colloid sol	NaCl	Crystal violet (CV) [M]							
	[M]	10^{-5}	10^{-6}	10^{-7}	10^{-8}	10^{-9}	10^{-10}	10^{-11}	10^{-12}
A	0.00	91±1	80±5	13±0.5	4±2	≤3	≤3	≤3	≤3
	0.01	30±5	15±2	8±1	≤3	≤3	≤3	≤3	≤3
	0.02	66±12	38±6	6±2	4±1	≤3	≤3	≤3	≤3
	0.03	75±12	68±4	7±2	≤3	≤3	≤3	≤3	≤3
	0.04	68±11	84±13	13±3	4±1	≤3	≤3	≤3	≤3
B	0.00	97±7	14±4	5±1	≤3	≤3	≤3	≤3	≤3
	0.01	79±17	104±8	26±5	26±13	3±0.5	20±20	23±10	13±12
	0.02	88±23	98±33	61±15	18±11	13±2.8	24±17	7±1	18±12
	0.03	117±18	124±10	98±12	39±14	22±12	6±2	23±8	24±2
	0.04	111±8	119±8	118±14	32±5	4±0.5	17±13	18±7	14±1
C	0.00	17±2	30±5	7±0	≤3	≤3	≤3	≤3	≤3
	0.01	47±7	59±6	19±1	5±0	≤3	≤3	≤3	≤3
	0.02	37±10	65±7	21±5	≤3	≤3	4±0	5±1	4±1
	0.03	22±7	212±16	26±3	17±2	36±7	6±1	7±1	9±4
	0.04	39±3	49±8	58±33	4±0	≤3	11±4	9±1	6±1
NR	0.00	≤3	≤3	≤3	≤3	≤3	≤3	≤3	≤3

SERS measurements employing an Ar^+ laser (514 nm) were carried out to prove the hypothesis that the use of smaller laser wavelength resulted in lower SERS enhancements (see table 6). Figure 35 show that due to salt addition, a redshift of the plasmon resonance and a broadening of the peaks occurred. An enhancement factor of 10^2 was obtained using green laser as excitation source when CV was measured in presence of silver colloid C. A tendency of increasing enhancement with increasing salt concentration was observed. The increase in signal was much lower using Ar^+ laser than obtained in the experiments applying He-Ne laser.

Table 6: Signal to noise ratios of SERS signals of CV mixed with colloid sol C and salt concentrations using Ar^+ laser (514 nm).

Colloid sol	NaCl	Crystal violet (CV) [M]					
	[M]	10^{-4}	10^{-5}	10^{-6}	10^{-7}	10^{-8}	10^{-9}
C	0.00	27	14	4	≤ 3	≤ 3	≤ 3
	0.01	30	30	4	≤ 3	≤ 3	≤ 3
	0.02	19	19	6	≤ 3	≤ 3	≤ 3
	0.03	17	32	10	≤ 3	≤ 3	≤ 3
	0.04	15	29	22	≤ 3	≤ 3	≤ 3
NR	0.00	4.6	≤ 3	≤ 3	≤ 3	≤ 3	≤ 3

Table 7: Silver colloidal sol parameters.

Colloid sol	λ_{max} [nm]	Particle diameter [nm]	Stability	Enhancement factor	Reaction temperature [°C]	Reproduci-bility
A	376	n.a	< 25 min	10^4	10	Good
B	417 - 441	n.a	> 3 weeks	10^8	100	Moderate
C	403	26	> 3 weeks	10^8	19	Good

n.a.: not applicable

4.2.2 Gold colloid sol

A known disadvantage of silver colloids is its toxicity towards bacteria. Silver possesses the ability to inhibit the initial stages of bacteria colonization [140]. Furthermore, the ions can attach to the cell membrane and block the respiration system. If the silver particles are smaller than 10 nm, ribosomes can be attacked and lead to cell destruction. Although the toxicity of Ag has been thoroughly discussed in the SERS community, a negative influence on the implementation in this work is unlikely, as the measurements are carried out right after adding the silver. Alternatively, it is possible to use Au colloids for SERS analysis of microorganisms [39]. Since mainly experiments on heat killed and autoclaved bacteria have been carried out, a comment on a potential toxic effect of the silver

on the analytes could not be made. Different procedures were carried out to produce different shapes and sizes of gold particles. These particles were examined using UV-Vis spectroscopy and TEM. Various preparation methods were tested on their reproducibility and sol stability. Both sphere- and rod-shaped particles were produced for this reason, all including the reduction of $HAuCl_4$. Finally, the SERS enhancement factor of the test molecule CV was derived with the optimal NaCl concentration. An overview of the results is summarized in table 8.

Colloid sol D (reducing agent: $NaBH_4$)

Figure 36a and 36b represent the UV-Vis spectra of the gold colloid sol produced by reducing $HAuCl_4$ with borohydride. In 36a it is shown that the preparation is both reproducible and gives monodisperse particles, as the extinction peak is narrow and has a maximum at 530 nm. Figure 36b proves that the sol is stable for more than 18 days. The TEM image shown in figure 37 illustrates the evenly sized Au particles of 7 nm diameter. For SERS enhancement, a sodium chloride concentration of 0.07 M gave the largest enhancement factor (10^3) for the test molecule CV. This signal enhancement is much lower than the one obtained with colloid sol C (10^8).

Colloid sol E (reducing agent: Na-citrate)

Gold colloids prepared by reducing $HAuCl_4$ with sodium citrate revealed a moderate reproducibility but a stability of over five weeks (see figure 38a and 38b). Preparation 1, 2 and 3 gave extinction maxima at 532, 528 and 519 nm respectively. The peaks differed in intensities and width for preparations 1 to 3. According to the TEM image in figure 39, the sphere-shaped particles were polydisperse with diameters of 7 – 49 nm (average diameter of 15 nm). Addition of 0.02 M sodium chloride gave the largest SERS enhancement factor of 10^4. This signal amplification is several factors smaller than the one obtained using silver colloid sol C (10^8).

Colloid sol F (reducing agent: $NaBH_4$, seed mediated)

The UV-Vis spectra of the rod-shaped Au particles produced by a non-seed preparation method showed the characteristic two maxima at ~510 nm and ~740 nm of gold nanorods. Reproducibility was good over three independent preparations and the colloid sol was stable more than seven days (see figure 40a and 40b). The resulting rods were monodisperse and of 18 nm length and 5 nm width in average according to the TEM image in figure 41. By adding 0.5 M sodium chloride, a SERS enhancement on CV of factor 10^1 was obtained. This was the smallest factor of signal increase obtained comparing sol A - G.

Colloid sol G (reducing agent: $NaBH_4$, non-seed mediated)

A second preparation method of rod-shaped Au colloid sol was tested. This preparation included a seed production with a following growing step. Due to minor reproducibility and stability, these colloids were not further investigated. These rods gave no signal enhancement of the test molecule CV.

A summary of the properties and parameters of the produced gold colloid sols is listed in table 8. The signal enhancements obtained with gold colloids were low in comparison to the enhancement using silver particles. The largest factor resulted by using gold nanoparticle spheres produced by reducing $HAuCl_4$ with sodium citrate (10^4). This preparation was not reproducible and the particles were polydisperse. In literature, it has been stated that nanorods create higher SERS enhancement than spheres due to the generation of higher electric fields at the tips of the rods and have large bent regions enhancing the signal as well [141, 142]. This was not observed in this investigation. Here, the nanorods obtained only a factor 10^1 signal enhancement compared to NR

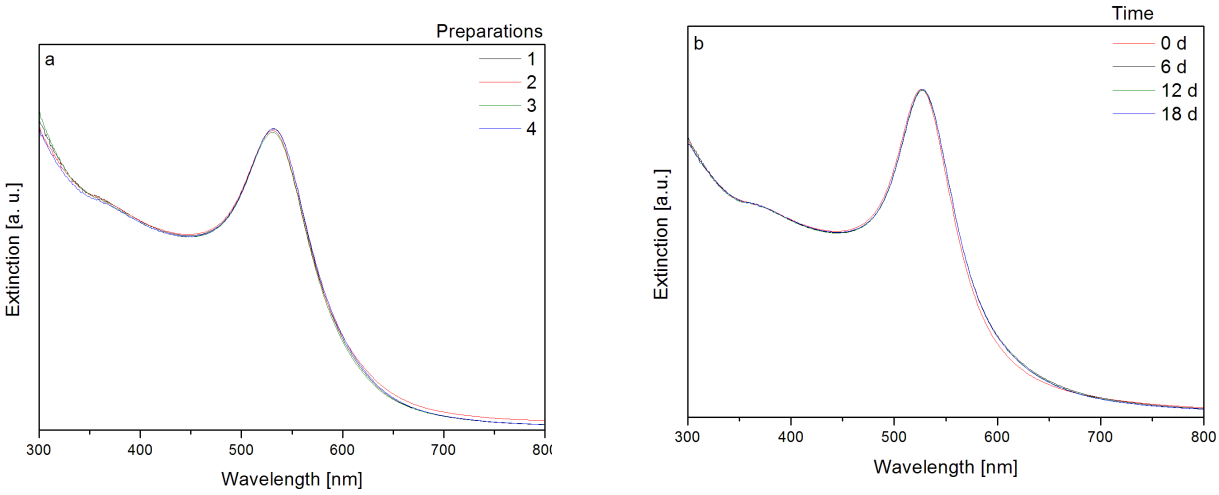

Figure 36: (a) UV-Vis spectra of four separate preparations of gold colloids using borohydride as reducing agent. The preparation method proved to be reproducible. (b) UV-Vis spectra measured after different time periods.

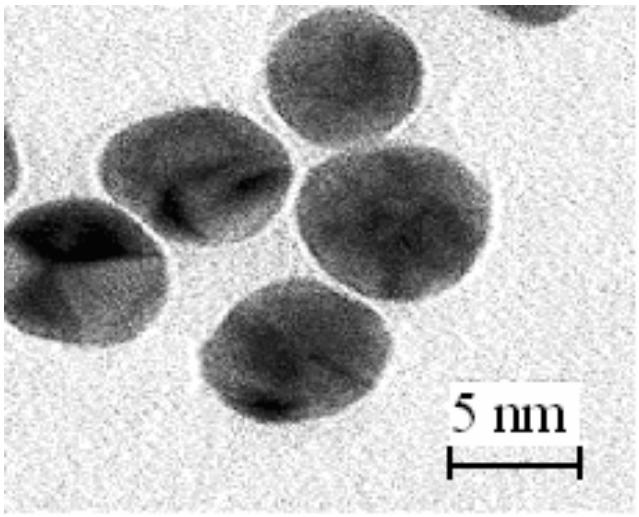

Figure 37: TEM image of Au particles produced by reducing $HAuCl_4$ with borohydride. The particles were of 7 nm diameter and were monodisperse.

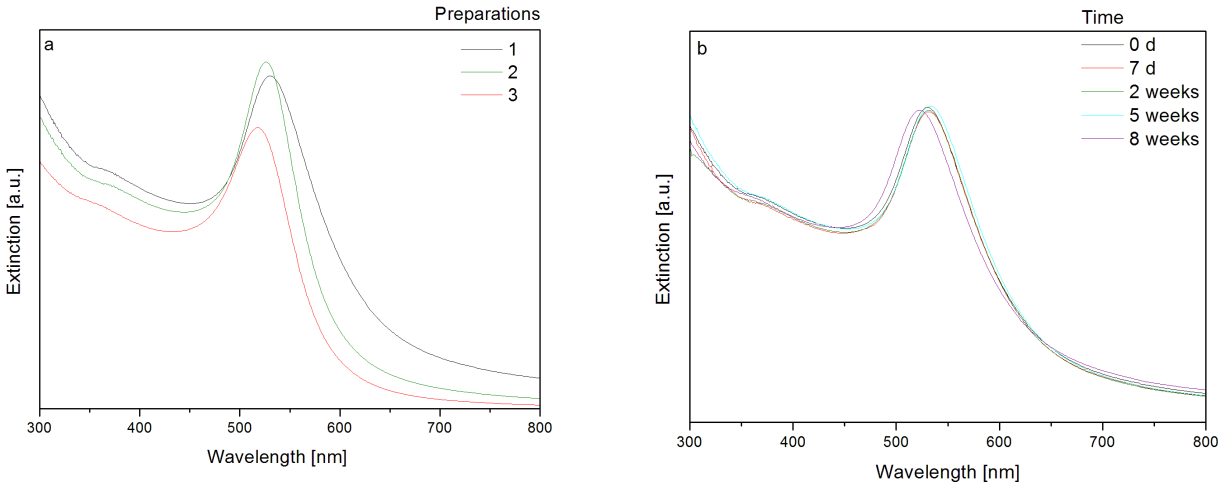

Figure 38: (a) UV-Vis spectra of three independent preparations of Au colloidal spheres produced by reducing $HAuCl_4$ with sodium citrate. The preparation proved not to be reproducible. (b) UV-Vis spectra measured for stability investigation of preparation 2. This sol was stable over five weeks.

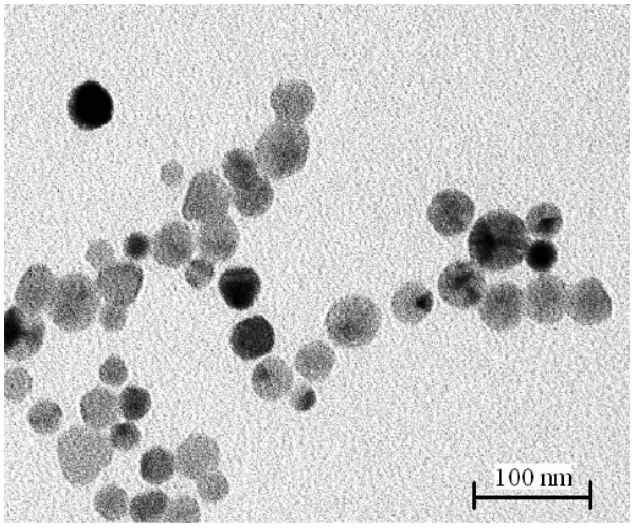

Figure 39: TEM image of Au sphere particles produced by reducing $HAuCl_4$ with sodium citrate. The particles were of 7 – 49 nm (15 nm in average) in diameter and were polydisperse.

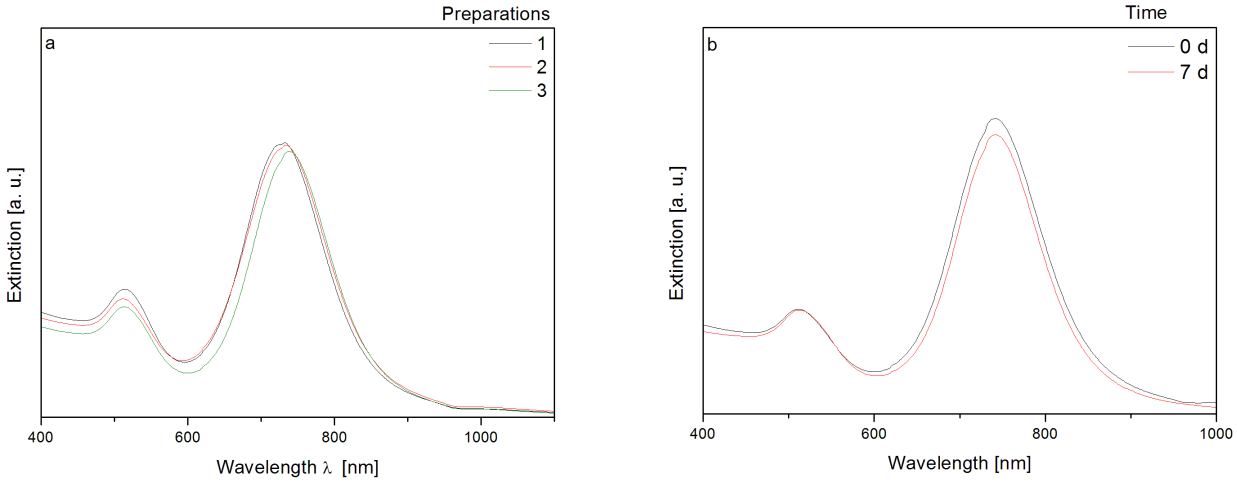

Figure 40: (a) UV-Vis spectra of three independent preparations of rod-shaped Au colloids produced by a seed mediated preparation. The procedure proved to be reproducible. (b) UV-Vis spectra measured for stability investigation of preparation 2. This sol was stable for more than seven days.

Figure 41: TEM image of rod-shaped Au particles produced by reducing $HAuCl_4$ with $NaBH_4$. The particles were of 10 – 25 nm length (18 nm in average) and 3 – 7 nm width (5 nm in average).

Table 8: Gold colloidal sol parameters.

Colloid sol	λ_{max} [nm]	Particle diameter [nm]	Stability	Enhancement factor	Reaction temperature [°C]	Reproducibility
D	530	7	> 18 d	10^3 (NaCl 0.07 M)	10	Good
E	519-530	15	> 5 weeks	10^4 (NaCl 0.02 M)	100	Moderate
F	510, 740	18 l, 5 w	> 7 d	10^1 (NaCl 0.5 M)	60	Good
G	-	-	-	0	19	Poor

The suitability of different Ag and Au colloid sols as SERS media for the label-free *in situ* analysis of microorganisms was studied. Comparing several preparation procedures and optimizing different parameters, a most advantageous approach was identified. Hereby, the effect of agglomeration of the colloids on the SERS cross section of CV was investigated. Stable, monodisperse silver colloid sols were prepared in a reproducible way by reducing silver nitrate with hydroxyl amine hydrochloride at room temperature, according to a modified procedure of Leopold and Lendl (colloid sol C). These colloids showed a shelf life of over three weeks and were later chosen as the optimal SERS media for microorganism detection in solution on a microarray. The silver particles had a diameter of 26 nm and a λ_{max} of 403 nm prior to salt addition. Using this colloid sol with the addition of 0.03 M NaCl, enhancement factors over 10^8 were reached. This optimal agglomeration of the particles obtained with test molecule CV, was successfully implemented in the reproducible detection of three different microorganisms (see section 4.3). The SERS detection of CV using an Ar^+ laser (514 nm) was less effective than the detection using a He-Ne laser (633 nm) as the absorption maxima of the colloids (403 nm) were redshifted and the peak underwent a broadening with the addition of salt. Hence, they were in resonance with higher wavelengths. Additionally, colloid sol C has been implemented in alternative applications since the modified preparation method was developed. The silver sol was for instance used as

precursors for core-shell SERS tags published by Liu *et al.* [143] and as tracers for groundwater research at the Institute of Hydrochemistry (IWC, TUM).

4.3 SERS on bacteria (stationary)

SERS is, compared to infrared spectroscopy, more appropriate for analyzing biological molecules like bacteria in aqueous samples, as water is a weak Raman scatterer. Additionally, SERS has a fluorescence quenching effect, thus further increases the sensitivity compared to normal Raman spectroscopy, like Zhao et al. discussed in detail by means of fullerene molecules and gold nanoparticles [144]. This is due to charge transfer and less radiation energy transfer to the metal surface.

In this thesis, metal particles are added as colloid sol and are surrounding the bacteria. It is expected that the SERS enhancement of the cell wall is at the strongest close to amide and carboxylate groups, as the metals are attracted to these functional groups. The charge of the analyte is important to the analyte-metal adsorption. Furthermore, one can expect a pH dependence of the SERS enhancement of some cell wall molecules like amino acids. The interior of the microorganisms are not detected unless the cells have been destroyed due to overheating or autoclaving. The use of labelling molecules should be avoided as this can result in false positive and false negative analysis due to unspecific binding and insufficient separation of excess labelling molecules. Additionally, the attachment of a Raman reporter molecule to a nanoparticle is limited and hard to reproduce. Moreover, the vibrational information of the reporter is revealed and not the ones of the bacterium cell wall.

The reproducible SERS detection of bacteria is challenging as the composition along the cell walls differs hence, the fingerprint spectra differ in dependence of site of laser focus. A second aspect is that living bacteria can eject different compounds called ejectosomes if they are exposed to light, various concentrations of oxygen, carbon dioxide, nutrition or different temperatures. The uptake of biomass also plays an important role to the bacterium content and changes with the age of the bacterium. In order to validate the method developed, dead bacteria were investigated to limit the variation of cell wall composition throughout the experiments. The first step of method validation was to establish a platform for the qualitative identification of different microorganisms. By carrying out negative controls, potential background signals could be eliminated.

4.3.1 Negative control

For a negative control, colloid sol C was added to the microarray platform holding anti-*Legionella* antibodies and a SERS map (static mode, 1100 cm^{-1} – 1500 cm^{-1}, 600 µm × 600 µm area, 25 µm steps, λ_0 = 633 nm, 1 s laser exposure) was developed on the microarray surface. No significant background signals were revealed from the surface material or the antibodies between 1100 cm^{-1} and 1500 cm^{-1}. Figure 42 illustrates a SERS map with no hits of 1380 cm^{-1} peak of the surface material. Hence, SERS spectra collected from bacteria immobilized to the surface will only reveal peaks originated from the bacterium itself in this wavenumber range. An explanation why the antibodies are SERS inactive on the microarray platform, could be that the concentration (1.3 mg/mL) is too low for SERS enhancement.

In solution, extended SERS spectra (extended mode, 400 cm^{-1} – 2000 cm^{-1}, λ_0 = 633 nm, 10 s laser exposure) were measured of reagents used for the microarray preparation (i.e. casein and coating buffer). Only a few weak peaks and a certain level of fluorescence was observed of both reagents (see figures 43 and 44).

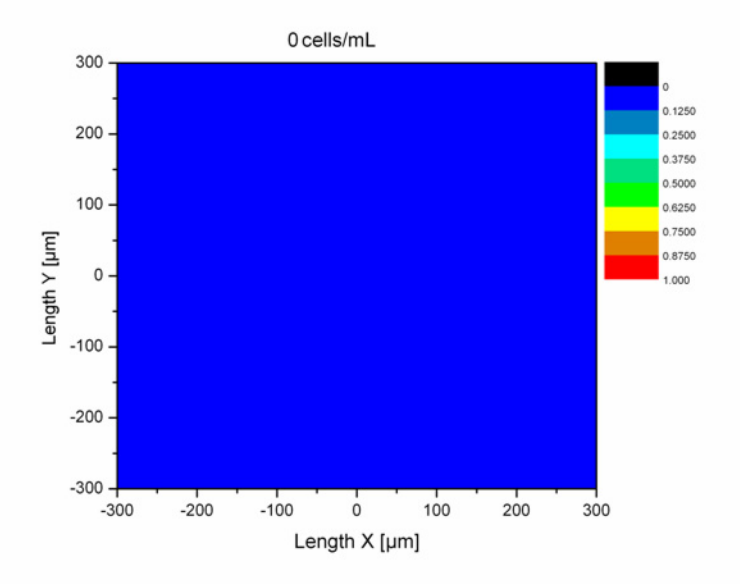

Figure 42: SERS map of microarray surface holding anti-*Legionella* antibodies using 1380 cm^{-1} peak. Blue colour represents a peak intensity of 0 a.u. No hit was detected.

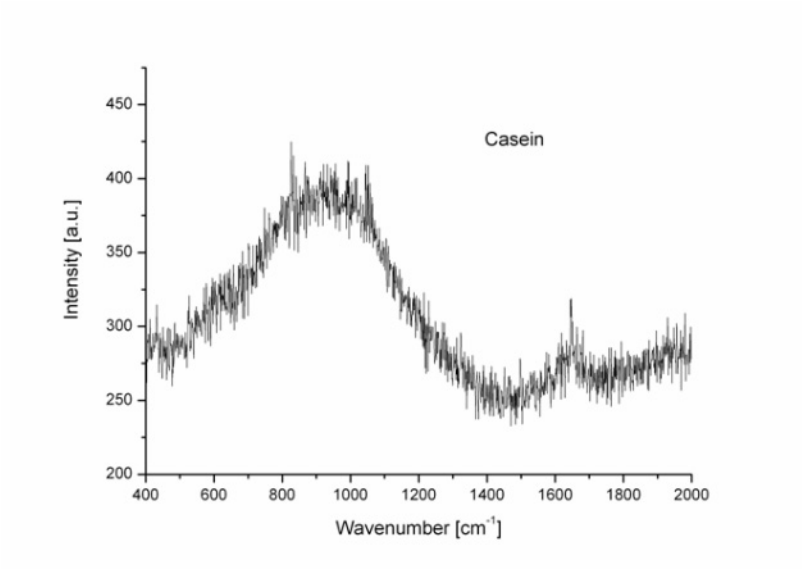

Figure 43: SERS fingerprint spectrum of casein.

Casein is a main component in milk and contains a mixture of large protein molecules. In the SERS spectra of casein, a broad peak at 950 cm^{-1} and a weak peak at 1680 cm^{-1} were observed. The intensities lied below 400 a.u. and represented no disturbance to the SERS detection of bacteria on the immunoassay. (SERS signals of microorganisms are stronger than 400 a.u.)

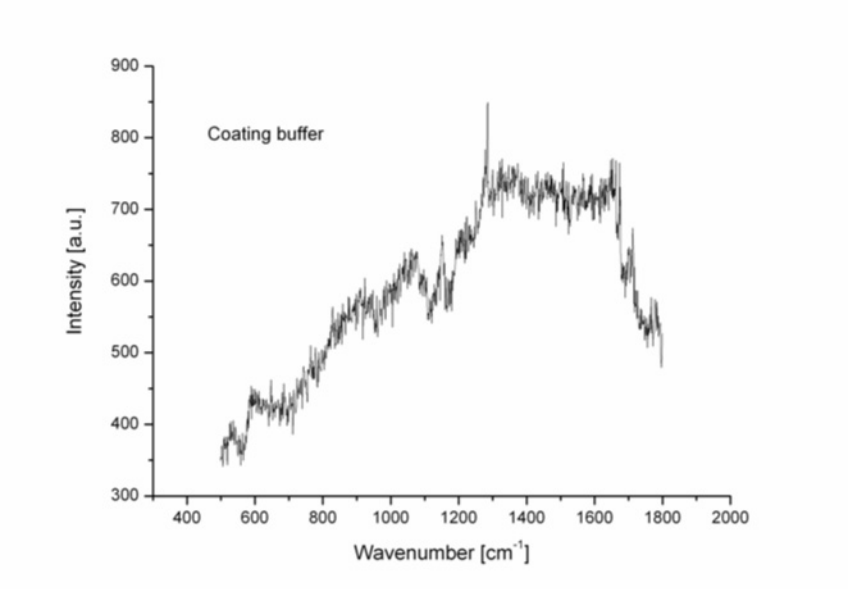

Figure 44: SERS fingerprint spectrum of coating buffer.

The fingerprint spectrum of coating buffer showed an increasing fluorescence background with increasing wavenumber. Weak peaks at 550 cm^{-1}, 1050 cm^{-1}, 1150 cm^{-1}, 1700 cm^{-1}, 1800 cm^{-1} were visible, but showed low SNR. Signal intensities did not exceed 850 a.u. and did not disturb SERS fingerprint spectra of bacteria which are usually observed > 1000 a.u.

Mapping of dehydrated bacteria

Literature states that a recognition and identification of numerous bacteria species is possible with SERS if the cells are dried on simple objective plates in the presence of noble metal particles (Ag, Au and Cu) at a specific size range (20 – 100 nm) [97]. It is also stated that dehydrated bacteria most probably exhibit differences in the SERS fingerprints compared to cells of same strain in solution. This approach is more complicated because the metal particles are in suspension as well and cannot be that easily attached to the cell wall in order to come in close contact to the analyte for SERS enhancement. As one of the approaches to validate the method of *in situ* SERS identification and quantification on a microarray, *L. pneumophila* cells mixed with colloid sol C (0.03 M NaCl) were examined on clean and empty glass objective plates. Several vibrational modes of the bacterium fingerprint were mapped and compared to the optical image of the scanned area (see figure 45).

The maps were collected with following parameters starting from top to bottom: (200 µm × 200 µm, 30 µm × 30 µm and 10 µm × 10 µm) of figure 45. A good reproduction of the optical images by SERS mapping was obtained at 1150, 1163, 1200, 1240, 1300, 1320, 1400, 1455 1526, 1570 and 1600 cm^{-1}, which are the vibrational modes of polysaccharides, proteins and lipids (see table 1) which are components of the bacterium cell wall. With this knowledge, a good starting point of the validation procedure had been set for the detection in water. How a controlled agglomeration of metal particles onto the bacterium cell wall by *in situ* SERS measurement can be carried out is discussed in section 4.3.2.

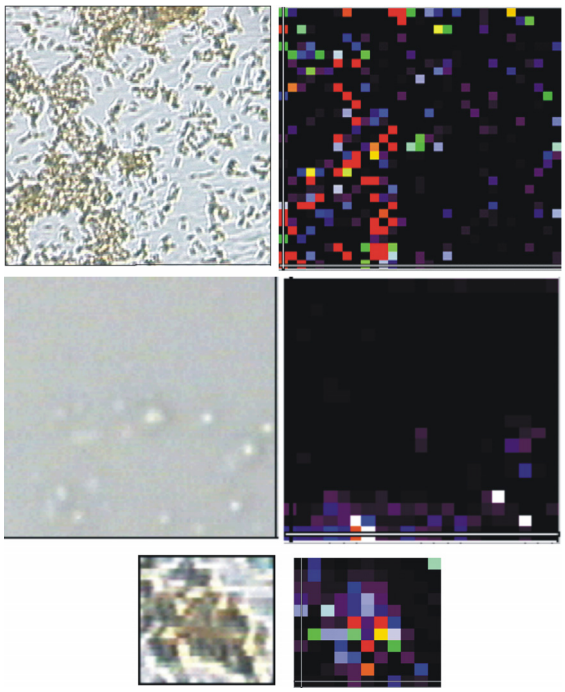

Figure 45: SERS imaging of *L. pneumophila* on clean glass slides. From the top to bottom the area of mapping is decreasing (200 µm × 200 µm, 30 µm × 30 µm and 10 µm × 10 µm). On the left hand sides the optical images of the SERS mapping area are shown and on their right the obtained SERS images respectively.

4.3.2 Importance of colloid agglomeration onto the bacteria

The extent and the way of Ag colloid agglomeration are important for the success of the SERS measurements. In order to optimize the agglomeration efficiency, two methods were tested to obtain directed formation of particle agglomerates onto the bacterial cell wall. Hereby, the bacteria suspension was diluted in either PBS buffer or carbonate buffer containing 0.01 % sodium azide. Sodium azide was added to the bacteria to obtain directed formation of particle agglomerates onto the bacterial cell wall. Azide binds to the cell wall and causes an additional negative charge on the outer wall [66]. This high negative charge attracts the metal nanoparticles and forces their agglomeration on the cell wall.

S. typhimurium and *L. pneumophila* cells were immobilized onto an diamino-PEG-ylated surface containing the corresponding antibodies. The microarray spots containing antibody-antigen immuno-complexes were 500 µm in diameter. Bacteria lengths were in the range of 2 – 20 µm. The time of measurement was 10 s for each spectrum. Silver colloid sol C with 0.03 M NaCl was applied, which gave the highest enhancement factor of the test

molecule CV. When the bacteria suspension was diluted and incubated in PBS on the microarray surface, a weak SERS signal was observed, resulting in only limited efficiency of microorganism detection for both *Salmonella*, *Legionella* and *E. coli*. In figure 46a this effect can be seen on a *Salmonella* cell. This limited efficiency was due to an inadequate rate of colloid agglomeration on the site of measurement. In addition, the site of agglomeration could have been too far away from the targets. In this case, SNRs were also relatively low (10) and high fluorescence background was observed. If the colloids were agglomerated directly onto the bacterial cell wall, over 90 % of the microorganisms visually identified on the chip revealed specific SERS spectra (see figure 46b for an example of the phenomenon on a *Salmonella* cell). This was accomplished by incubating the bacteria on the microarray surface in carbonate buffer, containing sodium azide. Hereby, the azide bound to the outer cell wall making it more negatively charged. The colloidal particles of colloid sol C, which possessed to 71.3 % negative Zeta potentials (see figure 32), experienced a higher attraction to the more negatively charged cell wall. A 6-fold raise of the SNR was obtained (from 10 to 59). The red and black dots in the figures indicate the sites of measurements.

Compared to conventional detection principles, the tool based on SERS has the potential of reaching higher sensitivities due to the low background noise and strong specific signal conversion. An optimization of the rate of silver particle agglomeration as well as the distribution of the particles on the cell wall, resulting in formation of “hot spots” on the bacteria surfaces was carried out. As a result, the label-free detection of *S. typhimurium*, *L. pneumophila* and *E. coli* on an immunoassay platform in water, with high resolution was feasible. In comparison to NR spectra of *S. typhimurium* (not shown), high enhancement factors by means of the described directed agglomeration of silver particles on the bacteria surface were obtained. The experiments were carried out *in situ*.

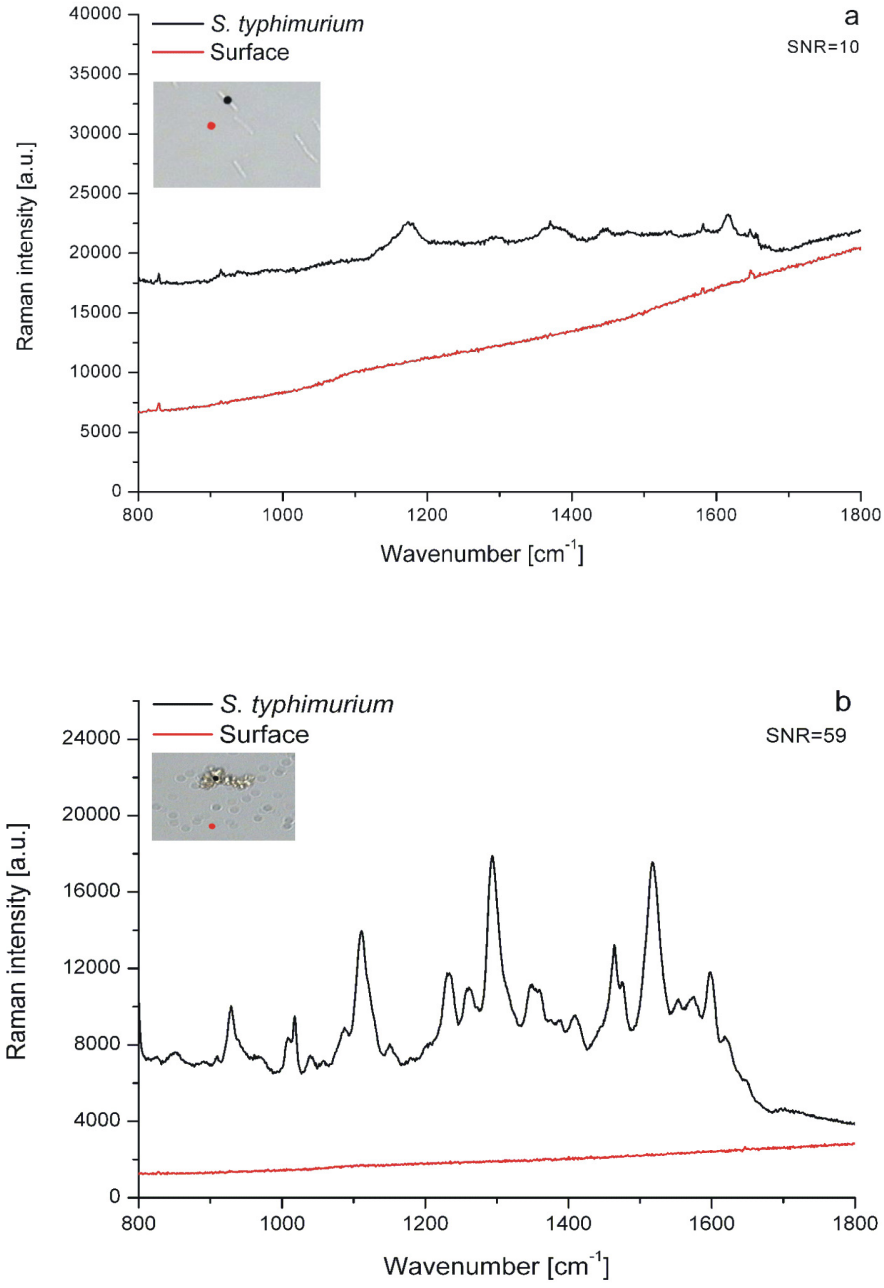

Figure 46: SERS spectra of *S. typhimurium*. (a) The surface material was detected under the same conditions as the analytes and showed no peaks in the fingerprint area of the bacterium (accumulation time 10 s). Incubation was carried out in PBS which resulted in only weak signals and a low probability of hit. (b) Incubation carried out in carbonate buffer containing azide, which induced specific agglomeration of the colloids at the site of bacteria cell wall, resulting in a signal enhancement and an evident increase of hit probability.

4.3.3 Identification of bacteria

It is known that bacteria exhibit specific fingerprint spectra below 1500 cm^{-1} and species specific differences in relative signal intensities can be distinguished [34]. Reliable identification of *L. pneumophila*, *S. typhimurium* and *E. coli* was possible by means of their whole-organism fingerprint spectra (see figures 47 - 50). Reproducible fingerprint spectra of *L. pneumophila* and *S. typhimurium* were collected from different sites on single bacterium cells (figures 47a and 48a) as well as from different cells (figures 47b and 48b) for both species. Minor shifts in the fingerprint spectra of bacteria occur in dependence of the site of measurement on the bacteria cell wall. The cell wall contains different structural features made of proteins, lipids, phosphate and carboxylate groups. The SERS enhancement occurs in dependence of the nanoparticle distance to the site of measurement, and due to this, the spectra collected on the same cell give subtle changes on the Raman response (see figures 47a and 48a). On the other hand, the spectra collected on three different bacteria are all made in the same region of the bacteria cell wall (tip of bacteria) where the silver nanoparticles tend to agglomerate preferably. We believe this is due to the higher negatively charge of the bacteria cell wall at this site after introducing sodium azide.

Differences in the cell wall consistency (e.g. proteins, lipids and carbohydrates) gave rise to the variations of vibrational mode compositions and, in consequence, relative signal intensities. Due to the signal enhancement caused by the silver nanoparticles, which were agglomerated directly on the cell walls, high signal to noise ratios were achieved and identification was possible for all analytes (see table 9). The largest differences were found in the Raman shift originated from Amide I, $\delta(CH_2)$ saturated lipids, Phe ring breath., $\rho(CH_2)$ and Phe skeletal bands found at 1640 – 1680 cm^{-1}, 1440 - 1460 cm^{-1}, ~1000 cm^{-1}, 720 – 730 cm^{-1} and 620 cm^{-1}, respectively (see figure 49). *L. pneumophila* exhibited strong peaks for the Amide I, II and III vibrational modes, while *S. typhimurium* featured strong peaks only for Amide II and III and a weak signal for the Amide I vibrational mode. In the case of *L. pneumophila* and *S. typhimurium*, these variations are not due to differences in particle agglomeration, as reproducible spectra were measured from several cells of the same colony. Experimental data of *E. coli* were only collected from one cell. Fingerprint spectrum of living *E. coli* was measured under the same conditions as described above for *L. pneumophila* and *S. typhimurium* (see figure 50). The combinations of vibrational modes were distinguishable from the ones derived from dead *L. pneumophila* and *S. typhimurium* cells. Strong signals of $\delta(CH_2)$ saturated lipids, $\nu(COO^-)$ symmetric, Amide III bands were found in the regions of

1440 - 1460 cm^{-1}, 1360 - 1440 cm^{-1} and 1250 – 1310 cm^{-1} respectively. Weak signals appeared of Amide I, Phe ring breath., $\rho(CH_2)$ and Phe skeletal bands found at 1640 – 1680 cm^{-1}, ~1000 cm^{-1}, 720 – 730 cm^{-1} and 620 cm^{-1}, respectively. Reproducible spectra from different sites on a single *E. coli* cell are illustrated in figure 51.

The coverage of the metal particles on the cell wall plays an important role for the reproducibility of the fingerprint spectra. In these stationary measurements, the agglomerated particles were assumed to be mainly sediments produced by adding sodium chloride to the colloid sol. Some of these particles probably agglomerate too large to produce SERS enhancement and could block the respective sites on the bacteria cell wall for SERS activity. These large agglomerates were observed by eye. Though, it can be assumed that mainly the agglomerated particles remain in the size range known for SERS enhancement (20 - 100 nm). Due to these differences in number of agglomerates in different size ranges, the obtained fingerprints may differ. This is a huge drawback of the SERS method and quantitative SERS analysis becomes difficult as the reproducibility of enhancement factors is poor. In the next chapter, this problem is solved and explains the reproducible quantitative analysis of multiple bacteria on microarray.

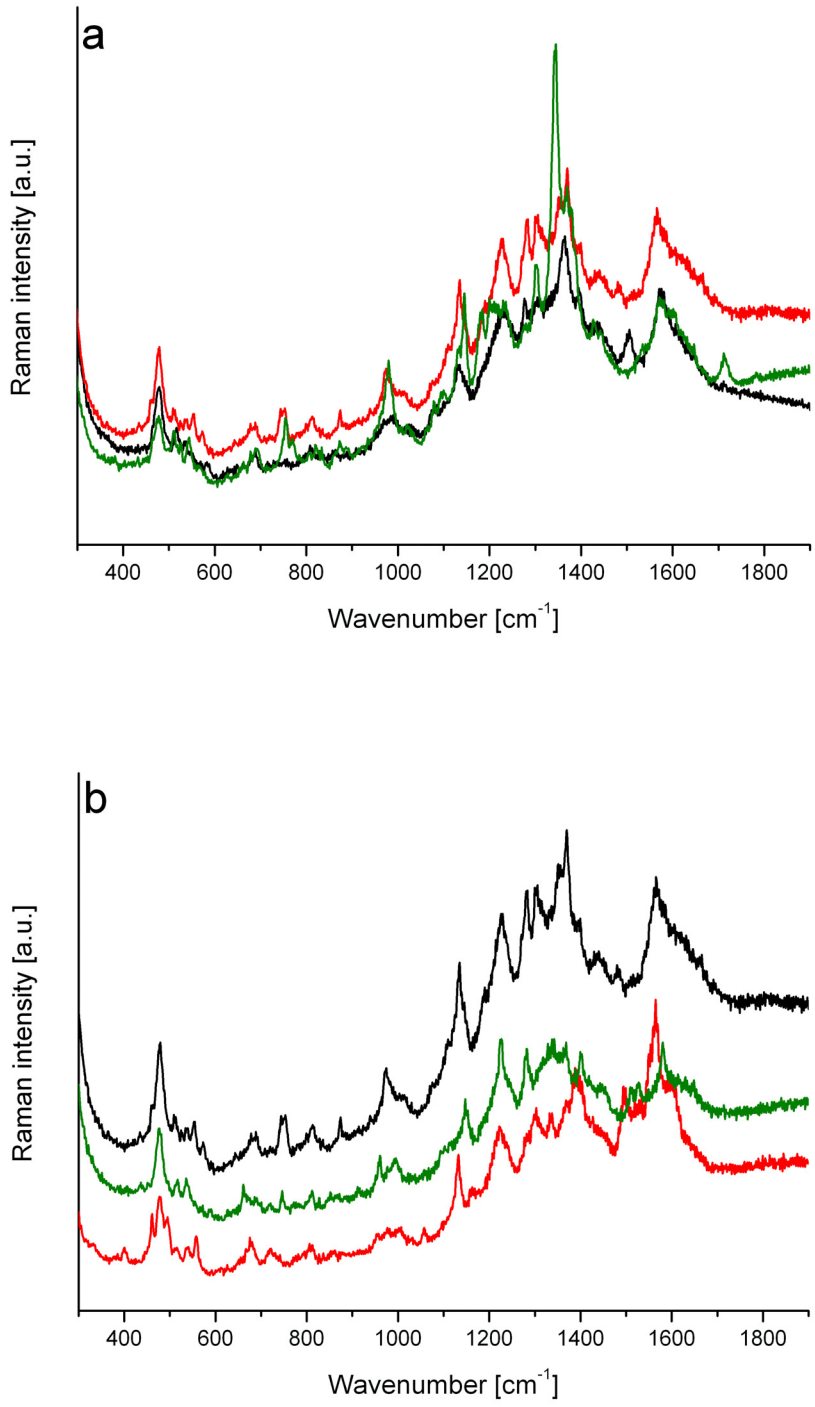

Figure 47: Reproducibility of SERS measurements on *L. pneumophila* cells. (a) Three different spectra measured at different sites on the same cell. (b) Three spectra from three different cells on the same microarray chip.

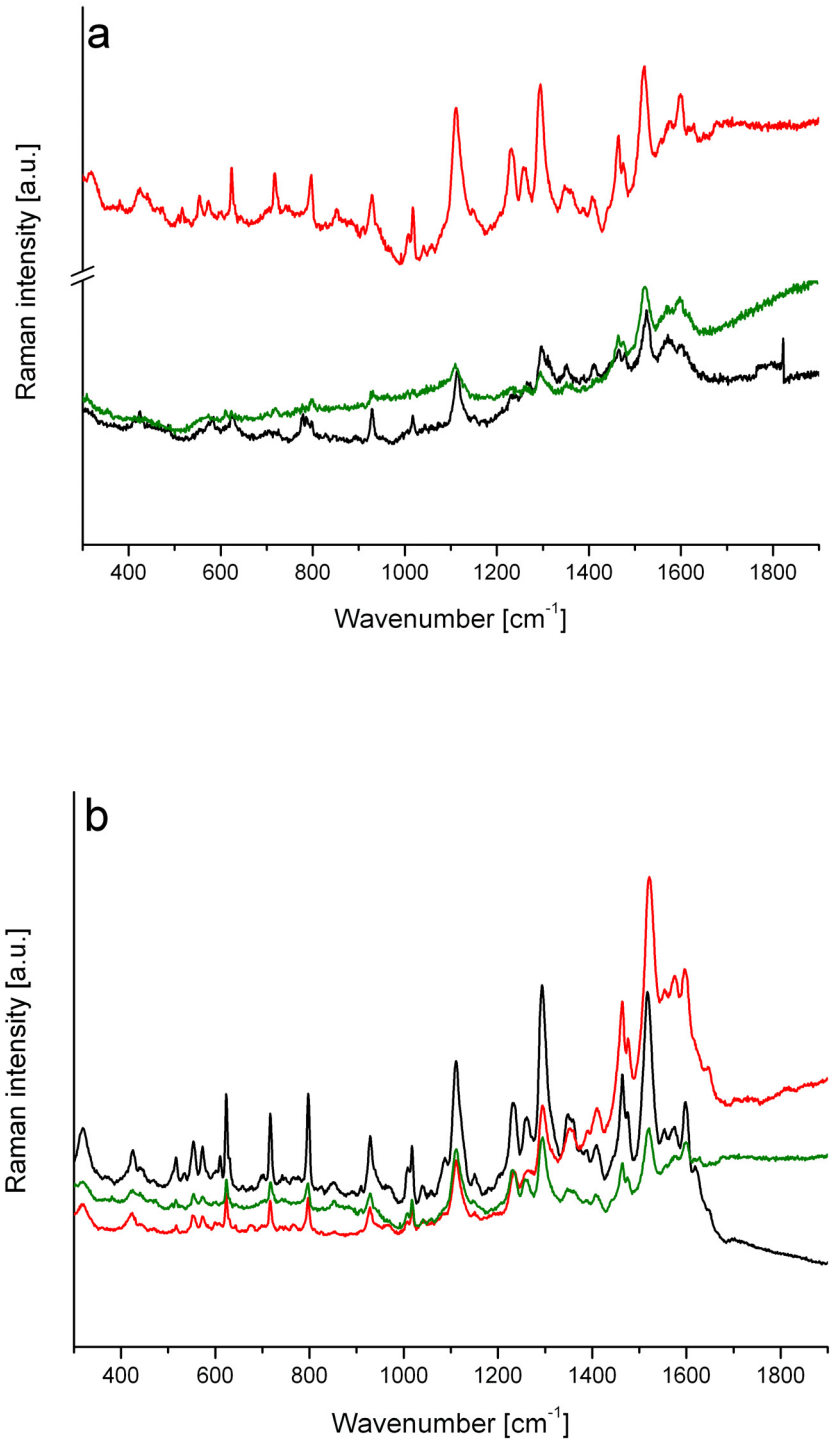

Figure 48: Reproducibility of SERS measurements on *S. typhimurium* cells. (a) Three different spectra measured at different sites on the same cell. (b) Three spectra from three different cells on the same microarray chip.

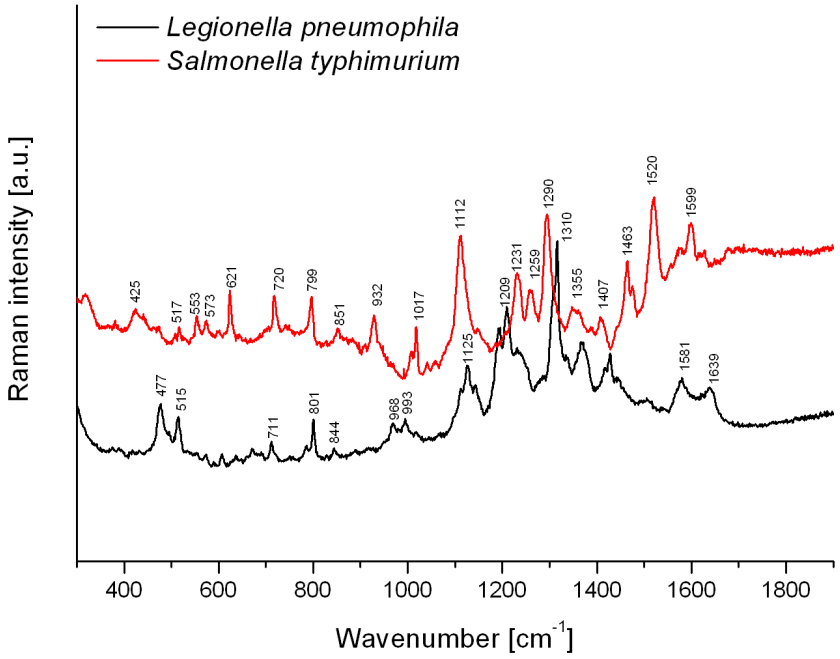

Figure 49: SERS spectra of *S. typhimurium* (red) and *L. pneumophila* (black).

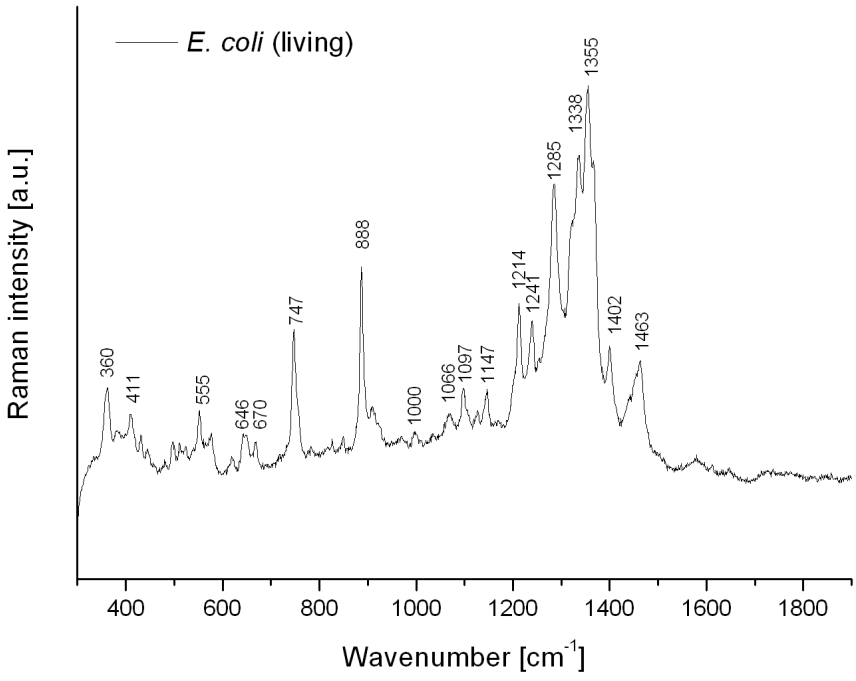

Figure 50: SERS spectra of living *E. coli.*

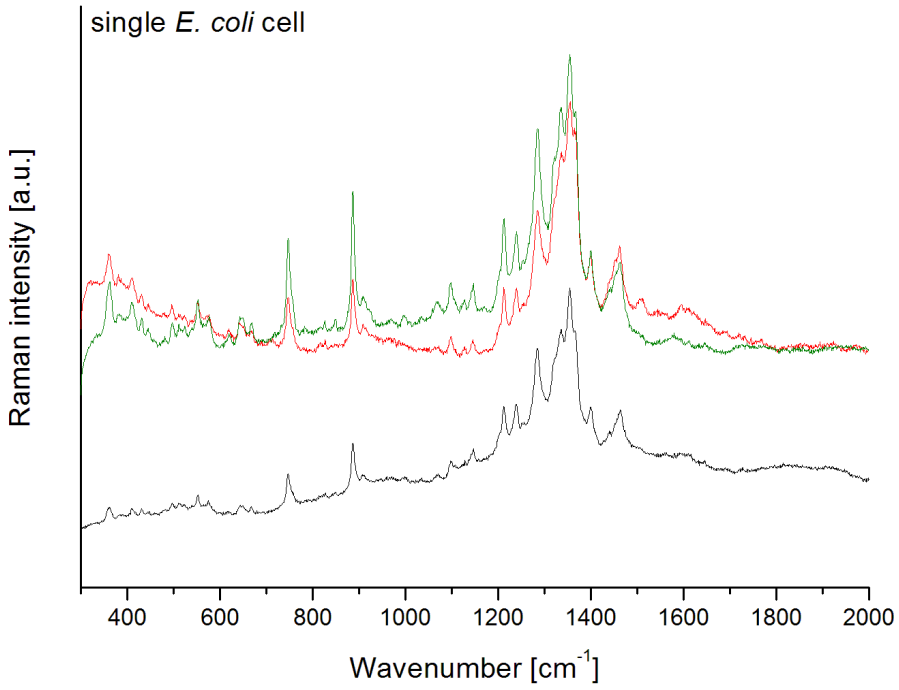

Figure 51: Reproducibility of SERS measurements on living *E. coli* cells where three different spectra were measured at different sites on the same cell.

In figure 52a, a TEM image of an MC4100 *E. coli* cell is shown which is covered by silver colloids. Hering *et al.* [145] published this photo originally made by Efrima *et al.* [35] with additionally SERS fingerprint spectra from two other research groups (Zeiri *et al.* 2004 and Jarvis *et al.* 2004) of *E. coli* (λ_0 633 nm) (figure 52b). These fingerprints were compared to the spectra obtained in this work on *E. coli* (λ_0 633 nm) (figure 50). It could be concluded that in the region between 1200 cm^{-1} and 1500 cm^{-1}, the fingerprints are very similar. The strong peaks of $\delta(CH_2)$ saturated lipids, $\nu(COO^-)$ symmetric, Amide III were found in all four fingerprint spectra. In the wavenumber region smaller than 1200 cm^{-1}, varieties were observed. The main differences of the cell properties of these four experiments were that in figure 52 only SERS spectra of dehydrated cells were discussed. These results suggest for varying composition of the molecular structures on the cell wall of a living cell. This explains the diversities of SERS fingerprints in figure 50 to figure 52

Furthermore, Segupta *et al.* published in 2007 a fingerprint spectrum of *E. coli* which had peaks at 1627, 1572, 1521, 1459, 1401, 1344, 1268, 1150, 1078, 828, 798, 739, 615, 543 and 1240 cm^{-1} [54]. Many of these vibrational bands were found in figure 50. Peaks in the

region 500 - 1100 cm^{-1} are due to the various functional groups that are present in the bacteria cell including glycosides, nucleic acids (cytidine, uracil), proteins (tyrosine), phenylalanine, carbohydrates and unsaturated fatty acids and lipids [107].

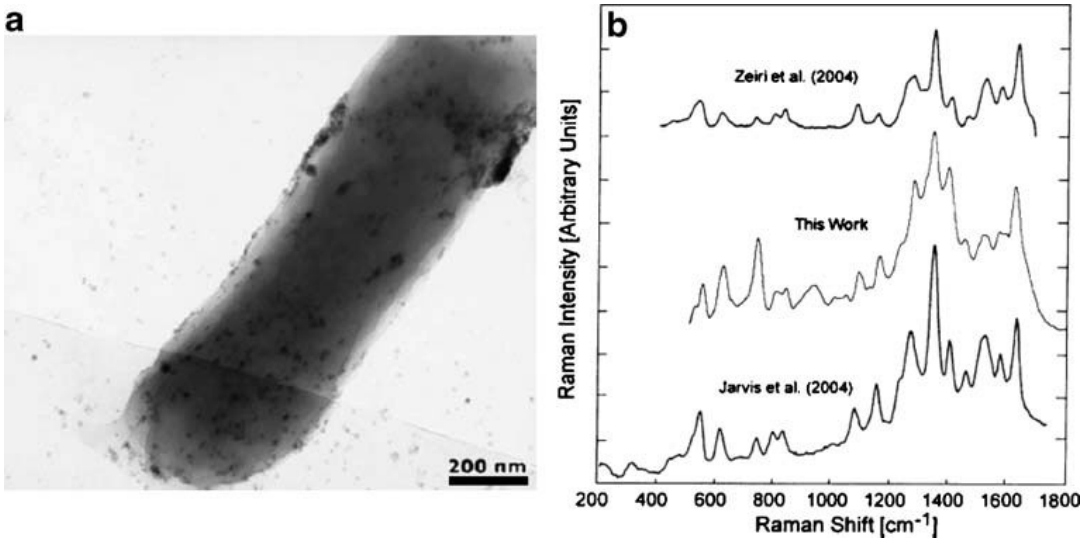

Figure 52: (a) A TEM image of an *E. coli* cell covered by silver nanoparticles [35]. (b) Fingerprint spectra of *E. coli* found by three different research groups [145].

Table 9: Raman shifts of *L. pneumophila, S. typhimurium* and *E. coli* and their relative intensities for qualitative analysis of SERS vibrational modes.

Vibrational mode	Wavenumber [cm^{-1}]	*L. pneumophila*	*S. typhimurium*	*E. coli*
Amide I	1640 – 1680	s	w	w
δ(NH)	1546 – 1645	s	s	w
ν(CN)	1546 – 1645	s	s	w
Amide II	1540 – 1645	s	s	w
δ(CH_2) saturated lipids	1440 – 1460	w	s	s
ν(COO^-) sym.	1360 – 1440	s	s	s
Amide III	1250 – 1310	s	s	s
(CC) ring breath. assym.	1150 – 1160	w	w	w
(CO) ring breath. assym.	1150 – 1160	w	w	w
ν(CC) aromatic ring (Phe)	~1000	w	s	w
ρ(CH_2)	720 – 730	w	s	w
Phe skeletal	625	w	s	w

δ, deformation; ν, stretching; ρ, rocking; Phe, phenylalanine; breath., breathing; s, strong; w, weak.

L. pneumophila, S. typhimurium and *E. coli DSM1116* revealed specific SERS spectra. In comparison to NR spectra of *L. pneumophila*, *S. typhimurium* and *E. coli* (not shown), high enhancement factors using the colloids produced by the modified procedure of Leopold and Lendl (colloid sol C) were obtained. The vibrational modes of the analytes are listed in table 9. Both, COO^- and NH_2 vibrational modes are present in the fingerprint spectra of *L. pneumophila*, *S. typhimurium* and *E. coli* in the wavenumber region of 1360 – 1440 cm^{-1} [109]. The presence of these modes suggests that at least some of the adsorbed silver colloids interact with the analyte through amine and carboxylate groups. The bands in the region 1250 - 1310 cm^{-1} are assigned to Amide III, which primarily involves NH bending and ν CN [32]. The bands at 1540 – 1645 cm^{-1} are assigned to Amide II, which arises mostly from NH bending [34]. The bands at 1640 – 1680 cm^{-1} are assigned to Amide I, which involves predominantly ν CO and ν CN [109].

4.3.4 Quantitative analysis of bacteria

For quantification, SERS spectra were collected in a given raster distributed over three different spots for each analyte and concentration on the microarray. The maps collected for the calibration curve in figure 54 were generated using single peak mapping of the respective fingerprint spectra, which were obtained in an 25-µm raster within an area of 600 µm × 600 µm (λ_0 = 633 nm, 1 s exposure time). Surface coverage of *S. typhimurium* was analyzed using these maps where suspensions of different concentrations were quantified by means of the Amide III band at 1290 cm^{-1}. If the peak area of the Amide III band was larger than six times of the standard deviation of background spectra, it was defined to be a positive detection. Nevertheless, these results revealed large standard deviations which were due to increasing agglomeration of the particles on the bacteria cell wall with time. The agglomeration was observed under microscope and was caused by a temperature rise in the laser exposed solution. This change in temperature developed as the time of laser radiation increased. In figure 53 a, b and c, microscopic images are shown of the site of SERS map origins of measurements after 40, 80 and 120 min laser exposure, respectively. An agglomeration with respect to laser exposure time was observed on this microarray holding *S. typhimurium* immuno-complexes. The same effect was observed with *Legionella* as analyte. In figure 55, the dependence on SERS intensity vs. particle agglomeration, caused by the increasing temperature of solution, is illustrated. In order to raise the reproducibility of the quantitative analysis, it was important to measure each concentration after identical time of laser exposure to the solution. Figures 55 and 56 highlight this effect. With increasing radiation time, the number of hits per map increased. If the quantitative mapping procedure was carried out after an equal time period of laser radiation in the solution, the number of hits per map stabilized. This was obtained by renewing the microarray platform prior to each quantitative experiment.

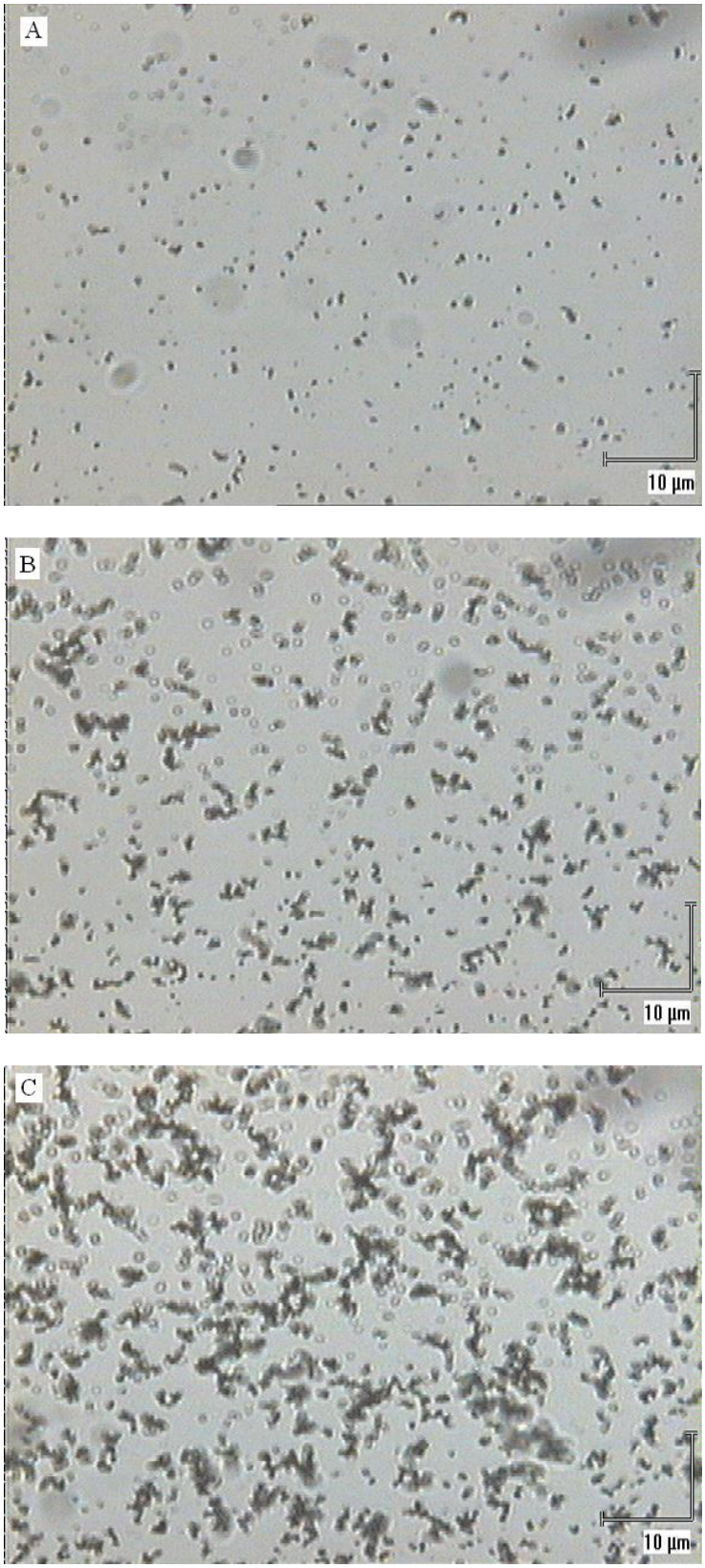

Figure 53: Microscopic images of the sites of SERS mapping origins after 20 min (a), 40 min (b) and 80 min (c) laser exposure to the solution. An increasing particle agglomeration with laser exposure time, is caused by increasing temperature of solution.

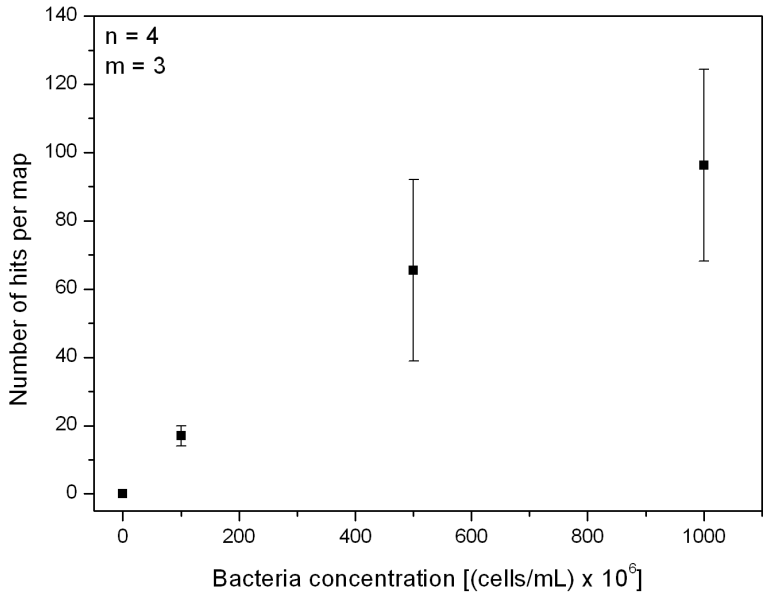

Figure 54: Calibration of *S. typhimurium* obtained by mapping the Amide III vibrational band.

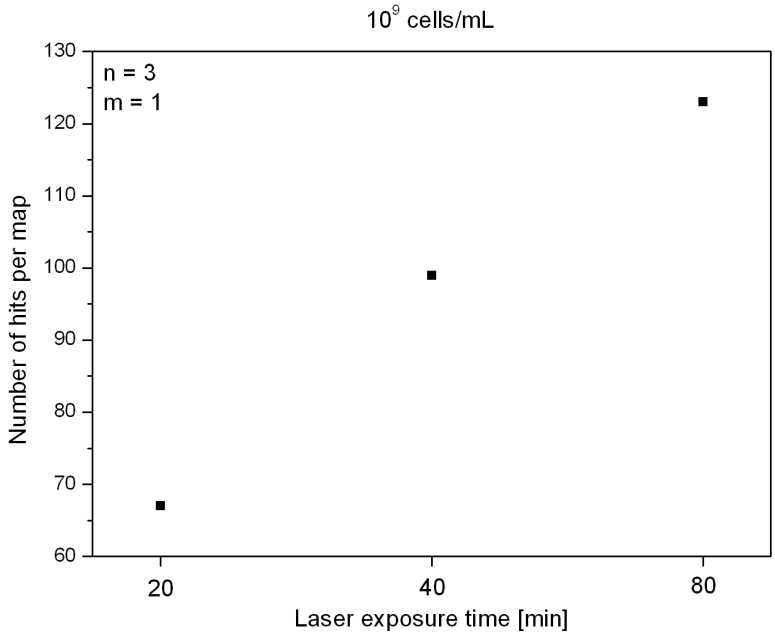

Figure 55: Quantitative results gained by mapping three different spots on the same microarray holding *S. typhimurium* with a concentration of 10^9 cells/mL. The maps were measured after 40, 80 and 120 min laser exposure to the solution.

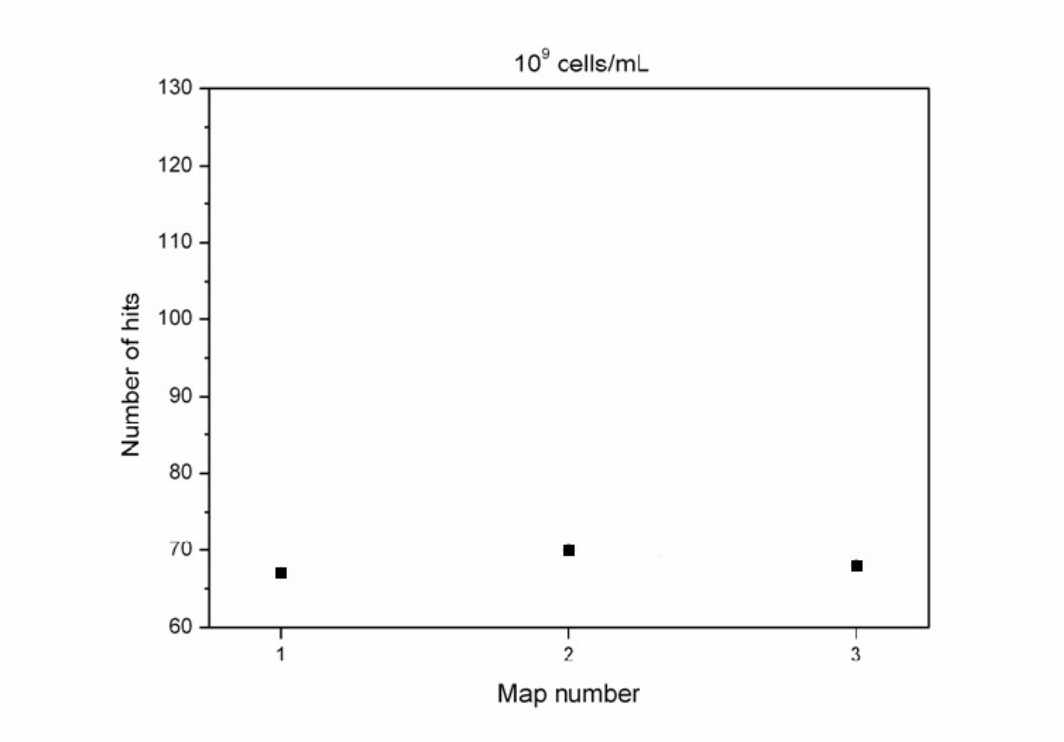

Figure 56: Quantitative results gained by mapping three different spots on different microarrays holding *S. typhimurium* with a concentration of 10^9 cells/mL. The maps 1-3 were measured after 40 min laser radiation to the solution.

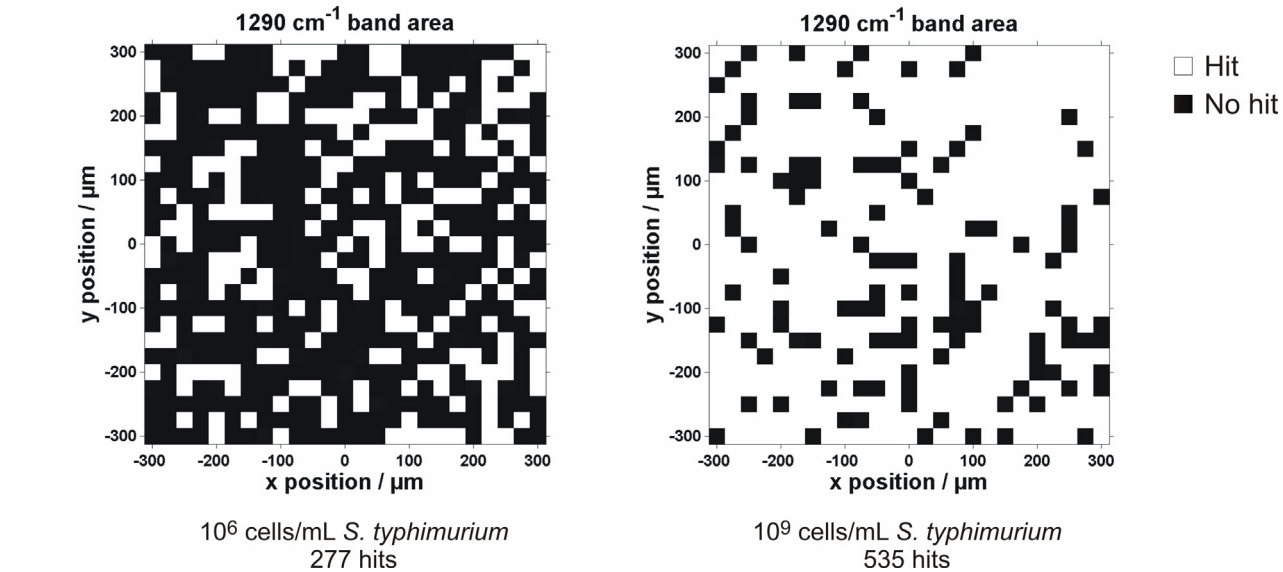

Figure 57: Typical SERS maps of a microarray surface covered with *S. typhimurium*. The white colour indicates a hit, and the black no hit. (left) A map of a spot holding 10^6 cells/mL which resulted in 277 hits. (right) A map of a spot holding 10^9 cells/mL which resulted in 535 hits.

A spatially resolved mapping analysis was used to create calibration curves for different species. Concentrations between 10^6 and 10^9 cells/mL were examined for *S. typhimurium* and between 10^8 and 10^9 cells/mL for *L. pneumophila*. Each concentration was measured three times on different microarray chips. Figure 57 shows typical Raman maps of a microarray surface covered with *S. typhimurium* concentrations of 10^6 and 10^9 cells/mL. Each visible white spot represents the presence of a bacterium. As the steps were larger than the largest possible bacteria, double counting of a single bacterium was ruled out. The signal intensities varied, probably due to variations in colloid agglomeration around a bacterium, but the fingerprint spectra remained constant. In figures 58 and 59 calibration curves of *S. typhimurium* and *L. pneumophila* suspensions are shown. All data points were obtained after 40 min laser radiation to the solution in the stationary tray. An increasing number of hits per map with increasing concentration of analyte was observed. In comparison to the calibration curve of *S. typhimurium* shown in figure 54, standard deviations decreased when time of laser exposure of solution was identical for each measurement.

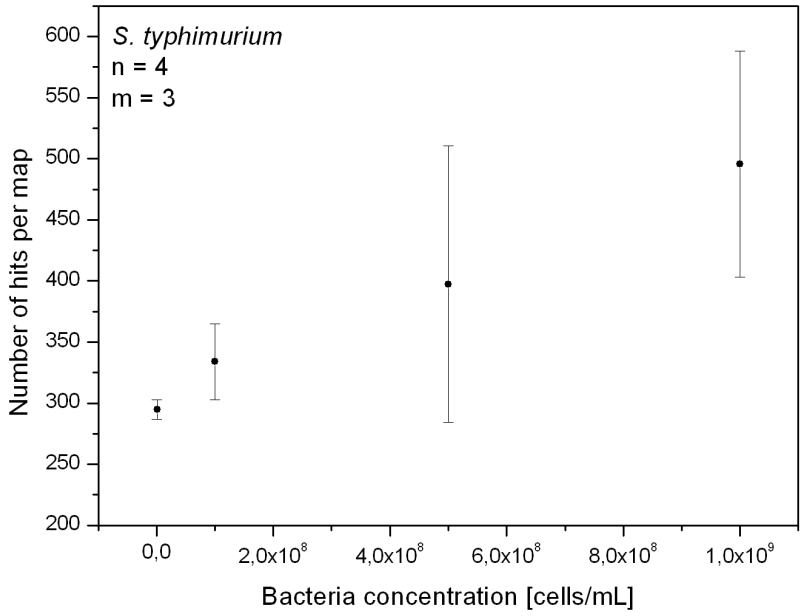

Figure 58: Calibration curve of *S. typhimurium.* An increasing number of hits per map with increasing bacteria concentration was obtained.

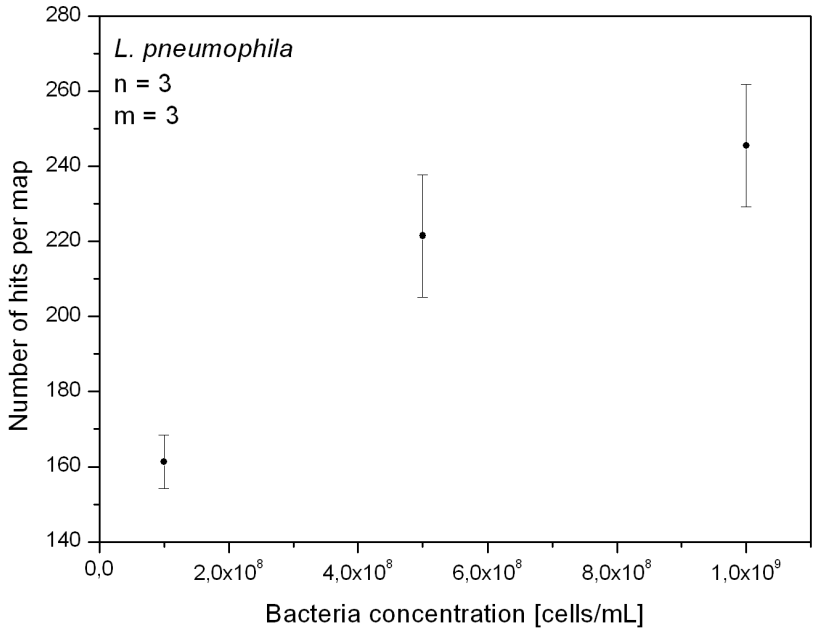

Figure 59: Calibration curve of *L. pneumophila.* An increasing number of hits per map with increasing bacteria concentration was obtained.

In this chapter, the validation of a label-free *in situ* detection principle of microorganisms on a microarray chip using SERS was presented. The total assay time of the method was 65 minutes and required a total reactant volume of 28 mL to analyze cells in a wet environment. The method offers the advantages of reduced assay times, simple handling and lower reactant volumes compared to methods where the target molecules need to be labelled. Little literature exists on systematic studies on silver colloid sols regarding the optimized *in situ* SERS detection of single bacteria. This was successfully evaluated here. Three different bacteria (*L. pneumophila, S. typhimurium* and *E. coli*) in aqueous environment were detected *in situ* and showed clearly distinct fingerprint spectra with high SNR. An optimized incubation solution of the analytes was found in order to direct the Ag particle agglomeration towards the cell wall, hence increased the number of particles surrounding the analyte during detection. This resulted in “hot spots” which again enabled us to reach higher sensitivities. An assignment of the SERS bands was carried out for both species. Calibration curves through SERS mapping of both *L. pneumophila* and *S. typhimurium* were developed. This thesis is the first to report on the quantitative *in situ* analysis of bacteria based on label-free SERS measurements in aqueous environment. Although this system requires further development, the results presented are evidence that the method worked. By optimizing the

method an expansion of the working range and a decrease in standard deviations can be obtained. This was realized by inserting a flow cell to the system setup (see section 4.4). The bacteria concentrations used in this establishing phase were fairly high and it is known that at high concentrations, the standard deviations increase. The combination of immunoassay microarrays with SERS detection was successful and has a high potential in microorganism analysis of water samples in the future.

4.4 SERS on bacteria (flow cell)

The use of flow cells in microarray analysis carries many advantages. The combination with immunoassay techniques offers the possibility to capture the antigens on specific sites in the flow cell. In that way, a SERS mapping procedure can be carried out on the spot, containing the immuno-complexes, resulting in a quantitative data plot. Furthermore, the analysis can be performed in aqueous environment and spare the analytes for dehydration. It was predicted that our microarray system allows higher reproducibility of SERS detection in flow cells, compared to mobile analyte detection. When the Raman signal is collected from a flowing stream (mobile analyte detection), the samples pass through a laser beam. At the laser detection point, SERS signals from different aggregates are accumulated and averaged [80]. Hence, a quantitative analysis is associated with large standard deviations. Another advantage of microassays is that any desirable number of spots of different antibodies of multiple targets can be added. Furthermore, a reduction of the assay time and the quantity of unspecifically bound analytes, as well as an improvement of the sensitivity is suggested [67]. A monitoring of chemical reactions can be possible [76, 113]. Additionally, the volume of reactants can be reduced because a higher precision of analyte dosage is warranted. Hence, less waste is generated. The flow can be connected in a circuit and diminish the loss of analytes, because excess analytes are repeatedly added to the microarray. In that way, the efficiency of the detection could be increased. In comparison to stationary systems, a flow-through system is a closed compartment in which pathogenic bacteria can be analyzed without risk of contaminations of environment and operator. The antibody spots are fixed and can be easily retrieved. Several flow cell constructions have been published describing different flow conditions of the reactants. Mainly, the importance of analyte/colloid mixing is highlighted [143, 146]. The fact that in our system the bacteria were immobilized onto the antibodies prior to the colloid addition diminished these problems. There is no need for a mixing procedure within the flow cell. The flow cell used in this thesis is shown in figure 60. For technical drawing please see App. A.

Figure 60: Image of the flow cell used for both qualitative and quantitative analysis of bacteria in aqueous environment.

4.4.1 Negative control

Background SERS signals originating from reagents used in the flow cell experiments can be eliminated as described in section 4.3.1. As quantitative evaluation was carried out by mapping of the vibrational band of carbohydrates at 565 cm^{-1} (for explanation see chapter 4.4.3), a negative control was assessed on an anti-*E. coli* microarray surface placed in the flow cell (see figure 61). Experimental parameters were set equal to the experiments with antigen solution, only here the concentration was 0 cells/mL

The optical image of the microarray used showed no bacteria present around the site (x = 0 µm, y = 0 µm) (figure 61 (top)). Quantitative evaluation of the negative control resulted in 4 ± 5.2 hits (figure 61 (bottom) an example with 3 hits is shown). It was expected that some hits would result as residue analytes were probably present in capillaries and windings after the washing procedure, due to geometry and age. LOD was calculated using this value in the quantitative experiments.

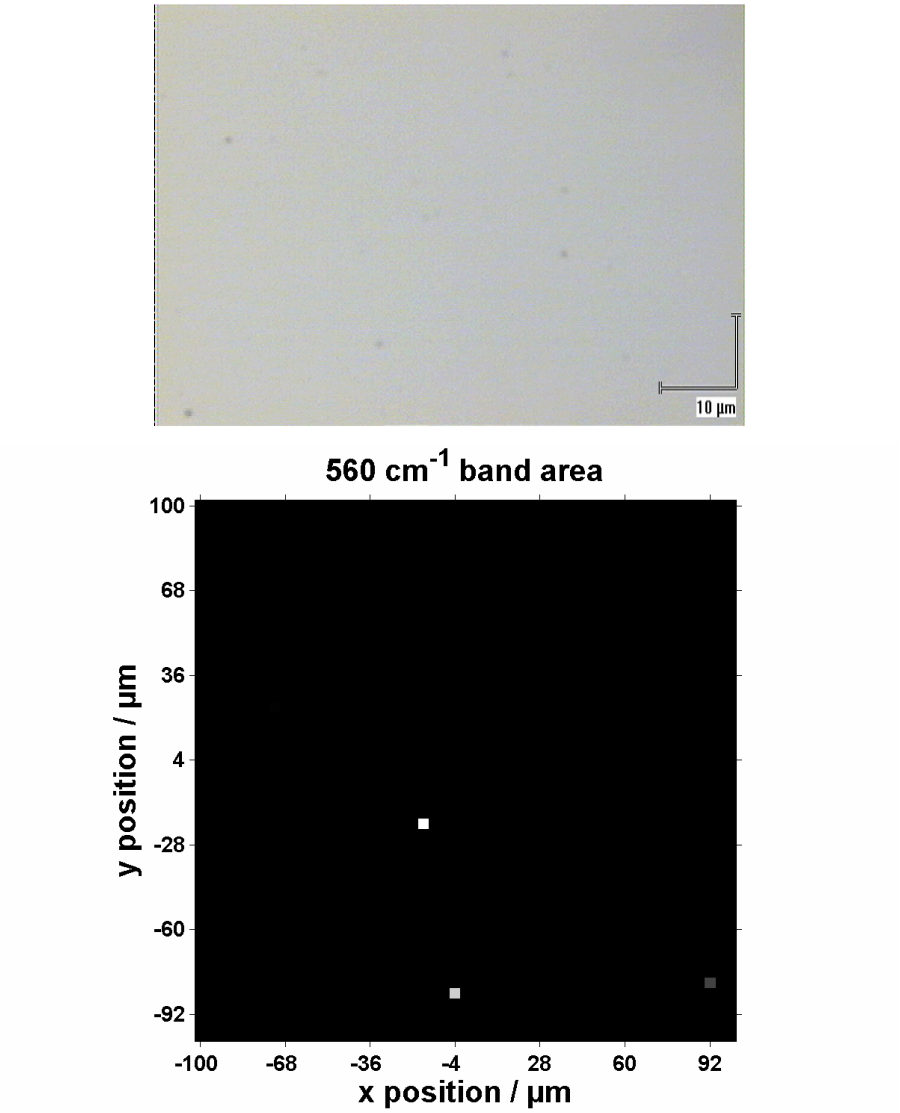

Figure 61: (Top) Optical image of the site of negative control map origin (x = 0 µm, y = 0 µm) on the microarray surface used for negative control. (Bottom) Quantitative evaluated map of negative control. Hits are illustrated with white colour and no sites with no hit are black.

4.4.2 Identification of bacteria

In order to identify the bacteria via fingerprint spectra, several procedures were carried out. In all flow cell experiments the analytes were incubated in PBS and not in carbonate buffer. This was to reduce external modifaction of the cell wall compositions. Single bacteria were localized through microscopy and analyzed by SERS mapping, so-called single cell SERS imaging. Furthermore, extended spectra of large wavenumber ranges were measured of single cells found on the microarray surface, to achieve more detailed chemical information. As the stationary experiments discussed in section 4.3 revealed large differences in fingerprint

spectra between autoclaved *L. pneumophila*, heat inactivated *S. typhimurium,* and living *E. coli DMS 1116*, the qualitative differentiation of the same antigens were expected to give comparable results. SERS measurements were successfully carried out in the flow cell by focusing the laser beam through the transparent microarray platform. Extended spectra (spectral range 400 – 3000 cm^{-1}, 10 s laser exposure, 633 nm laser) of these are shown in figure 62. In figure 63, the range is set to 400 – 1800 cm^{-1} to visualise differences in the SERS fingerprints.

By comparing the fingerprint spectra of *E. coli* reported by Sengupta *et al*., there are similarities of amino acid spectra to the ones in figure 61 [92]. As bacteria cell walls contain amino acids in large amount, this was expected. Sengupta *et al*. also showed that in the range of 500 – 900 cm^{-1} there are spectral differences between *S. typhimurium* and *E. coli*. This was also observed in our experiments. The following spectral differences were found in figure 63 between the three analytes: *S. typhimurium* fingerprint possessed peaks at 438, 869 and 1015 cm^{-1}, which were not present in the other spectra. *L. pneumophila* lacked the peaks at 712, 1274, 1453 and 1644 cm^{-1} in comparison to the other two analytes. Here, vibrational bands which did only appear in *L. pneumophila* fingerprint were 436, 1072, 1305, 1450 and 1624 cm^{-1}. In the fingerprint spectrum of *E. coli*, peaks at 440 and 479 cm^{-1} were observed which were missing in the spectra of *S. typhimurium* and *L. pneumophila*. It is in particular interesting that all three analytes (*L. pneumophila, S. typhimurium* and *E. coli*) reveal peaks at 436, 438 and 440 cm^{-1} respectively. In future, these vibrational modes can be used to gain qualitative results in addition to the vibrational band of carbohydrates at ~560 cm^{-1}. In order to carry out an evaluation of multiple peaks simultaneously, an upgraded Matlab program should be developed.

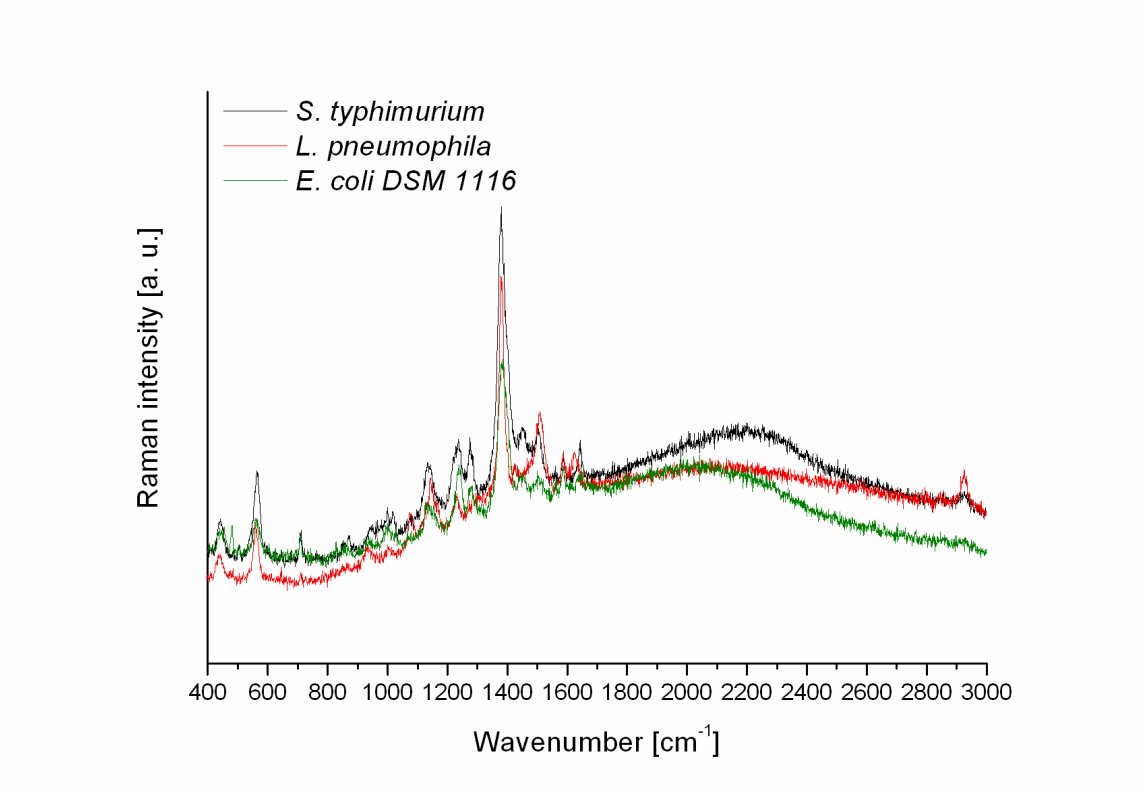

Figure 62: Fingerprint spectra of heat inactivated *S. typhimurium* (black), autoclaved *L. pneumophila* (red) and living *E. coli* (green).

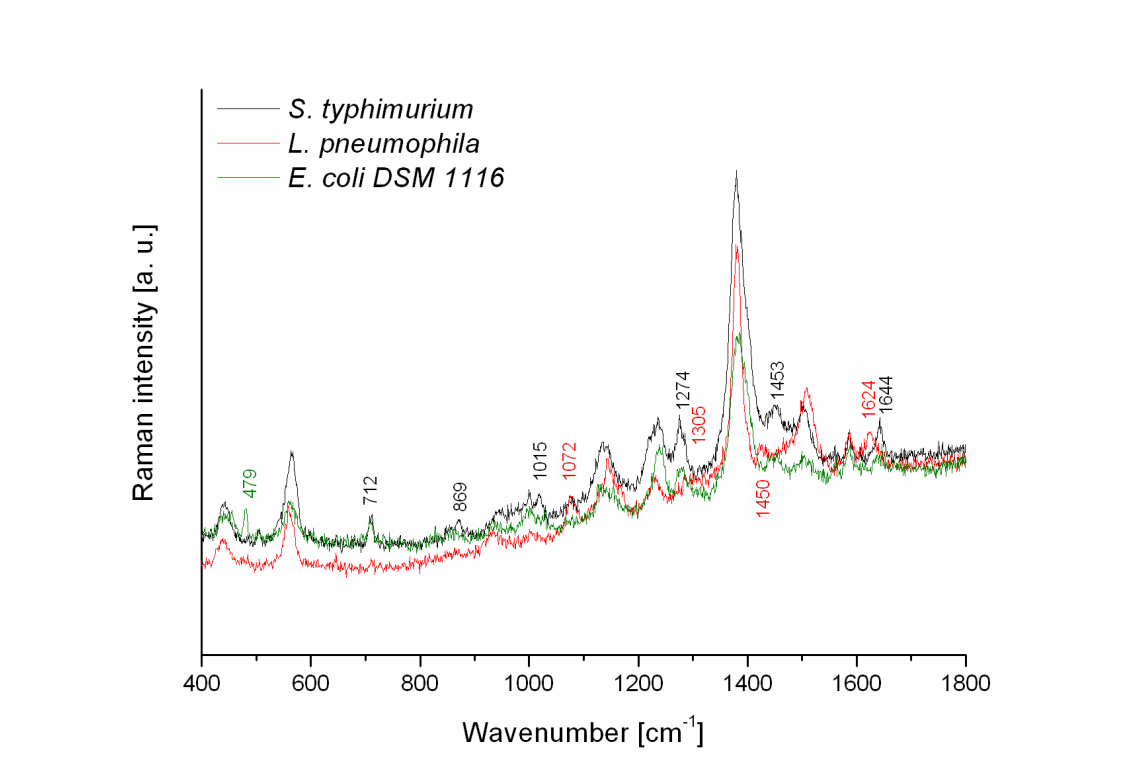

Figure 63: Enlarged graphic of the fingerprint spectra of heat inactivated *S. typhimurium* (black), autoclaved *L. pneumophila* (red) and living *E. coli* (green) cells.

Apparently, there were some factors contributing to differences in the fingerprint spectra of the three analytes when using a flow cell out of metal. These diversities in comparison to the stationary method can be due to electrostatic attraction properties of the flow cell metal as the colloids might agglomerate differently in a polycarbonate tray. Furthermore, the absence of azide during bacteria incubation could have caused differences in the spectra. In order to specify the significant vibrational bands to the right bacteria, chemometric is needed. Though, experiments were carried out to certain that the spectra belong to the analytes (i.e. SERS imaging and mapping procedures). As the surface material was SERS-inactive, an imaging of single bacteria was possible. The surface material did not affect the quality of the mapping because here, only fluorescence signals were detected. In figure 64 such SERS images of autoclaved *L. pneumophila,* heat inactivated *S. typhimurium* and living *E. coli* cells are shown. Here, two *L. pneumophila* cells, one *S. typhimurium* cell and one *E. coli* cell were mapped on spots in the flow cell. SERS mapping was carried out in a wavenumber range of 186 – 794 cm^{-1}, with 0.5 µm, 0.5 µm and 1 µm steps, respectively. The vibrational mode at 565 cm^{-1}, attributed to carbohydrates [31, 32], was analyzed over the mapping areas resulting in 1:1 compliance with the light microscopic pictures on the left of figure 64. This vibrational mode gave a strong SERS signal in the fingerprint spectrum of *L. pneumophila*, *S. typhimurium* and *E. coli*. Hence, it was very convenient for image processing. This vibrational band was also used for quantitative measurements. In chapter 4.4.3, the choice of this peak is discussed in more detail.

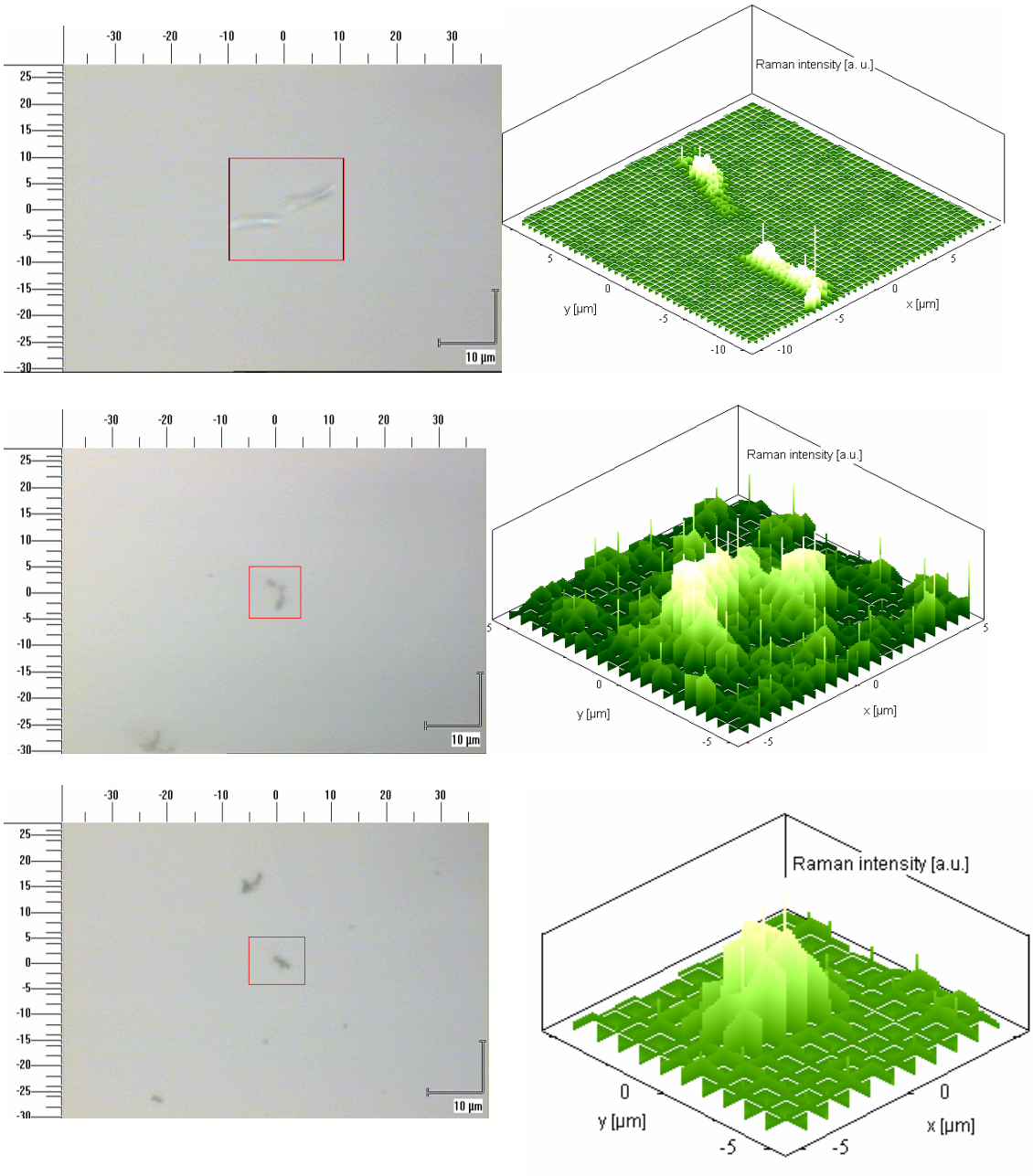

Figure 64: From top image to bottom image: SERS images of two autoclaved *L. pneumophila* cells, one heat inactivated *S. typhimurium* cell and one living *E. coli* cell on microarray surface in flow cell. (Left) Optical images of the bacteria. The red squares are framing the areas of SERS mapping. (Right) The corresponding single cell SERS maps of the bacteria.

4.4.3 Effects of environmental stress on bacteria

By using SERS-based immunoassay detection, even single bacteria can be detected label-free [97]. Though, there are several aspects which have to be considered prior to both qualitative and quantitative analysis of bacteria. The SERS fingerprint spectrum can change if the storage parameters of the cells differ. This is due to the possibility of variations in the cell wall composition, which depends on the environmental condition in the bacterium surroundings. With differences in nutrition supply, temperature of storage or experiment, lack of water etc., the bacterium can undergo several steps of self protection. This includes the production of a polysaccharide layer, enzymes and even shrinking and destruction of the cell wall. Hence, it can be important to keep the experimental conditions and the preparation steps constant. The dependence on environmental parameters to fingerprint spectra of *E. coli* was investigated. Thereby, SERS spectra were measured after storing the cells in different nutrient solutions (PBS, Lennox and NYCYM) over different time periods and temperatures.

It was found that environmental stress towards the bacteria induces fluctuations in the fingerprint spectra in the higher wavenumber range, whereas the band at 565 cm^{-1} does not change when exposing the cells to stress situations. No significant differences in the fingerprint spectra of living and autoclaved *E. coli* stored 14 days in PBS were observed (see figure 65). This was unexpected as during autoclaving high temperatures and pressure cause chemical changes in the cell wall composition. An explanation to the similarity of the two fingerprints could be that only whole cells were measured and the cells were at the same growth-stage. The living bacteria stored in different nutrient media showed significant differences with respect to the vibrational modes of carbohydrates in the Raman shift region between 440 and 1143 cm^{-1} (see figure 66). In the SERS spectra recorded after 7 days of storage in PBS (see figure 67), peaks at 440, 565, 930, 1144, 1229 and 1380 cm^{-1} were observed regardless of the storage temperature (4 °C, 20 °C and 37 °C). There are significant differences between the spectra of the bacteria stored at 37 °C for 7 and 12 days (see figure 68). Peaks at 558, 934, 1144, 1230 and 1380 cm^{-1} were observed in both spectra. The peak at 440 cm^{-1} was visible after 7 days. After 12 days it was shifted to higher wavenumber (435 - 445 cm^{-1}). The peaks around 640, 870 and 1010 cm^{-1} were no longer present after 12 days. Further vibrational modes in both spectra occurred in the area of 1420 - 1435 cm^{-1} and 1500 - 1515 cm^{-1}. The signal assignments refer to the several cell components, carbohydrates, proteins, amino acids and DNA bases. The stretching vibration of the aromatic ring at 1010 cm^{-1} is due to the amino acid phenylalanine [108, 109]. The vibrational mode of carbohydrates at 565 cm^{-1} and the asymmetric ring breathing at 1144 cm^{-1} probably originates

from polysaccharides, as well as the carboxylate stretching vibration at 1380 cm^{-1} [109, 147]. It is also observable in various carbohydrates like glucose or dextrose [148]. The peak at 871 cm^{-1} could refer to the single bond ν(CN) stretching vibrations of the amino acids proline and valine [149]. The amino acid tyrosine is observable as aromatic ring skeletal of proteins at 640 cm^{-1} [50, 149]. Further components of proteins like the torsion mode of amines are visible in the spectra at 1144 cm^{-1} [50]. Differences in the fingerprint spectra of *E. coli* stored over different time periods in Lennox and NZCYM, are probably caused by the different growth phases the cells underwent (see figures 69 and 70). The fact that after 12 days, some peaks are missing correlates with the theory [150]. The bacteria pass various growing phases (see figure 70). First the lag phase, where the bacteria mature and prepare for the metabolism. Then the bacterial growing begins in the acceleration phase, followed by the exponential growth phase. Once the nutrients are consumed or the population density becomes too high, the bacteria enter the retardation phase and after that the stationary phase. Finally, the bacteria start to evolve toxins, so that the population decreases. This is called the dying-off phase. During these phases, particularly the proteins in the cells change [50] which may be the reason for the variances in the spectra. This highlights the importance of information about the bacteria conditions prior to SERS measurements. A temperature dependence of the SERS could not be determined, but it cannot be excluded.

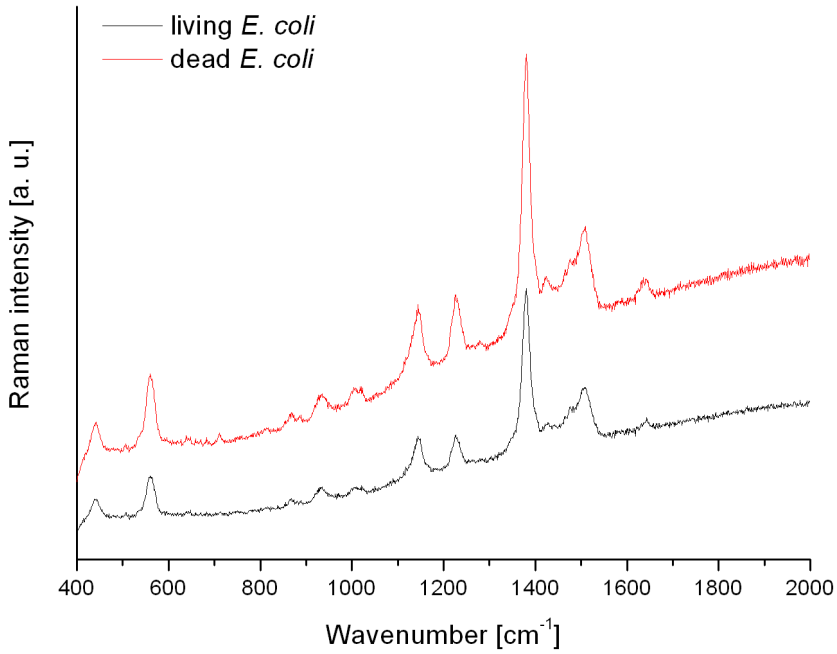

Figure 65: SERS fingerprint spectra of living (black) and dead (red) *E. coli* cells stored 14 d in PBS.

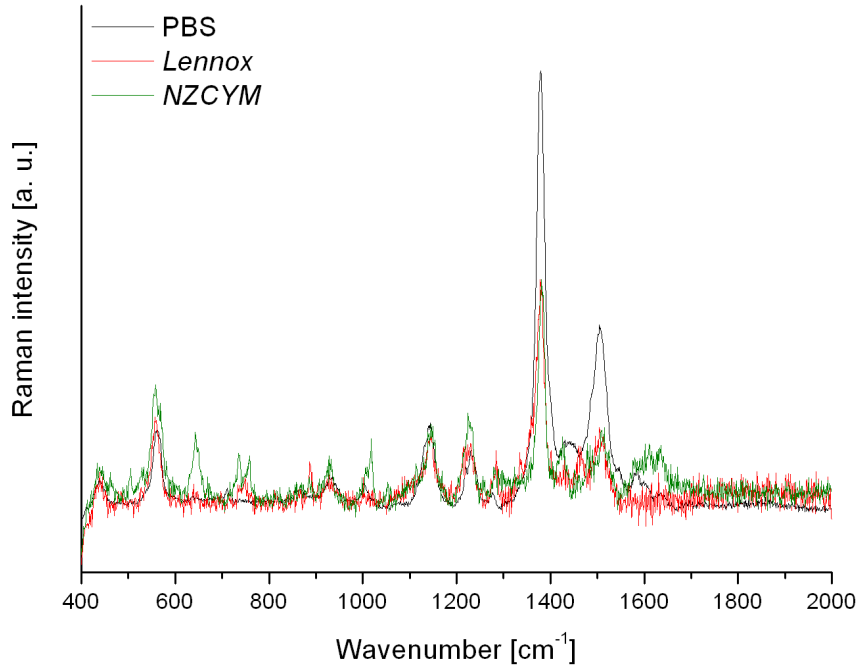

Figure 66: SERS fingerprint spectra of living *E. coli* cells stored in different nutrition media; PBS (black), Lennox (red) and NZCYM (green).

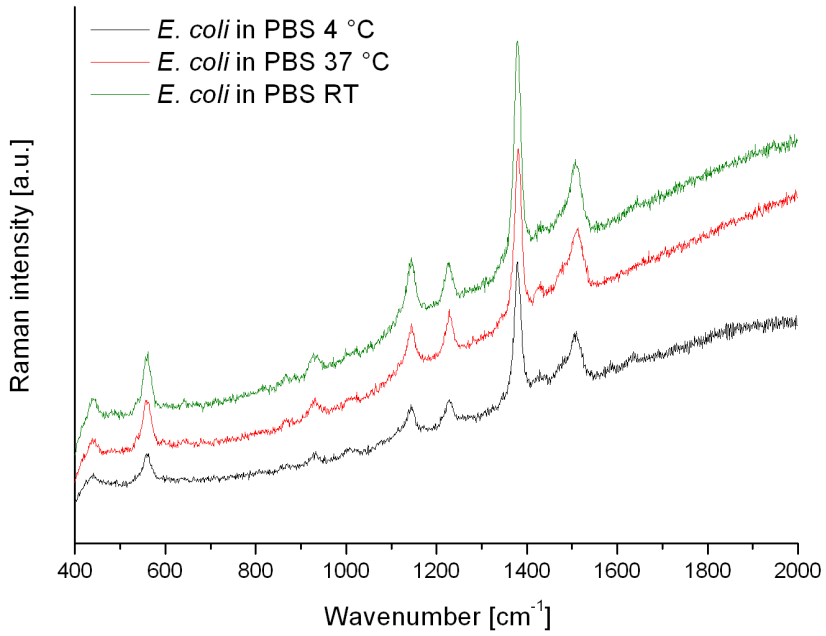

Figure 67: SERS fingerprint spectra of living *E. coli* cells stored for 7 d in PBS at different temperatures.

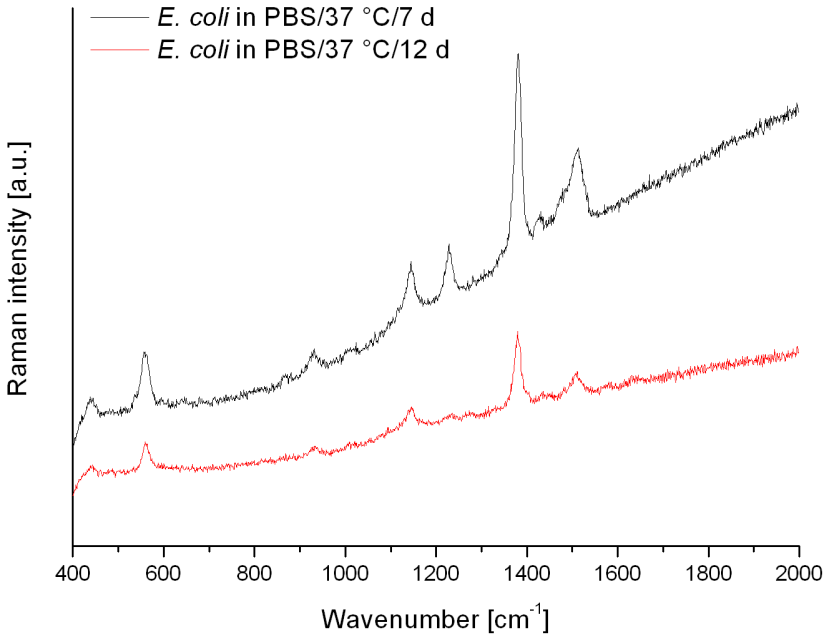

Figure 68: SERS fingerprint spectra of living *E. coli* cells stored in PBS at 37 °C over different time periods; 7 d (black), 12 d (red).

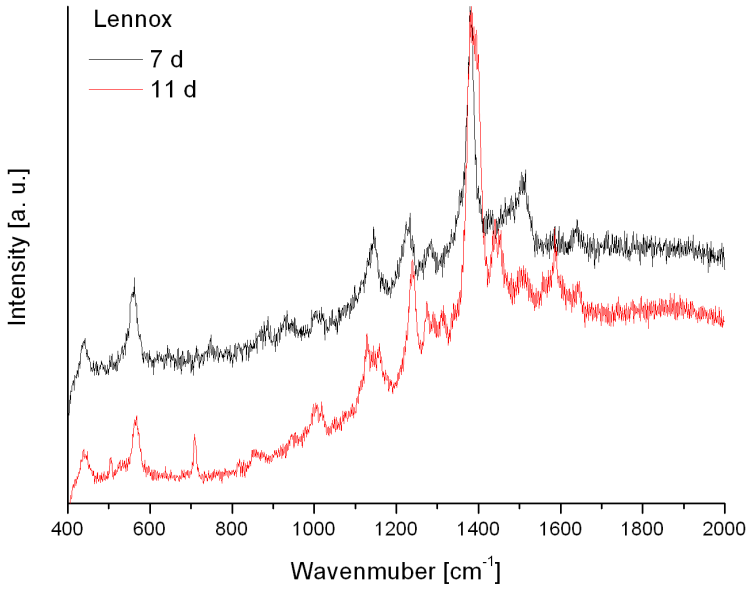

Figure 69: SERS fingerprint spectra of living *E. coli* cells stored in Lennox over a 7 d (black) and 11 d (red) period of time.

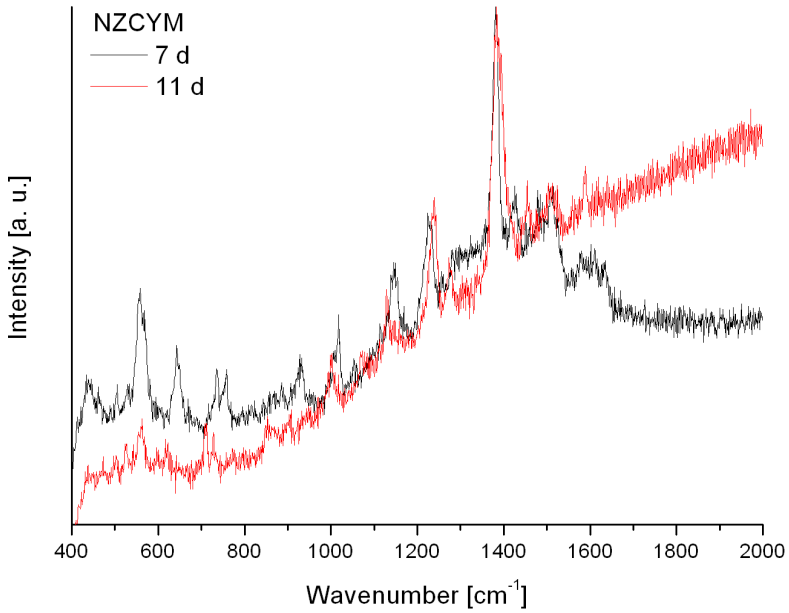

Figure 70: SERS fingerprint spectra of living *E. coli* cells stored in NZCYM over a 7 d (black) and 11 d (red) period of time.

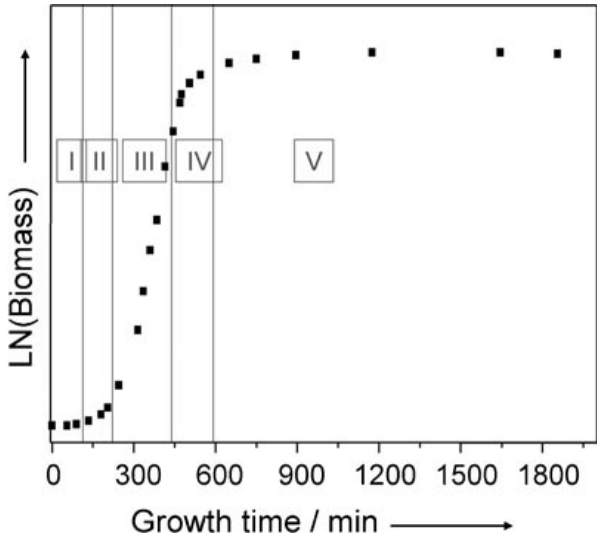

Figure 71: Bacteria growth diagram. (I) Lag phase, (II) acceleration phase, (III) exponential growth phase, (IV) retardation phase, (V) stationary phase [50].

In order to increase the reproducibility of the quantitative analysis, a vibrational mode was chosen which was not affected by environmental stress. This peak was attributed to carbohydrates and appeared at ~565 cm^{-1}. The choice of a peak at this low wavenumber was additionally realized due to possible fluctuations in higher wavenumber ranges. If the focal point of the laser beam bears too much energy, a charring process can occur. This is a known phenomenon and is visible in the SERS spectra as temporal fluctuations in the wavenumber region of NIR (800 – 1500 cm^{-1}) and two broad inhomogeneous bands above 1300 cm^{-1} due to photodecomposition. Changes in the intensities of vibrational bands are known as SERS blinking. Suggested explanations are that nonresonant aromatic molecules form complexes with the silver surfaces, thermal diffusion of molecules in and out of SERS active spots, structural changes of the SERS particles, changes in binding and orientation of adsorbates and overall different behaviour of single or a few molecules [151-153].

An experiment was carried out to assign the bacterium specific vibrational modes in the fingerprint of *E. coli.* An area of an anti-*E. coli* spot, covered by *E. coli* cells and a high concentration of silver nanoparticles, was scanned in order to force a soot generation process on the surface. Single spectra, which were collected within the map, were analyzed and attributed to either the bacterium or the soot. In figure 72, optical images made at the site of mapping before and after the soot generation are illustrated. Figure 73 shows examples of evaluated SERS maps of peaks assigned either to the bacterium (left) or to the soot (right). A summary of the vibrational modes examined is shown in table 10.

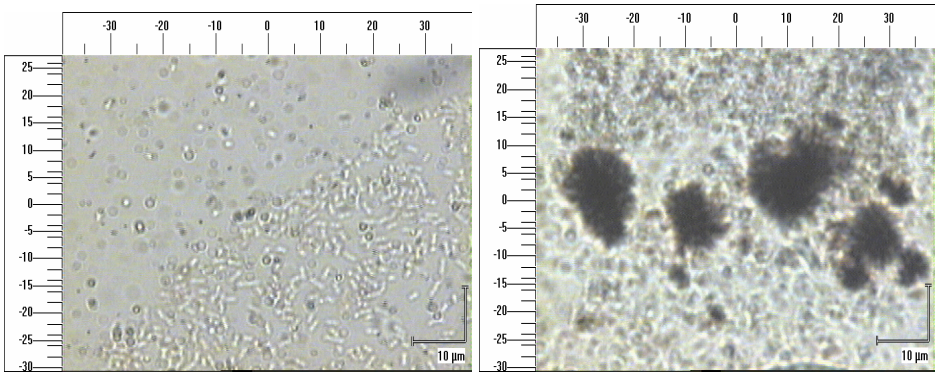

Figure 72: (Left) Optical image of an anti-*E. coli* spot covered with *E. coli* cells and SERS media prior to SERS mapping. (Right) Optical image of the same site on the antibody spot after SERS mapping over an area of 60 µm × 60 µm. A soot generation process on the surface due to the high concentration of silver metal had occurred which is seen as black spots in the image.

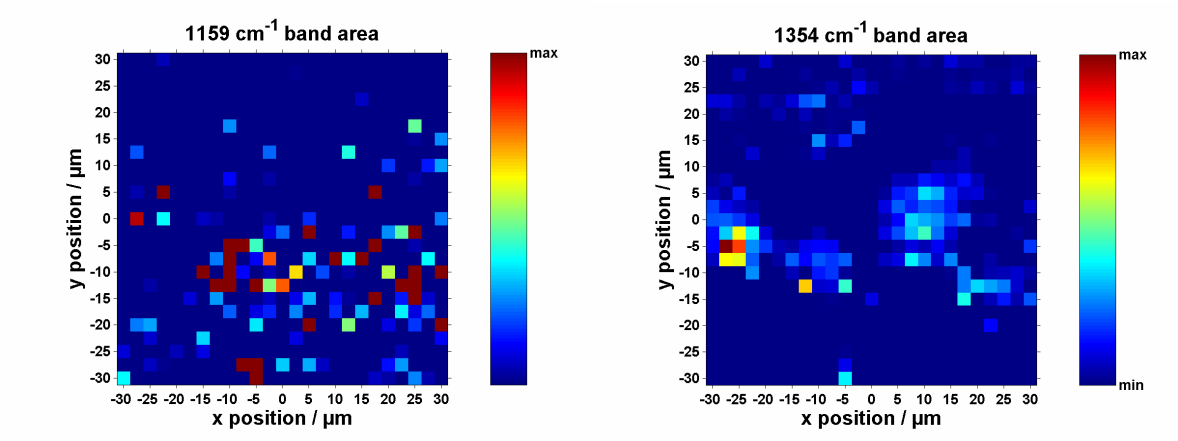

Figure 73: (Left) SERS map of the vibrational band at 1159 cm^{-1}, which could be attributed to the fingerprint spectrum of *E. coli*, as it shows a 1:1 compliance to the optical image of the site of bacteria in figure 72. (Right) SERS map of the vibrational band at 1354 cm^{-1}, which could be attributed as a peak originated from the soot generation process.

Table 10: Assignments of vibrational modes.

Vibrational mode [cm^{-1}]	*E. coli*	Soot
565	X	
1159	X	
1198	X	
1212		X
1223	X	
1238		X
1300	X	
1354		X
1400		X
1463		X
1575		X

4.4.4 Quantitative analysis of bacteria

The quantification of *E. coli* suspensions was carried out by SERS mapping of the vibrational mode of carbohydrates at 565 cm^{-1} with 4-µm scanning steps in a map of 200 µm × 200 µm area. Each concentration was analyzed three times and error bars calculated by standard deviation of the results. A linear range was found between 4.3×10^3 and 4.3×10^5 cells/mL (see figures 74 and 75). Above this concentration, standard deviation significantly increased due to agglomeration of the bacteria, which was observed under the microscope (see figure 76).

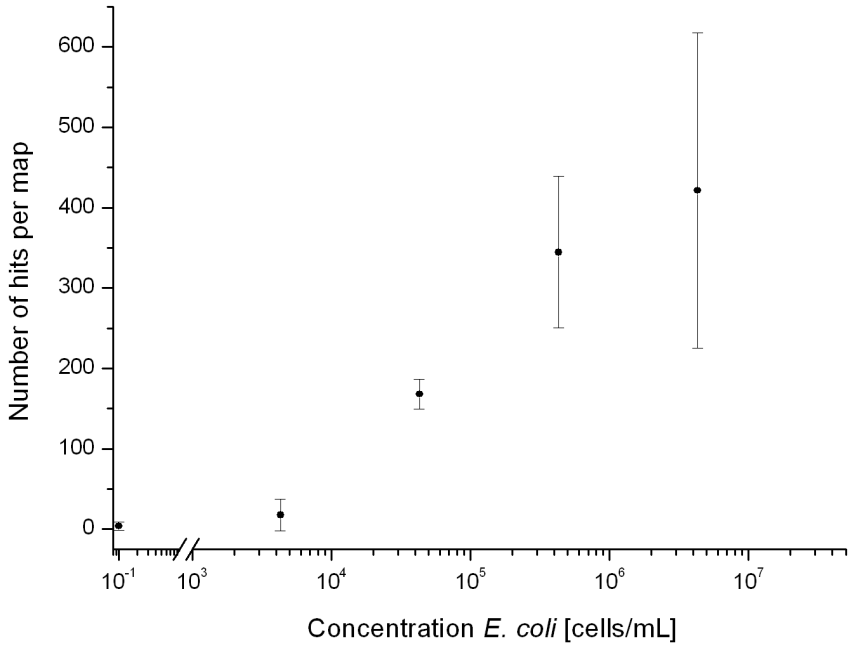

Figure 74: Calibration curve for living *E. coli* obtained by label-free *in situ* SERS mapping of immunocomplex microarray spots of 1 mL bacteria sample. This data was developed with single measurement LOD of 3 s.

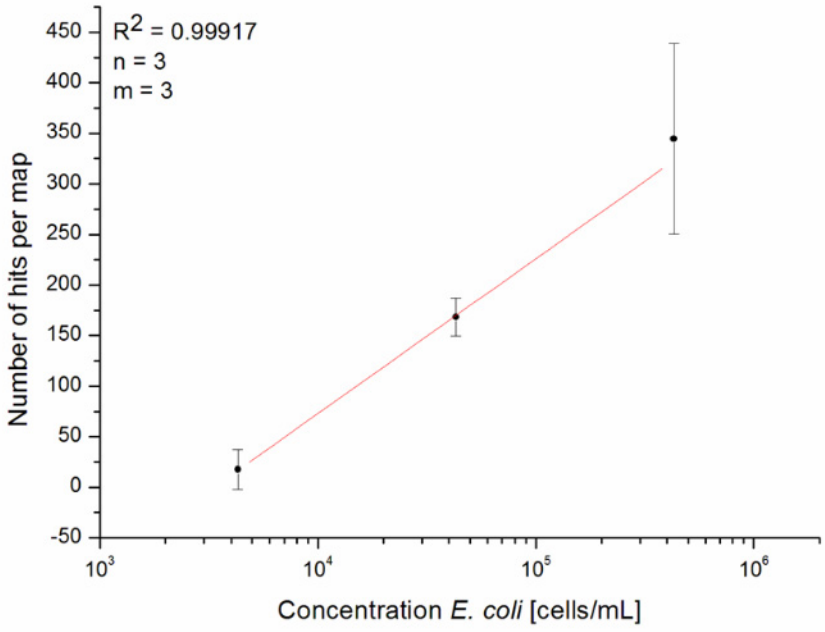

Figure 75: Linear range between 4.3×10^3 to 4.3×10^5 cells/mL of the calibration curve for living *E. coli* obtained by label-free *in situ* SERS mapping of immunocomplex microarray spots of 1 mL bacteria sample. This data was developed with single measurement LOD of 3 s.

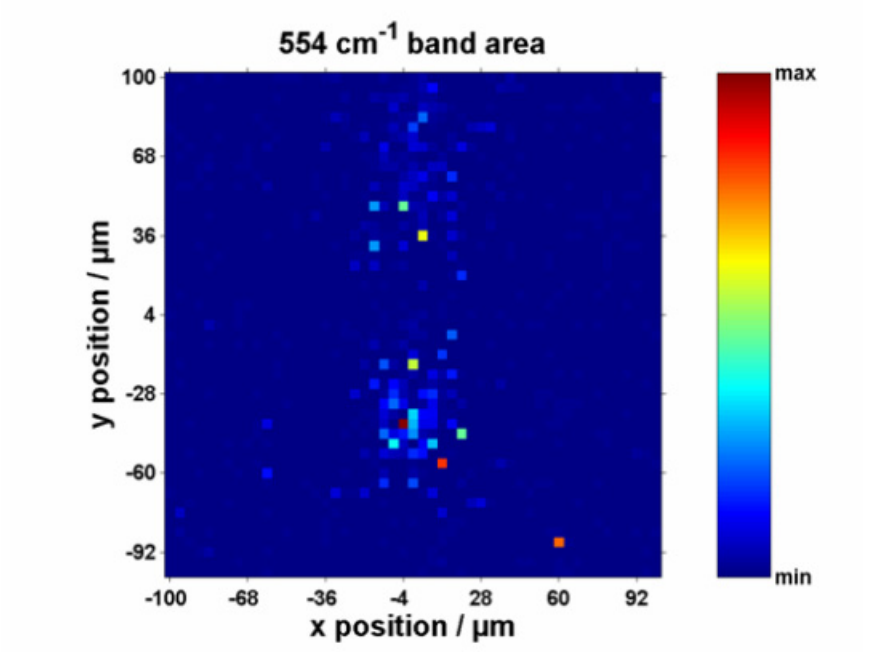

Figure 76: SERS map on an *E. coli* spot holding 4.3×10^6 cells/mL. The light blue to dark red spots are hits of bacteria. Two large clusters of bacteria are visible and indicate an agglomeration of bacteria.

The dynamic range of the system is limited by the number of points per map, hence the time of measurement, which can be increased. According to IUPAC definitions, the LOD of the method is 4485 cells/mL, LOQ is 7755 cells/mL. It could be shown that *E. coli* spiked aqueous samples could be analyzed quantitatively, which resulted in a calibration curve with linear range of 4.3×10^3 to 4.3×10^5 cells/mL. A lower standard deviation and LOD were obtained by means of the flow cell application in comparison to the stationary platform discussed in section 4.3. It should be mentioned that the standard deviation of the background, i.e. the signal generated by a blank signal, is only 4 ± 5 hits. This is due to the high selectivity of the double approach of antibody capture plus SERS readout. The background fluctuation could be even lowered by more careful flushing and cleaning the flow system, as we attribute the false positive values mostly to cross-contamination by highly concentrated samples we measured before the background measurement. Consequently, this thesis suggests that this method can be routinely applied for water sample analysis, allowing a fast and straight-forward screening of germs.

A flow-through system for the *in situ* SERS detection of living *E. coli* on a microarray was successfully applied. The method is non-destructive and fast. Additionally, there is no

risk of contamination of the sample, since the flow cell is a closed compartment. The silver nanoparticles surrounded the bacteria evenly distributed. In this way, the flow could be kept laminar throughout the entire measurement. This kind of aqueous microorganism analysis in combination to SERS is a completely new application and offers the advantage of antigen capturing prior to detection. In order to perform a quantitative detection, removal of any unbound antibody or antigen has to take place. The corresponding binding partner has to be fixed to the surface. By using a microarray as an immunoassay platform, there is no need of additional separation of the analytes as a SERS mapping procedure can be carried out on the spot, containing the immuno-complexes, resulting in a quantitative data plot. In addition, the complete analysis can be performed in aqueous environment and spare the analytes for dehydration.

For drinking water, the legal regulation in Germany requires that a volume of 100 mL must not contain a single cell; hence a suitable detection system needs to be able to see this concentration [60]. Most existing water analysis methods require an enrichment step to meet this, which is time consuming. The method presented in this work is promising for the capturing of bacteria cells and the label-free quantification on immuno-complex microarray without pre-enrichment. Though, a higher sensitivity is required for this purpose. The implementation into a continuous flow system allows for automation and brings the system closer to routine application.

4.5 SERS analysis of airborne bacteria

An alternative application of the developed SERS method is the detection of airborne bacteria. A prototype test chamber was developed for the first approach towards the application in which aerosol samples were collected for SERS analysis. Existing detection methods for bioaerosols are various sampling methods followed by for instance PCR, platen based counting or ELISA.

4.5.1 Aerosol sampling

E. coli (heat killed) aerosol was collected in a closed chamber by a wet sampler and evaluated qualitatively and quantitatively by SERS in flow cell. The aerosol concentration in the chamber, produced by nebulizing a bacteria suspension, was measured by APS. A linear increase of particle concentration with increasing spraying time was observed (see figure 77). These results gave a good starting point for the quantitative analysis of the collected samples. The background lied between 0 and 3 particles per cm^3 (aerodydamic particle size range 0.8 µm – 14.5 µm).

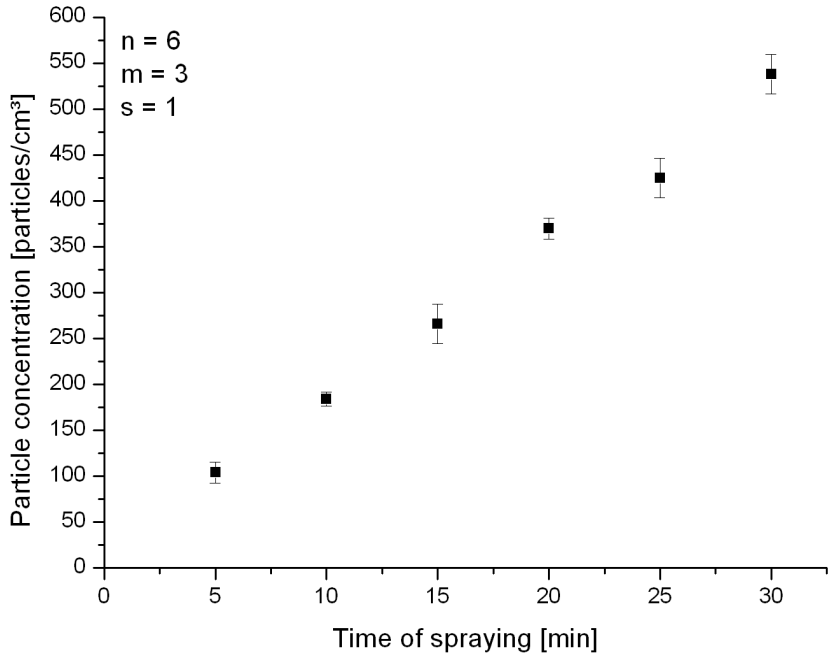

Figure 77: Time of *E. coli* aerosol spraying versus particle concentration in the aerosol chamber.

4.5.2 Identification of bacteria

An identification of the bacteria in the aerosol was carried out with SERS analysis in the flow cell. Figure 78 illustrates the fingerprint spectrum obtained by focusing the laser beam on a single cell on the microarray. The fingerprint spectra corresponded to the qualitative analysis of *E. coli* in chapter 4.4.

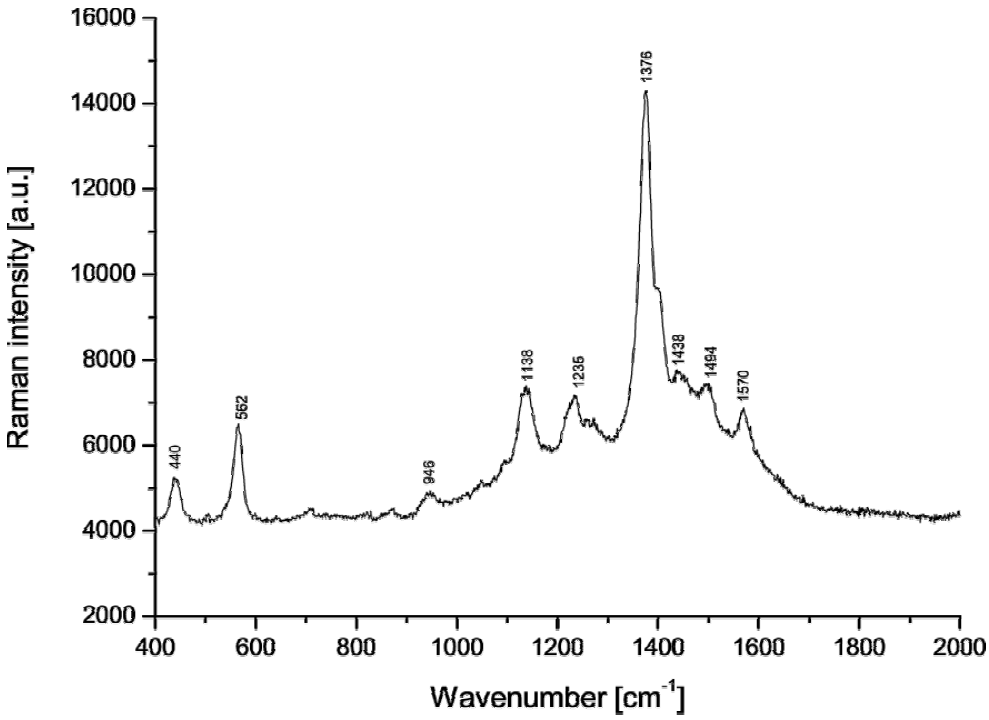

Figure 78: Fingerprint spectrum of *E. coli* collected by Coriolis® sampler in the aerosol chamber and measured by SERS in the microarray flow cell.

4.5.3 Quantitative analysis of bacteria

The quantification of *E. coli* aerosols was successfully carried out by SERS mapping of the vibrational mode of carbohydrates at 562 cm^{-1} with 4-µm scanning steps in a map of 200 µm × 200 µm area. Each concentration was analyzed three times and error bars calculated by standard deviation of the results.

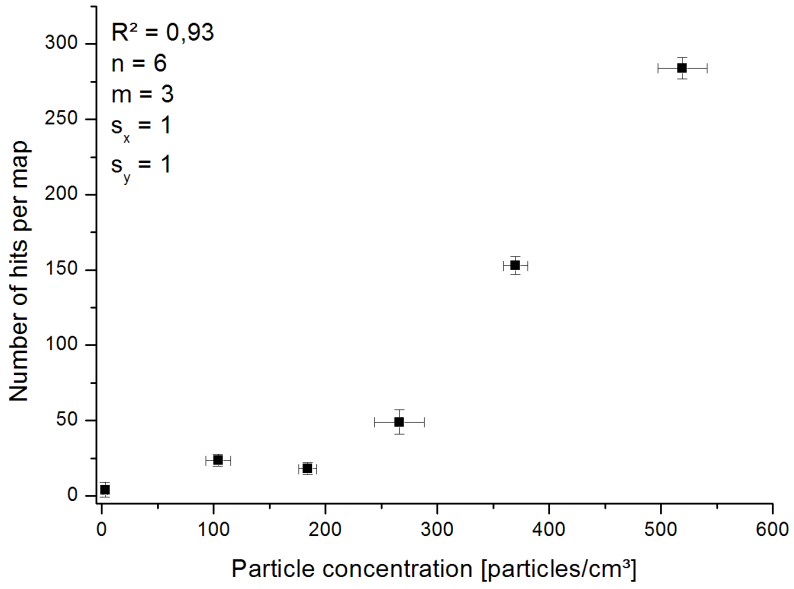

Figure 79: Calibration curve of *E. coli* obtained by label-free *in situ* SERS mapping of immunocomplex microarray spots of 1 mL collected bacteria aerosol sample. This data was developed with single measurement LOD of 3 s.

A calibration curve of *E. coli* was successfully developed between 0 and 600 particles/cm^3 (see figure 79). The dynamic range of the system was limited by the number of spectra per map, hence the time of measurement, which can be increased. The LOD (according to IUPAC) of the method is 114 particles/cm^3, LOQ is 178 particles/cm^3. At low particle consentrations (<200 particles/cm^3), the number of hits per map were nearly constant. This effect was caused by poor aerosol mixing in the chamber at low concentrations. It is to mention that a destruction of the bacteria during the nebulizing process was observed by microscopic analysis (see figure 80). Furthermore, the main threat of bioaerosols is the presence of *Legionellas*. Therefore, in the future the method must be made more sensitive and calibrated for *Legionella* in order to draw interest of the bioaerosol analysis industry for eventual commercialization. In figure 81, preliminary results are shown of the collection and SERS imaging of *Legionella* from the aerosol chamber. A whole cell was recovered in the flow cell and a 10 µm x 10 µm SERS map of 0.5-µm step (1 s laser exposure, λ_0 = 633 nm) was obtained of the vibrational band at 565 cm^{-1}. These results suggest for a successful analysis of *Legionella* using the developed aerosol readout method.

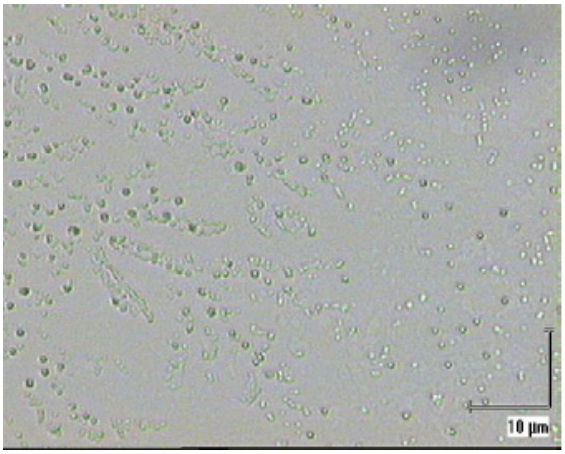

Figure 80: Microscopic image of liquidized *E. coli* aerosol sample. A major part of the cells had been destructed in the process.

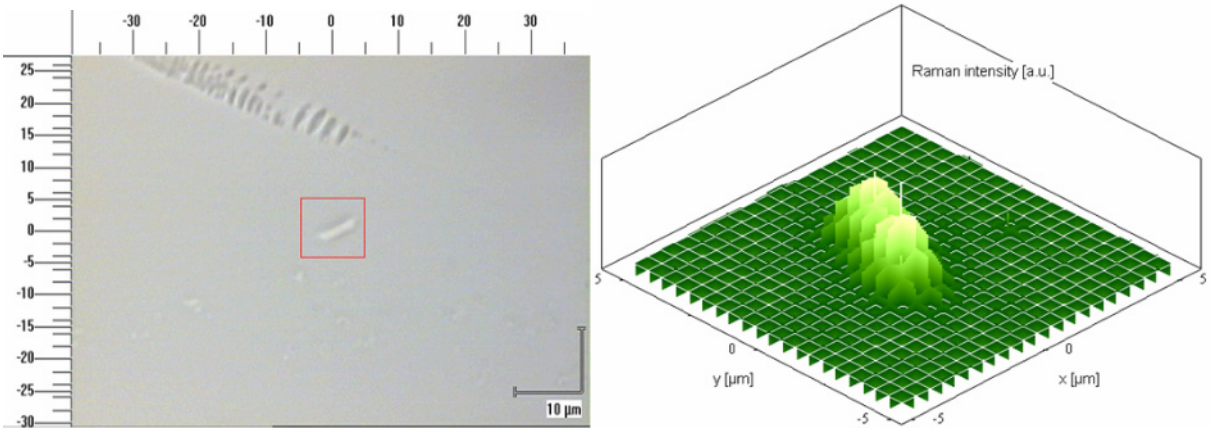

Figure 81: SERS imaging of a single *Legionella* cell collected from aerosol state. (left) Optical image of the bacterium, the red square indicates the area of SERS mapping. Top left of the picture, defects in the glass surface are visible. (right) SERS image of a single *Legionella* cell captured on a microarray surface in flow cell.

5 Summary and Outlook

In this thesis, the development of a new readout method for microarray detection of microorganisms is discussed. The detection is based on surface-enhanced Raman scattering (SERS) and enables the label-free detection of bacteria in water and aerosol matrices *in situ*. The advantages of the method are a label-free, fast and selective analysis of multiple bacteria. The characterization is feasible in water which prevents the analytes from dehydration and denaturation. For the analysis of the molecular composition of cell walls, this could be of advantage. Additionally, it presents the facility to analyze microarrays quantitatively with Raman. In this work, a completely new approach for the identification and quantification of bacteria is demonstrated.

Within the scope of this work, a modified preparation procedure of Ag colloid sol for the implementation as SERS media on microorganism detection was developed. A study towards its suitability for qualitative and quantitative SERS analysis of bacteria was performed. Using this colloid sol, enhancement factors of up to 10^8 were reached for the test molecule crystal violet. The colloid sol had a shelf life of over three weeks. Advantages of the proposed procedure are the straightforward, fast and inexpensive production at room temperature and the high reproducibility of the resulting particles. The rate of silver particle agglomeration was optimized by means of NaCl (0.03 M) addition. The distribution of the particles on the cell wall was optimized, resulting in formation of "hot spots" on the bacteria surfaces. As a result, a detection of three different microorganisms was enabled in a completely label-free way on an immunoassay platform. For the fingerprint spectra measurements, only 10s laser exposure time was needed.

An examination of the SERS fingerprint spectra of *E. coli* exposed to various environmental stress situations revealed fluctuations of vibrational bands depending on temperature, time of storage and nutrition supply. It was concluded that the vibrational mode of hydrocarbons at 565 cm^{-1} remained stable independent of the environmental changes. A mapping of this band was convenient for quantitative analysis of *E. coli*. Changes in fingerprint spectrum of living and autoclaved *E. coli* were not detected.

For the setup validation, single cell imaging as well as qualitative and quantitative stationary analyses of *L. pneumophila, S. typhimurium* and *E. coli* in contaminated aqueous samples were shown. The current time to image a single cell is 30 min with a resolution of 0.5 µm steps, 10 µm × 10 µm map (laser exposure: 1 s, static mode, total number of spectra: 484) based on the narrow vibrational band of hydrocarbons ν at 565 cm^{-1}. A successful integration in an automatic fluidic system was obtained which enabled a calibration of living

E. coli suspensions by means of a scanning procedure of the immuno-complex spots (4 µm steps, 200 µm × 200 µm map (laser exposure: 1 s, static mode, total number of spectra: 2601, mapping of vibrational band at 565 cm^{-1}) with a LOD of 4485 cells/mL and LOQ of 7755 cells/mL. An implementation in aerosol analysis, which is a new field to SERS analysis, was possible by developing a sample chamber to generate an aerosol sample. Combined with the flow-through SERS readout method, a calibration of heat killed *E. coli* suspensions was possible. A LOD of 114 particles/cm^3 and LOQ of 178 particles/cm^3 was obtained (4-µm steps, 200 µm × 200 µm map (laser exposure: 1 s, static mode, total number of spectra: 2601, mapping of vibrational band at 565 cm^{-1}). It was proven that aerosolized autoclaved *L. pneumophila* suspensions could be qualitatively detected with this setup. Hence, in a qualified laboratory, the successful real sample analysis of living *Legionella* aerosols is promising.

This is the first report on the label-free single cell imaging of *E. coli* cells based on SERS in water (living) and aerosols (heat killed). The results suggest that by this method, information on the biochemical reactions in bacteria cell walls can be gained. As the detection is carried out in aqueous environment, an online analysis is possible. The method can provide new information about the binding between antigen and antibody in the future, which again can give us a better knowledge on biochemical activities in microorganisms. Fully exploiting the high selectivity of SERS may even allow the use of the less selective receptor structures for immobilization of microorganisms, which would facilitate quantitative multicomponent detection. The method can be of use in real water and aerosol sample analysis for a fast and straight forward screening of germs. A huge advantage is that single cells can be detected and quantified without any risks for the user.

To further optimize the method, *in vitro* agglomeration of the SERS media could be carried out. With this method, the particles can be immobilized on specific sites, rich in amide and thiol functional groups, for different recognition purposes. To improve the sensitivity, an expansion of the size of the SERS maps on the antibody-antigen spots and reduction of the scanning steps need to be realized. For drinking water analysis, the method is promising, but the sensitivity needs to be increased. The use of larger sample volumes could improve the LOD of the system. Moreover, chemometric data analyses are important to fully exploit the spectral differences between the analytes in the flow cell compartment. Microarray platforms holding different antibodies can be applied for simultaneous qualitative and quantitative detection of multiple antigens. In this way, an ultrafast screening of drinking water can be realized. The analysis of living cells is interesting for further investigation on the biochemical

reactions of, for instance, growth and immuno-complex binding mechanisms, and their physiological states.

6 Abbreviations

AA	Ascorbic acid
AFM	Atomic force microscopy
APS	Aerodynamic particle sizer
ASTM	American Society for Testing and Materials
a. u.	Arbitrary unit
breath.	Breathing
CARS	Coherent anti-Stokes Raman spectroscopy
CCD	Charge-coupled device
CE	Chemical enhancement
CNC	Condensation nucleus counter
CTAB	Cetrimonium bromide
CV	Crystal violet
DMAP	4-Dimethylaminopyridine
DMF	2,5-Dimethylfuran
DMSO	Dimethyl sulfoxide
DNA	Deoxyribonucleic acid
DSC	*N,N´*-Disuccinimidyl carbonate
DTNB	5,5'-Dithiobis-2-nitrobenzoic acid
E. coli	Escherichia coli
ELISA	Enzyme-linked immunosorbent assay
EME	Electromagnetic enhancement
FEM	Finite element methods
FISH	Fluorescence *in situ* hybridization
FWHM	Full width at half maximum
GOPTS	3-Glycidyloxypropyltrimethoxysilane
HOMO	Highest occupied molecular orbital
HRP	Horseradish peroxidase

IUPAC	International Union of Pure and Applied Chemistry
IWC	Institute of Hydrochemistry
LOD	Limit of detection
LOQ	Limit of quantitation
L. pneumophila	Legionella pneumophila
LPS	Lipopolysaccharides
LUMO	Lowest unoccupied molecular orbital
NA	Numerical aperture
NHS	N-Hydroxysuccinimid
NR	Normal Raman
PBS	Phosphate buffered saline
PCR	Polymerase chain reaction
PDMS	Polydimethylsiloxane
PEG	Polyethylene glycol
PEO	Polyethylene oxide
Phe	Phenylalanin
PPO	Polypropylene oxide
RCS	Reuter centrifugal sampler
RM	Raman microscopy
RNA	Ribonucleic acid
RS	Raman spectroscopy
s	Strong
SAS	Surface air sampler
SERHS	Surface-enhanced hyper Raman spectroscopy
SERS	Surface-enhanced Raman scattering
SERRS	Surface-enhanced resonance Raman scattering
SMA	Sterilizable microbiological atrium

SNR	Signal to noise ratio
S. typhimurium	Salmonella typhimurium
TEM	Transmission electron microscopy
TERS	Tip-enhanced Raman scattering
THF	Tetrahydrofuran
UV	Ultra violet
VBNC	Viable but not culturable
w	Weak
δ	Deformation
ν	Stretching
ρ	Rocking

7 Appendix

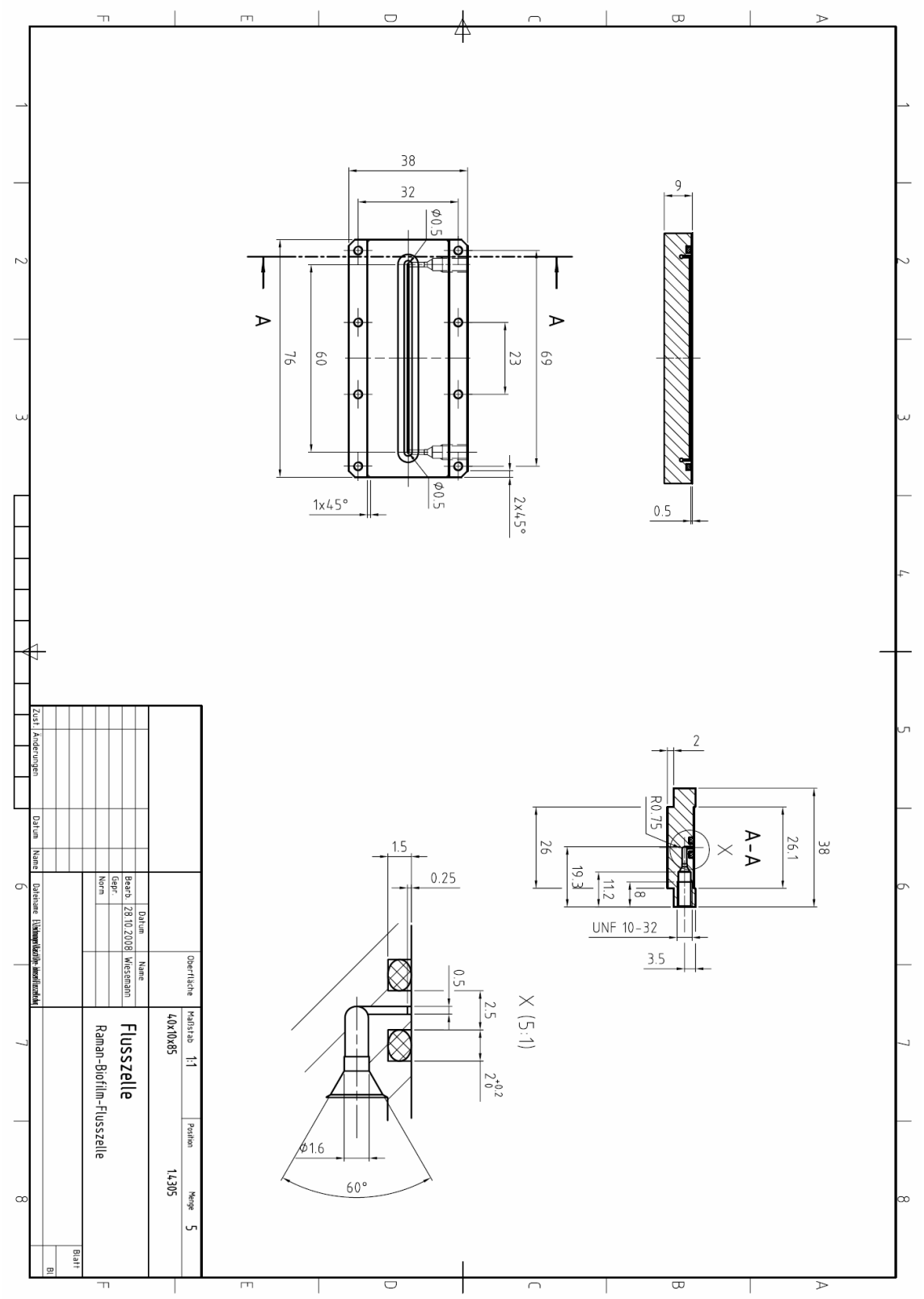

App. 1: Technical drawing of flow cell.

8 Literature

[1] Leopold, N.; Lendl, B. *A new method for fast preparation of highly surface-enhanced Raman-scattering (SERS) active colloids at room temperature by reduction of silver nitrate with hydroxylamine hydrochloride*, J. Phys. Chem. B, **2003**, *107*, 5723-5727.

[2] Gray, N. F. *Drinking water quality, problems and solutions*; Cambridge University Press: Cambridge, **2008**, 2.

[3] **TrinkwV**, http://www.dvgw.de/wasser/recht-trinkwasserverordnung/, *10.10.2011*.

[4] Creighton, J. A.; Blatchford, C. G.; Albrecht, M. G. *Plasma resonance enhancement of Raman scattering by pyridine adsorbed on silver or gold sol particles of size comparable to the exitation wavelength*, J. Chem. Soc., Faraday Trans., **1979**, *75*, 790-798.

[5] Eustis, S.; El-Sayed, M. A. *Why gold nanoparticles are more precious than pretty gold: Noble metal surface plasmon resonance and its enhancement of the radiative and nonradiative properties of nanocrystals of different shapes*, Chem. Soc. Rev., **2006**, *35*, 209-217.

[6] Liz-Marzán, L. M. *Tailoring surface plasmons through the morphology and assembly of metal nanoparticles*, Langmuir, **2006**, *22*, 32-41.

[7] Schwartzberg, A. M.; Oshiro, T. Y.; Zhang, J. Z.; Huser, T.; Talley, C. E. *Improving nanoprobes using surface-enhanced Raman scattering from 30-nm hollow gold particles*, Anal. Chem., **2006**, *78*, 4732-4736.

[8] Stuart, D. A.; Yuen, J. M.; Shah, N.; Lyandres, O.; Yonzon, C. R.; Glucksberg, M. R.; Walsh, J. T.; Van Duyne, R. P. *In vivo glucose measurement by surface-enhanced Raman spectroscopy*, Anal. Chem., **2006**, *78*, 7211-7215.

[9] Driskell, J. D.; Shanmukh, S.; Liu, Y.-J.; Hennigan, S.; Jones, L.; Zhao, Y.-P.; Dluhy, R. A.; Krause, D. C.; Tripp, R. A. *Infectious agent detection with SERS-active silver nanorod arrays prepared by oblique angle deposition*, IEEE Sens. J., **2008**, *8*, 863-870.

[10] Pignataro, B.; De Bonis, A.; Compagnini, G.; Sassi, P.; Cataliotti, R. S. *The role of micro- and nanomorphology of rough silver surfaces of different nature in surface enhanced Raman scattering effect: A combined study of scanning force microscopy and low-frequency Raman modes*, Journal of Chemical Physics, **2000**, *113*, 5947-5953.

[11] Stamplecoskie, K. G.; Scaiano, J. C.; Tiwari, V. S.; Anis, H. *Optimal size of silver nanoparticles for surface-enhanced Raman spectroscopy*, Journal of Physical Chemistry C, **2011**, *115*, 1403-1409.

[12] Willets, K. A. *Surface-enhanced Raman scattering (SERS) for probing internal cellular structure and dynamics*, Anal. Bioanal. Chem., **2009**, *394*, 85-94.

[13] Smitha, S. L.; Gopchandran, K. G.; Ravindran, T. R.; Prasad, V. S. *Gold nanorods with finely tunable longitudinal surface plasmon resonance as SERS substrates*, Nanotechnology, **2011**, *22*, 265705-265711.

[14] Liu, X. J.; Knauer, M.; Ivleva, N. P.; Niessner, R.; Haisch, C. *Synthesis of core-shell surface-enhanced Raman tags for bioimaging*, Analytical Chemistry, **2010**, *82*, 441-446.

[15] Merlen, A.; Chevallier, V.; Valmalette, J. C.; Patrone, L.; Torchio, P.; Vedraine, S.; Flory, F.; Moula, G. *Surface enhanced spectroscopy with gold nanostructures on silicon and glass substrates*, Surface Science, **2011**, *605*, 1214-1218.

[16] Ren, B.; Liu, G. K.; Lian, X. B.; Yang, Z. L.; Tian, Z. Q. *Raman spectroscopy on transition metals*, Analytical and Bioanalytical Chemistry, **2007**, *388*, 29-45.

[17] Ren, B.; Lin, X. F.; Yang, Z. L.; Liu, G. K.; Aroca, R. F.; Mao, B. W.; Tian, Z. Q. *Surface-enhanced Raman scattering in the ultraviolet spectral region: UV-SERS on rhodium and ruthenium electrodes*, Journal of the American Chemical Society, **2003**, *125*, 9598-9599.

[18] Wang, L. M.; Wang, L. H.; Tan, E. Z.; Li, L. D.; Guo, L.; Han, X. D. *Flower-shaped PdI2 nanomaterials with remarkable surface-enhanced Raman scattering activity*, Journal of Materials Chemistry, **2011**, *21*, 2369-2373.

[19] Tian, Z. Q.; Ren, B.; Wu, D. Y. *Surface-enhanced Raman scattering: From noble to transition metals and from rough surfaces to ordered nanostructures*, Journal of Physical Chemistry B, **2002**, *106*, 9463-9483.

[20] Ooka, A. A.; Kuhar, K. A.; Cho, N.; Garrell, R. L. *Surface interactions of a homologous series of α, ω-amino acids on colloidal silver and gold*, Biospectroscopy, **1999**, *5*, 9-17.

[21] Lee, P. C.; Meisel, D. *Adsorption and surface-enhanced Raman of dyes on silver and gold sols*, J. Phys. Chem. , **1982**, *86*, 3391-3395.

[22] Munro, C. H.; Smith, W. E.; Garner, M.; Clarkson, J.; White, P. C. *Characterization of the surface of a citrate-reduced colloid optimized for use as a substrate for SERS*, Langmuir, **1995**, *11*, 3712-3720.

[23] Holt, R. E.; Cotton, T. M. *Surface-enhanced resonance Raman and electrochemical investigation of glucose-oxidase catalysis at a silver electrode*, Journal of the American Chemical Society, **1989**, *111*, 2815-2821.

[24] Wilson, R.; Monaghan, P.; Bowden, S. A.; Parnell, J.; Cooper, J. M. *Surface-enhanced Raman signatures of pigmentation of cyanobacteria from within geological samples in a spectroscopic-microfluidic flow cell*, Anal. Chem., **2007**, *79*, 7036-7041.

[25] Temur, E.; Boyaci, I. H.; Tamer, U.; Unsal, H.; Aydogan, N. *A highly sensitive detection platform based on surface-enhanced Raman scattering for Escherichia coli enumeration*, Anal. Bioanal. Chem., **2010**, *397*, 1595-1604.

[26] Kneipp, J.; Kneipp, H.; Rajadurai, A.; Redmond, R. W.; Kneipp, K. *Optical probing and imaging of live cells using SERS labels*, J. Raman Spectrosc., **2009**, *40*, 1-5.

[27] Premasiri, W. R.; Moir, D. T.; Klempner, M. S.; Krieger, N.; Jones II, G.; Ziegler, L. D. *Characterization of the surface enhanced Raman scattering (SERS) of bacteria*, J. Phys. Chem. B, **2005**, *109*, 312-320.

[28] Walter, A.; Marz, A.; Schumacher, W.; Rosch, P.; Popp, J. *Towards a fast, high specific and reliable discrimination of bacteria on strain level by means of SERS in a microfluidic device*, Lab on a Chip, **2011**, *11*, 1013-1021.

[29] Zeiri, L.; Bronk, B. V.; Shabtai, Y.; Eichler, J.; Efrima, S. *Surface-enhanced Raman spectroscopy as a tool for probing specific biochemical components in bacteria*, Applied Spectroscopy, **2004**, *58*, 33-40.

[30] Kahraman, M.; Yazici, M. M.; Sahin, F.; Bayrak, O. F.; Topcu, E.; Culha, M. *Towards single-microorganism detection using surface-enhanced Raman spectroscopy*, International Journal of Environmental Analytical Chemistry, **2007**, *87*, 763-770.

[31] Kahraman, M.; Yazici, M. M.; Sahin, F.; Culha, M. *Convective assembly of bacteria for surface-enhanced Raman scattering* Langmuir, **2008**, *24*, 894-901.

[32] Laucks, M. L.; Sengputa, A.; Junge, K.; Davis, E. J.; Swanson, B. D. *Comparison of psychro-active arctic marine bacteria and common mesophilic bacteria using surface-enhanced Raman spectroscopy*, Appl. Spectrosc., **2005**, *59*, 1222-1228.

[33] Wigginton, K. R.; Vikesland, P. J. *Gold-coated polycarbonate membrane filter for pathogen concentration and SERS-based detection*, Analyst, **2010**, *135*, 1320-1326.

[34] Jarvis, R. M.; Law, N.; Shadi, L. T.; O'Brien, P.; Lloyd, J. R.; Goodacre, R. *Surface-enhanced Raman scattering from intracellular and extracellular bacterial locations*, Anal. Chem., **2008**, *80*, 6741-6746.

[35] Efrima, S.; Zeiri, L. *Understanding SERS of bacteria*, J. Raman Spectrosc., **2009**, *40*, 277-288.

[36] Ivleva, N. P.; Wagner, M.; Horn, H.; Niessner, R.; Haisch, C. *In situ surface-enhanced Raman scattering analysis of biofilm*, Anal. Chem., **2008**, *80*, 8538-8544.

[37] Ivleva, N. P.; Wagner, M.; Szkola, A.; Horn, H.; Niessner, R.; Haisch, C. *Label-free in situ SERS imaging of biofilms*, J. Phys. Chem. B, **2010**, *114*, 10184-10194.

[38] Ravindranath, S. P.; Wang, Y. L.; Irudayaraj, J. *SERS driven cross-platform based multiplex pathogen detection*, Sens. Actuator B-Chem., **2011**, *152*, 183-190.

[39] Zeiri, L.; Efrima, S. *Surface-enhanced Raman spectroscopy of bacteria: The effect of excitation wavelength and chemical modification of the colloidal milieu*, J. Raman Spectrosc., **2005**, *36*, 667-675.

[40] Cheng, I. F.; Lin, C. C.; Lin, D. Y.; Chang, H. *A dielectrophoretic chip with a roughened metal surface for on-chip surface-enhanced Raman scattering analysis of bacteria*, Biomicrofluidics, **2010**, *4*, 03410401-03410411.

[41] Yan, B.; Thubagere, A.; Premasiri, W. R.; Ziegler, L. D.; Dal Negro, L.; Reinhard, B. M. *Engineered SERS substrates with multiscale signal enhancement: Nanoparticle cluster arrays*, ACS Nano, **2009**, *3*, 1190-1202.

[42] Yang, X.; Gu, C.; Qian, F.; Li, Y.; Zhang, J. Z. *Highly sensitive detection of proteins and bacteria in aqueous solution using surface-enhanced Raman scattering and optical fibers*, Anal. Chem., **2011**, *83*, 5888-5894.

[43] Berthod, A.; Laserna, J. J.; Winefordner, J. D. *Surface enhanced Raman-spectrometry on silver hydrosols studied by flow-injection analysis*, Applied Spectroscopy, **1987**, *41*, 1137-1141.

[44] Strehle, K. R.; Cialla, D.; Rösch, P.; Henkel, T.; Köhler, M.; Popp, J. *A reproducible surface-enhanced Raman spectroscopy approach. online SERS measurements in a segmented microfluidic system*, Anal. Chem., **2007**, *79*, 1542-1547.

[45] Park, T.; Lee, S.; Seong, G. H.; Choo, J.; Lee, E. K.; Kim, Y. S.; Ji, W. H.; Hwang, S. Y.; Gweon, D.-G.; Lee, S. *Highly sensitive signal detection of duplex dye-labelled DNA oligonucleotides in a PDMS microfluidic chip: Confocal surface-enhanced Raman spectroscopic study*, Lab on a Chip, **2005**, *5*, 437-442.

[46] Yea, K.-h.; Lee, S.; Kyong, J. B.; Choo, J.; Lee, E. K.; Joo, S.-W.; Lee, S. *Ultra-sensitive trace analysis of cyanide water pollutant in a PDMS microfluidic channel using surface-enhanced Raman spectroscopy*, Analyst, **2005**, *130*, 1009-1011.

[47] Hou, D.; Maheshwari, S.; Chang, H.-C. *Rapid bioparticle concentration and detection by combining a discharge driven vortex with surface enhanced Raman scattering*, Biomicrofluidics, **2007**, *1*, 01410601-01410613.

[48] Guven, B.; Basaran-Akgul, N.; Temur, E.; Tamer, U.; Boyaci, I. H. *SERS-based sandwich immunoassay using antibody coated magnetic nanoparticles for Escherichia coli enumeration*, Analyst, **2011**, *136*, 740-748.

[49] Picorel, R.; Holt, R. E.; Heald, R.; Cotton, T. M.; Seibert, M. *Stability of isolated bacterial and photosystem-Ii reaction center complexes on Ag electrode surfaces - a surface-enhanced resonance Raman-study*, Journal of the American Chemical Society, **1991**, *113*, 2839-2843.

[50] Neugebauer, U.; Schmid, U.; Baumann, K.; Ziebuhr, W.; Kozitskaya, S.; Deckert, V.; Schmitt, M.; Popp, J. *Towards a detailed understanding of bacterial metabolism - Spectroscopic characterization of Staphylococcus epidermidis*, Chem. Phys. Chem, **2007**, *8*, 124-137.

[51] Chan, J.; Fore, S.; Wachsmann-Hogiu, S.; Huser, T. *Raman spectroscopy and microscopy of individual cells and cellular components*, Laser & Photon. Rev., **2008**, *2*, 325-349.

[52] Tian, Z. Q. *Surface-enhanced Raman spectroscopy: Advancements and applications*, J. Raman Spectr., **2005**, *36*, 466-470.

[53] Sengupta, A.; Laucks, M. L.; Dildine, N.; Drapala, E.; Davis, E. J. *Bioaerosol characterization by surface-enhanced Raman spectroscopy (SERS)*, Journal of Aerosol Science, **2005**, *36*, 651-664.

[54] Sengupta, A.; Brar, N.; Davis, E. J. *Bioaerosol detection and characterization by surface-enhanced Raman spectroscopy*, Journal of Colloid and Interface Science, **2007**, *309*, 36-43.

[55] Miram, W.; Scharf, K.-H. *Biologie heute SII*; Schroedel Diesterweg Schöningh Winklers GmbH: Braunschweig, **2000**, 1.

[56] Osborn, M. J. *Studies on gram-negative cell wall .1. evidence for role of 2-Keto-3deoxyoctonate in lipopolysaccharide of Salmonella typhimurium*, Proceedings of the National Academy of Sciences of the United States of America, **1963**, *50*, 499-506.

[57] Rozhok, S.; Holz, R. *Electrochemical attachment of motile bacterial cells to gold*, Talanta, **2005**, *67*, 538-542.

[58] Sigua, G. C.; Palhares, J. C. P.; Kich, J. D.; Mulinari, M. R.; Mattei, R. M.; Klein, J. B.; Muller, S.; Plieske, G. *Microbiological quality assessment of watershed associated with animal-based agriculture in Santa Catarina, Brazil*, Water Air and Soil Pollut., **2010**, *210*, 307-316.

[59] Lee, C. M.; Griffith, J. F.; Kaiser, W.; Jay, J. A. *Covalently linked immunomagnetic separation/adenosine triphosphate technique (Cov-IMS/ATP) enables rapid, in-field detection and quantification of Escherichia coli and Enterococcus spp. in freshwater and marine environments*, J. of Appl. Microbiol., **2010**, *109*, 324-333.

[60] Wolter, A.; Niessner, R.; Seidel, M. *Detection of Escheria coli O157:H7, Salmonella typhimurium amd Legionella pneumophila in water using a flow-through chemiluminescence microarray readout system*, Anal. Chem., **2008**, *80*, 5854-5863.

[61] Oukacine, F.; Quirino, J. P.; Garrelly, L.; Romestand, B.; Zou, T.; Cottet, H. *Simultaneous electrokinetic and hydrodynamic injection for high sensitivity bacteria analysis in capillary electrophoresis*, Analytical Chemistry, **2011**, *83*, 4949-4954.

[62] Pinto, D.; Almeida, V.; Santos, M. A.; Chambel, L. *Resuscitation of Escherichia coli VBNC cells depends on a variety of environmental or chemical stimuli*, J. Appl. Microbiol., **2011**, *110*, 1601-1611.

[63] Hammes, F.; Egli, T. *Cytometric methods for measuring bacteria in water: Advantages, pitfalls and applications*, Anal. Bioanal. Chem., **2010**, *397*, 1083-1095.

[64] Griffitt, K. J.; Noriea, N. F.; Johnson, C. N.; Grimes, D. J. *Enumeration of Vibrio parahaemolyticus in the viable but nonculturable state using direct plate counts and recognition of individual gene fluorescence in situ hybridization*, Journal of Microbiological Methods, **2011**, *85*, 114-118.

[65] Wolter, A.; Niessner, R.; Seidel, M. *Preparation and characterization of functional poly(ethylene glycol) surfaces for the use of antibody microarrays*, Anal. Chem., **2007**, *79*, 4529-4537.

[66] Knauer, M.; Ivleva, N. P.; Liu, X.; Niessner, R.; Haisch, C. *SERS-based label-free microarray readout for the detection of microorganisms*, Anal. Chem., **2010**, *82*, 2766-2772.

[67] Seidel, M.; Niessner, R. *Automated analytical microarrays: A critical review*, Anal. Bioanal. Chem., **2008**, *391*, 1521-1544.

[68] Suo, Z. Y.; Avci, R.; Yang, X. H.; Pascual, D. W. *Efficient immobilization and patterning of live bacterial cells*, Langmuir, **2008**, *24*, 4161-4167.

[69] Madigan, M.; Martinko, J. *Brock biology of microorganisms*; Prentice-Hall Inc.: New Jersey, **2005**, 11.

[70] Costerton, J. W. *Biofilm highlights (Springers series on biofilm)*; Springer-Verlag GmbH: Berlin and Heidelberg, **2011**, 1.

[71] Schets, F. M.; Nobel, P. J.; Strating, S.; Mooijman, K. A.; Engels, G. B.; Brouwer, A. *EU drinking water directive reference methods for enumeration of total coliforms and Escheria coli compared with alternative methods*, Let. Appl. Microbiol., **2002**, *34*, 227-231.

[72] Lashkari, D. A.; Derisi, J. L.; McCusker, J. H.; Namath, A. F.; Gentile, C.; Hwang, S. Y.; Brown, P. O.; Davis, R. W. *Yeast microarrays for genome wide parallel genetic and gene expression analysis*, Proc. Nat. Acad. Sci. USA, **1997**, *94*, 13057-13062.

[73] Campbell, C. J.; O´Looney, N.; Kwan, M. C.; Robb, J. S.; Ross, A. J.; Beattie, J. S.; Petrik, J.; Ghazal, P. *Cell interaction microarray for blood phenotyping*, Anal. Chem., **2006**, *78*, 1930-1938.

[74] Simon, R.; Sauter, G. *Tissue microarrays for miniaturized high-throughput molecular profiling of tumors*, Exp. Hemat., **2002**, *30*, 1365-1372.

[75] Fodor, S. P. A.; Read, J. L.; Pirrung, M. C.; Stryer, L.; Lu, A. T.; Solas, D. *Light-directed, spatially addressable parallel chemical synthesis*, Science, **1991**, *251*, 767-773.

[76] Kloth, K.; Rye-Johnsen, M.; Didier, A.; Dietrich, R.; Märtlbauer, E.; Niessner, R.; Seidel, M. *A regenerable immunochip for the rapid determination of 13 different antibiotics in raw milk*, Analyst, **2009**, *134*, 1433-1439.

[77] Han, X. X.; Jia, H. Y.; Wang, Y. F.; Lu, Z. C.; Wang, C. X.; Xu, W. Q.; Zhao, B.; Ozaki, Y. *Analytical technique for label-free multi-protein detection based on western blot and surface-enhanced Raman scattering*, Anal. Chem., **2008**, *80*, 2799-2804.

[78] Grow, A. E.; Wood, L. L.; Claycomb, J. L.; Thompson, P. A. *New biochip technology for label-free detection of pathogens and their toxins*, journal of Microbiological Methods, **2003**, *53*, 221-233.

[79] Hudson, S. D.; Chumanov, G. *Bioanalytical applications of SERS (surface-enhanced Raman spectroscopy)*, Analytical and Bioanalytical Chemistry, **2009**, *394*, 679-686.

[80] Chen, L.; Choo, J. *Recent advances in surface-enhanced Raman scattering detection technology for microfluidic chips*, Electrophoresis, **2008**, *29*, 1815-1828.

[81] Lindenmeier, G.; Horn, F.; Moc, I.; Grillhösl, C.; Berghold, S.; Schneider, N. *Biochemie des Menschen*; Georg Thieme Verlag KG: Stuttgart, **2005**, 3.

[82] Löffler, G. *Basiswissen Biochemie*; Springer-Verlag GmbH: Berlin and Heidelberg, **2005**, 6.

[83] Voet, D.; Voet, J. G.; Pratt, W.; Beck-Sickinger, A. G.; Hahn, U. *Lehrbuch der Biochemie*; Wiley-VCH Verlag GmbH: Weinheim, **2002**, 2.

[84] Kohler, G.; Milstein, C. *Continuous cultures of fused cells secreting antibody of predefined specificity*, Nature, **1975**, *256*, 495-497.

[85] Cuello, A.; Milstein, C.; Galfre, G. *Preparation and application of monoclonal antibodies for immunohistochemistry and immunocytochemistry*, IBRO Handbook Series, **1983**, *3*, 215-256.

[86] Easty, G. C.; Mercer, E. H. *Electron microscopic studies of the antigen-antibody complex*, Immunology, **1958**, *1*, 353-364.

[87] Camman, K. *Instrumentelle Analytische Chemie*, **2001**, Heidelberg.

[88] Stryer, L. *Biochemie*; Spektrum Akademischer Verlag: Heidelberg, **1996**, 4.

[89] Kellner, R.; Mermet, J. M.; Otto, M.; Valcàrcel, M.; Widmer, H. M. *Analytical chemistry: A modern approach to analytical science*; Wiley-VCH Verlag GmbH: Weinheim, **2004**, 2.

[90] Harz, M.; Rösch, P.; Popp, J. *Vibrational spectroscopy- a powerful tool for the rapid identification of microbial cells at the single-cell level*, Cytometry Part A, **2009**, *75A*, 104-113.

[91] Kneipp, K.; Wang, Y.; Kneipp, H.; Perelman, L. T.; Itzkan, I.; Dasari, R. R.; Feld, M. S. *Single molecule detection using surface-enhanced Raman scattering (SERS)*, Phys. Rev. Let., **1997**, *78*, 1667-1670.

[92] Segupta, A.; Mujacic, M.; Davis, E. J. *Detection of bacteria by surface-enhanced Raman spectroscopy*, Anal. Bioanal. Chem., **2006**, *386*, 1379-1386.

[93] Fleischmann, M.; Hendra, P. J.; McQuilla, A. *Raman-spectra of pyridine adsorbed at a silver electrode*, Chemical Physics Letters, **1974**, *26*, 163-166.

[94] Moskovits, M. *Surface-enhanced Raman spectroscopy: a brief retrospective*, J. Raman Spectrosc., **2005**, *36*, 485-496.

[95] Noginov, M. A.; Zhu, G.; Mayy, M.; Ritzo, B. A.; Noginova, N.; Podolskiy, V. A. *Simulated emission of surface plasmon polaritons*, Phys. Rev. Let., **2008**, *101*, 226806-226809.

[96] Khlebtsov, N. G.; Dykman, L. A.; Krasnov, Y. M.; Mel´nikov, A. G. *Light absorption by the clusters of colloidal gold and silver particles formed during slow and fast aggregation*, Colloidal J., **2000**, *67*, 765-779.

[97] Kneipp, J.; Kneipp, H.; Kneipp, K. *SERS - a single-molecule and nanoscale tool for bioanalytics*, Chem. Soc. Rev., **2008**, *37*, 1052-1060.

[98] Luo, Y. L. Y.; Aubry, A.; Pendry, J. B. *Electromagnetic contribution to surface-enhanced Raman scattering from rough metal surfaces: A transformation optics approach*, Phys. Rev. B, **2011**, *83*, 155422-155432.

[99] Brown, R. J. C.; Wang, J.; Milton, M. J. T. *Electromagnetic modelling of Raman enhancement from nanoscale structures as a means to predict the efficacy of SERS substrates*, J. Nanomat., **2007**, *1*, 1-10.

[100] Lombardi, J. R.; Birke, R. L.; Lu, T.; Xu, J. *Charge-transfer theory of surface enhanced Raman spectroscopy: Herzberg-Teller contributions*, J. Chem. Phys., **1986**, *84*, 4174-4181.

[101] Persson, B. N. J. *On the theory of surface-enhanced Raman scattering*, Chem. Phys. Lett., **1981**, *82*, 561-565.

[102] Schlucker, S. *SERS microscopy: Nanoparticle probes and biomedical applications*, Chem. Phys. Chem., **2009**, *10*, 1344-1354.

[103] Li, Y.-S.; Cheng, J.; Wang, Y. *Surface-enhanced Raman spectra of dyes and organic acids in silver solutions: Chloride ion effect*, Spectrochim. Acta A, **2000**, *56*, 2067-2072.

[104] Bengter, H.; Tengroth, C.; Jacobsson, S. P. *New light on Ag-colloid preparation for surface-enhanced FT-Raman spectroscopy: The role of aggregation*, J. Raman Spectrosc., **2005**, *36*, 1015-1022.

[105] Knauer, M.; Ivleva, N. P.; Niessner, R.; Haisch, C. *Optimized surface-enhanced Raman scattering (SERS) colloids for the characterization of microorganisms*, Anal. Sci., **2010**, *26*, 761-766.

[106] Petit, C.; Lixon, P.; Pileni, M.-P. *In situ synthesis of silver nanocluster in AOT reverse micelles*, J. Phys. Chem., **1993**, *97*, 12974-12983.

[107] Schuster, K. C.; Reese, I.; Urlaub, E.; Gapes, J. R.; Lendl, B. *Multidimensional information on the chemical composition of single bacterial cells by confocal Raman microspectroscopy*, Analytical Chemistry, **2000**, *72*, 5529-5534.

[108] Ivleva, N. P.; Wagner, M.; Horn, H.; Niessner, R.; Haisch, C. *Raman microscopy and surface-enhanced Raman scattering (SERS) for in situ analysis of biofilms*, J. of Biophoton., **2010**, *3*, 548-556.

[109] Ivleva, N. P.; Wagner, M.; Horn, H.; Niessner, R.; Haisch, C. *Towards a nondestructive chemical characterization of biofilm matrix by Raman microscopy*, Anal. Bioanal. Chem., **2009**, *393*, 197-206.

[110] Alak, A. M.; Vo-Dinh, T. *Surface-enhanced Raman-spectrometry of organophosphorus chemical-agents*, Analytical Chemistry, **1987**, *59*, 2149-2153.

[111] Kneipp, J.; Kneipp, H.; Rajadurai, A.; Redmond, R. W.; Kneipp, K. *Optical probing and imaging of live cells using SERS labels*, J. Raman Spectrosc., **2009**, *40*, 1-5.

[112] Pearman, W. F.; Lawrence-Snyder, M.; Angel, M. S.; Decho, A. W. *Surface-enhanced Raman spectroscopy for in situ measurements of signaling molecules (autoinducers) relevant to bacteria quorum sensing*, Appl. Spectrosc., **2007**, *61*, 1295-1300.

[113] Karsunke, X. Y. Z.; Niessner, R.; Seidel, M. *Development of a multichannel flow-through chemiluminescence microarray chip for parallel calibration and detection of pathogenic bacteria*, Anal. Bioanal. Chem., **2009**, *395*, 1623-1630.

[114] Bayraktar, T.; Pidugu, S. B. *Characterization of liquid flows in microfluidic systems*, International Journal of Heat and Mass Transfer, **2006**, *49*, 815-824.

[115] Sritharan, K.; Strobl, C. J.; Schneider, M. F.; Wixforth, A.; Guttenberg, Z. *Acoustic mixing at low Reynold's numbers*, Appl. Phys. Lett., **2006**, *88*, 0541021-0541023.

[116] Brook, R. D.; Franklin, B.; Cascio, W.; Hong, Y.; Howard, G.; Lipsett, M.; Luepker, R.; Mittleman, M.; Samet, J.; Smith, S. C.; Tager, I. *Air pollution and cardiovascular disease*, Circulation, **2004**, *109*, 2655-2671.

[117] Dungan, R. S.; Leytem, A. B. *Qualitative and quantitative methodologies for determination of airborne microorganisms at concentrated animal-feeding operations*, World J. Microbiol. & Biotechn., **2009**, *25*, 1505-1518.

[118] Brooks, J. P.; Tanner, B. D.; Josephson, K. L.; Gerba, C. P.; Haas, C. N.; Pepper, I. L. *A national study on the residential impact of biological aerosols from the land application of biosolids*, J. Appl. Microbiol., **2005**, *99*, 310-322.

[119] Hasegawa, N.; Yamasaki, S.; Horiguchi, Y. *A study of bacterial culturability during bioaerosol challenge test using a test chamber*, Journal of Aerosol Science, **2011**, *42*, 397-407.

[120] Lundholm, I. M. *Comparison of methods for quantitative-determinations of airborne bacteria and evaluation of total viable counts*, Applied and Environmental Microbiology, **1982**, *44*, 179-183.

[121] Duchaine, C.; Thorne, P. S.; Mériaux, A.; Grimard, Y.; Whitten, P.; Cormier, Y. *Comparison of endotoxin exposure assessment by bioaerosol impinger and filter-sampling methods*, Appl. Environ. Microbiol., **2001**, *67*, 2775-2780.

[122] Mainelis, G.; Grinshpun, S. A.; Willeke, K.; Reponen, T.; Ulevicius, V.; Hintz, P. J. *Collection of airborne microorganisms by electrostatic percipitation*, Aerosol Science and Technology, **1999**, *30*, 127-144.

[123] Bures, P.; Huang, Y. B.; Oral, E.; Peppas, N. A. *Surface modifications and molecular imprinting of polymers in medical and pharmaceutical applications*, Journal of Controlled Release, **2001**, *72*, 25-33.

[124] Sigal, G. B.; Bamdad, C.; Barberis, A.; Strominger, J.; Whitesides, G. M. *A self-assembled monolayer for the binding and study of histidine tagged proteins by surface plasmon resonance*, Analytical Chemistry, **1996**, *68*, 490-497.

[125] Peluso, P.; Wilson, D. S.; Do, D.; Tran, H.; Venkatasubbaiah, M.; Quincy, D.; Heidecker, B.; Poindexter, K.; Tolani, N.; Phelan, M.; Witte, K.; Jung, L. S.; Wagner, P.; Nock, S. *Optimizing antibody immobilization strategies for the construction of protein microarrays*, Analytical Biochemistry, **2003**, *312*, 113-124.

[126] Becker, H. G. O.; Berger, W.; Domschke, G. *Organikum*; Wiley-VCH Verlag GmbH & Co. KGaA: Weinheim, **2004**, 22.

[127] Kim, J. K.; Shin, D. S.; Chung, W. J.; Jang, K. H.; Lee, K. N.; Kim, Y. K.; Lee, Y. S. *Effects of polymer grafting on a glass surface for protein chip applications*, Coll. and Surf. B-Biointerf., **2004**, *33*, 67-75.

[128] Kingshott, P.; Griesser, H. J. *Surfaces that resist bioadhesion*, Curr. Opinion in Solid State & Mat. Sci., **1999**, *4*, 403-412.

[129] Norman, A. I.; Ho, D. L.; Greer, S. C. *Partitioning, fractionation, and conformations of star poly(ethylene glycol) in isobutyric acid and water*, Macromolecules, **2007**, *40*, 9628-9639.

[130] Groll, J.; Haubensak, W.; Ameringer, T.; Moeller, M. *Ultrathin coatings from isocyanate terminated star PEG prepolymers: Patterning of proteins on the layers*, Langmuir, **2005**, *21*, 3076-3083.

[131] Yacoub-George, E.; Hell, W.; Meixner, L.; Wenninger, F.; Bock, K.; Lindner, P.; Wolf, H.; Kloth, T.; Feller, K. A. *Automated 10-channel capillary chip immunodetector for biological agents detection*, Biosensors & Bioelectronics, **2007**, *22*, 1368-1375.

[132] Gotz, H.; Beginn, U.; Bartelink, C. F.; Grunbauer, H. J. M.; Moller, M. *Preparation of isophorone diisocyanate terminated star polyethers*, Macromolecular Materials and Engineering, **2002**, *287*, 223-230.

[133] Vasheghani, F. B.; Rajabi, F. H.; Ahmadi, M. H. *Thermodynamic study of multi-component polymer complexes of varying composition in a mixed solvent*, J. Macromol. Sci. Part A - Pure and Appl. Chem., **2007**, *44*, 113-118.

[134] Jana, N. R.; Gearheart, L.; Murphy, C. J. *Seed-mediated growth approach for shape-controlled synthesis of spheroidal and rod-like gold nanoparticles using a surfactant template*, Adv. Mater., **2001**, *13*, 1389-1393.

[135] Frens, G. *Controlled nucleation for the regulation of the particle size in monodisperse gold suspensions*, Nature, **1973**, *241*, 20-22.

[136] Gao, J.; Bender, C. M.; Murphy, C. J. *Dependence of the gold nanorod aspect ratio on the nature of the directing surfactant in aqueous solution*, Langmuir, **2003**, *21*, 9065-9070.

[137] Jana, N. R. *Gram-scale synthesis of soluble, near-monodisperse gold nanorods and other anisotropic nanoparticles*, Small, **2005**, *1*, 875-882.

[138] Chu, H. Y.; Huang, Y. W.; Zhao, Y. P. *Silver nanorod arrays as a surface-enhanced Raman scattering substrate for foodborne pathogenic bacteria detection*, Appl. Spectr., **2008**, *62*, 922-931.

[139] ASTM standard D, *American Society for Testing Materials*, Zeta potential of colloids in water and waste water, **1985**, 4182-4187.

[140] Bosetti, M.; Masse, A.; Tobin, E.; Cannas, M. *Silver coated materials for external fixation devices: In vitro biocompatibility and genotoxicity*, Biomaterials, **2002**, *23*, 887-892.

[141] Hao, E.; Schatz, G.; Hupp, J. *Synthesis and optical properties of anisotropic metal nanoparticles*, J. Fluoresc., **2004**, *14*, 331-341.

[142] Nikoobakht, B.; El-Sayed, M. A. *Surface-enhanced Raman scattering studies on aggregated gold nanorods*, J. Phys. Chem. A, **2003**, *107*, 3372-3378.

[143] Chon, H.; Lim, C.; Ha, S.-M.; Ahn, Y.; Lee, E. K.; Chang, S.-I.; Seong, G. H.; Choo, J. *On-chip immunoassay using surface-enhanced Raman scattering of hollow gold nanospheres*, Anal. Chem., **2010**, *82*, 5290-5295.

[144] Zhao, Y.; Jiang, Y.; Fang, Y. *Quenching and enhancement of fluorescence of fullerene molecules on gold particle*, Chemical Physics, **2006**, *323*, 169-172.

[145] Hering, K.; Cialla, D.; Ackermann, K.; Dörfer, T.; Möller, R.; Schneidewind, H.; Mattheis, R.; Fritzsche, W.; Rösch, P.; Popp, J. *SERS: A versatile tool in chemical and biochemical diagnostics*, Anal. Bioanal. Chem., **2008**, *390*, 113-124.

[146] Wilson, R.; Bowden, S. A.; Parnell, J.; Cooper, J. M. *Signal enhancement of surface enhanced Raman scattering and surface enhanced resonance Raman scattering using in situ colloidal synthesis in microfluidics*, Anal. Chem., **2010**, *82*, 2119-2123.

[147] Schenzel, K.; Fischer, S. *NIR FT Raman spectroscopy - a rapid analytical tool for detecting the transformation of cellulose polymorphs*, Cellulose, **2001**, *8*, 49-57.

[148] De Gussem, K.; Vandenabeele, P.; Verbeken, A.; Moens, L. *Raman spectroscopic study of Lactarius spores (Russulales, Fungi)*, Spectrochim. Acta Part A - Molecul. and Biomolecul. Spectr., **2005**, *61*, 2896-2908.

[149] Movasaghi, Z.; Rehman, S.; Rehman, I. U. *Raman spectroscopy of biological tissues*, Applied Spectroscopy Reviews, **2007**, *42*, 493-541.

[150] Moritz, T. J.; Taylor, D. S.; Polage, C. R.; Krol, D. M.; Lane, S. M.; Chan, J. W. *Effect of cefazolin treatment on the nonresonant Raman signatures of the metabolic state of individual Escherichia coil cells*, Analytical Chemistry, **2010**, *82*, 2703-2710.

[151] Futamata, M.; Maruyama, Y.; Ishikawa, M. *Local electric field and scattering cross section of Ag nanoparticles under surface plasmon resonance by finite difference time domain method*, Journal of Physical Chemistry B, **2003**, *107*, 7607-7617.

[152] Maruyama, Y.; Ishikawa, M.; Futamata, M. *Surface-enhanced Raman scattering of single adenine molecules on silver colloidal particles*, Chemistry Letters, **2001**, 834-835.

[153] Sladkova, M.; Vlckova, B.; Mojzes, P.; Slouf, M.; Naudin, C.; Le Bourdon, G. *Probing strong optical fields in compact aggregates of silver nanoparticles by SERRS of protoporphyrin IX*, Faraday Discussions, **2006**, *132*, 121-134.